

**Design and Comparative Analysis of Single-layer Graphene
Microstrip Patch Antennas Operating at Terahertz
Frequencies**

By

Syed Abid Sahdman

19121153

Kazi Shihabul Islam

15121014

SK Shahabuddin Ahmed

15121019

Samir Sakir Siddiqui

19121149

A thesis submitted to the Department of Electrical and Electronic Engineering in partial fulfillment of the requirements for the degree of Bachelor of Science in Electrical and Electronic Engineering

Electrical and Electronic Engineering
Brac University
April 2019

© 2019. Brac University
All rights reserved.

Declaration

It is hereby declared that

1. The thesis submitted is my/our own original work while completing degree at Brac University.
2. The thesis does not contain material previously published or written by a third party, except where this is appropriately cited through full and accurate referencing.
3. The thesis does not contain material which has been accepted, or submitted, for any other degree or diploma at a university or other institution.
4. I/We have acknowledged all main sources of help.

Student's Full Name & Signature:

Syed Abid Sahnman
19121153

Kazi Shihabul Islam
15121014

SK Shahabuddin Ahmed
15121019

Samir Sakir Siddiqui
19121149

Approval

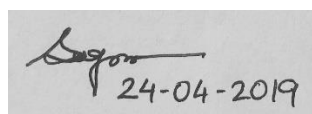
The thesis/project titled “Design and Comparative Analysis of Single-layer Graphene Microstrip Patch Antennas Operating at Terahertz Frequencies” submitted by

1. [Syed Abid Sahnman (19121153)]
2. [Kazi Shihabul Islam (15121014)]
3. [SK Shahabuddin Ahmed (15121019)]
4. [Samir Sakir Siddiqui (19121149)]

of Spring, 2019 has been accepted as satisfactory in partial fulfillment of the requirement for the degree of Bachelor of Science in Electrical and Electronic Engineering on April 25, 2019.

Examining Committee:

Supervisor:
(Member)



Dr. Md. Hasanuzzaman Sagor
Lecturer (Assistant Professor), School of Electronic
Engineering and Computer Science
Queen Mary University of London, UK

Program Coordinator:
(Member)

Dr. Saifur Rahman Sabuj
Assistant Professor, Department of Electrical and Electronic
Engineering
Brac University

Departmental Head:
(Chair)

Dr. Shahidul Islam Khan
Professor and Chairperson, Department of Electrical and
Electronic Engineering
Brac University

Abstract

The solution to the growing demand of higher speed wireless communication is the terahertz (THz) band, which will reduce the shortage of spectrum and capacity limitations of current wireless systems and will open new fields of applications in communication and networking domains. However, the existing wireless systems, comprising of classical copper antennas, are ill-equipped to handle this band of frequencies. Graphene, an allotrope of carbon, is a wonder material that proves to be a fine choice for an antenna material operating at the terahertz region. For our research, we have chosen the microstrip patch antenna to carry out our analyses because of its wide range of applications and ease of fabrication and modifications. Our research focuses on the comparison of antenna performances of three different shapes of the single layer graphene patch, and four substrates with different dielectric constants. The range of the operating frequencies were between 6 to 8THz. We have conducted our simulations on the software Computer Simulation Technology (CST), which is a specialized tool for accurate electro-magnetic simulations. Our goal was to find out the best combination of substrate and patch shape on the microstrip patch antenna that will give excellent performances at the terahertz frequency region. The comparisons have shown that combination of rectangular single-layer graphene patch shape with Teflon as the dielectric substrate provides the best antenna performances among all of them. Our findings will facilitate the researches and works towards finding the best practical solution for the difficulties faced in making terahertz communication possible and will contribute to a better and faster wireless communication system for all.

Keywords: Microstrip patch antenna; Single layer graphene patch; Terahertz frequencies; Patch shapes; Dielectric substrates; Graphene antenna performance comparison.

WE HAPPILY DEDICATE THIS PAPER TO OUR PARENTS

Acknowledgement

This paper is the work of Syed Abid Sahdman, Kazi Shihabul Islam, SK Shahabuddin Ahmed and Samir Sakir Siddiqui, students of Electrical and Electronics Engineering (EEE) Department of BRAC University. The paper has been prepared as an effort to compile the knowledge of our years of study in the University and produce a final thesis paper, which addresses “Design and Comparative Analysis of Single-layer Graphene Microstrip Patch Antennas Operating at Terahertz Frequencies”.

To begin with, we would like to express our sincere and earnest gratitude to Almighty Allah (S.W.T) for helping us successfully complete our undergraduate thesis in Electrical and Electronics Engineering.

We would like to express our sincere gratefulness and gratitude to our advisor and supervisor Dr. Md. Hasanuzzaman Sagor for his undivided support, immense knowledge and guidance. He was extremely supportive and helped us in every step of our thesis work. He was also extremely inspirational and motivating. Without his supervision, instructions and feedbacks, we could have never completed our work. The authors would also like to thank Dr. Saifur Rahman Sabuj, Ms Farzana Shabnam, Shifur Rahman and Swad Al Nahiyen for helping and supporting us.

Table of Contents

Declaration	ii
Approval.....	iii
Abstract	iv
Acknowledgement	vi
Table of Contents	vii
List of Figures.....	viii
List of Tables.....	xv
Chapter 1: Antenna Overview and Basics	1
Chapter 2: Introduction to Microstrip Patch Antenna	19
Chapter 3: Introduction to Graphene	37
Chapter 4: Graphene Modelling.....	43
Chapter 5: Literature Review and Methodology.....	53
Chapter 6: Simulation and Results.....	59
Chapter 7: Conclusion and Future Scope.....	101
References.....	103

List of Figures

Figure 1: Antenna as transition device.....	1
Figure 2: Half-Wave Dipole Antenna.....	2
Figure 3: Folded Dipole Antenna.....	3
Figure 4: Helical Antenna.....	4
Figure 5: Yagi-Uda Antenna.....	4
Figure 6: Rectangular Microstrip Patch Antenna.....	5
Figure 7: Planar Inverted-F Antenna.....	6
Figure 8: A Cassegrain Antenna used for Large Satellite Communication.....	7
Figure 9: A VSAT (Very Small Aperture Terminal) antenna used for home or business satellite communications.....	7
Figure 10: Log Periodic Dipole Antenna.....	8
Figure 11: Waveguide Antenna.....	9
Figure 12: Horn Antenna.....	10
Figure 13: Slot Antenna.....	10
Figure 14: Radiation Pattern in 2D.....	11
Figure 15: Omnidirectional Antenna Radiation Pattern.....	12
Figure 16: Isotropic Antenna Radiation Pattern.....	12
Figure 17: 3D Radiation Pattern of Isotropic Antenna.....	13
Figure 18: Yagi Antenna Directional Pattern.....	13
Figure 19: 3D Representation of Gain.....	14
Figure 20: S-Parameter of Antenna.....	16
Figure 21: A microstrip patch antenna.....	19
Figure 22: Side-view of a microstrip patch antenna.....	19

Figure 23: Typical feeds for microstrip antennas.....	22
Figure 24: Equivalent circuits for typical feeds.....	23
Figure 25: Microstrip line and its electric field lines, and effective dielectric constant geometry.....	24
Figure 26: Effective dielectric constant vs frequency for typical substrates.....	25
Figure 27: Physical and effective lengths of the rectangular microstrip patch.....	26
Figure 28: Recessed microstrip-line feed.....	27
Figure 29: Charge distribution and current density creation on microstrip patch.....	28
Figure 30: Rectangular microstrip patch geometry.....	29
Figure 31: Field configurations (modes) for rectangular microstrip patch.....	30
Figure 32: Geometry for circular microstrip patch antenna.....	31
Figure 33: Directivity vs effective radius for circular microstrip patch antenna operating in dominant TM_{110}^x mode.....	34
Figure 34: Triangular microstrip patch antenna design.....	34
Figure 35: Illustration of Orbitals.....	38
Figure 36: The honeycomb lattice of graphene.....	39
Figure 37: The Brillouin zone of graphene.....	40
Figure 38: Energy band structure of graphene for whole 1 st Brillouin zone.....	41
Figure 39: Energy band structure of graphene around Dirac point $K' = K_2$. K is given in units of $1/a$. Cone structure for low energies is clearly visible.....	42
Figure 40: Real part of intraband conductivity at room temperature ($T = 300k$) for different values of chemical potential.....	45
Figure 41: Imaginary part of intraband conductivity at room temperature ($T = 300k$) for different values of chemical potential.....	45
Figure 42: Real(a) and imaginary (b) part of effective permittivity at room temperature (300K) at $\mu_c = 0$ eV.....	47

Figure 43: Dependence of the absorption cross section of a graphenna as a function of its width.....	48
Figure 44: Log-log plots of the real (above) and imaginary (below) parts of the electrical conductivity of graphene as a function of the frequency, for different values of the chemical potential.....	49
Figure 45: Absorption cross-section of graphene slab with respect to frequency for different values of chemical potential.....	50
Figure 46: Log-log plots of the real (above) and imaginary (below) parts of the electrical conductivity of graphene as a function of the frequency.....	51
Figure 47: Absorption cross section (in logarithmic scale) of a graphenna as a function of frequency, for different values of the relaxation time.....	52
Figure 48: Single Layer Graphene Rectangular Patch Antenna.....	59
Figure 49: S Parameter for single layer graphene rectangular patch antenna using Teflon as Substrate.....	60
Figure 50: VSWR for single layer graphene rectangular patch antenna using Teflon as Substrate.....	60
Figure 51: Radiation Pattern of single layer graphene rectangular patch antenna using Teflon as Substrate.....	61
Figure 52: Polar Plot of Directivity of single layer graphene rectangular patch antenna using Teflon as Substrate.....	61
Figure 53: S Parameter for single layer graphene rectangular patch antenna using Polyimide as Substrate.....	62
Figure 54: VSWR for single layer graphene rectangular patch antenna using Polyimide as Substrate.....	63
Figure 55: Radiation Pattern of single layer graphene rectangular patch antenna using Polyimide as Substrate.....	63
Figure 56: Polar Plot of Directivity of single layer graphene rectangular patch antenna using Polyimide as Substrate.....	64

Figure 57: S Parameter for single layer graphene rectangular patch antenna using FR-4 as Substrate.....	64
Figure 58: VSWR for single layer graphene rectangular patch antenna using FR-4 as Substrate.....	65
Figure 59: Radiation Pattern of single layer graphene rectangular patch antenna using FR-4 as Substrate.....	65
Figure 60: Radiation Pattern of single layer graphene rectangular patch antenna using FR-4 as Substrate.....	66
Figure 61: S Parameter for single layer graphene rectangular patch antenna using Alumina as Substrate.....	67
Figure 62: VSWR for single layer graphene rectangular patch antenna using Alumina as Substrate.....	67
Figure 63: Radiation Pattern of single layer graphene rectangular patch antenna using Alumina as Substrate.....	68
Figure 64: Polar Plot of Directivity of single layer graphene rectangular patch antenna using Alumina as Substrate.....	68
Figure 65: Comparison of s-parameter of rectangular patch antenna for different substrates.....	69
Figure 66: Polar plot of rectangular patch antenna for different substrates.....	69
Figure 67: Single Layer Graphene Circular Patch Antenna.....	71
Figure 68: S Parameter for single layer graphene circular patch antenna using Teflon as Substrate.....	72
Figure 69: VSWR for single layer graphene circular patch antenna using Teflon as Substrate.....	72
Figure 70: Radiation Pattern of single layer graphene circular patch antenna using Teflon as Substrate.....	73
Figure 71: Polar Plot of Directivity of single layer graphene circular patch antenna using Teflon as Substrate.....	73

Figure 72: S Parameter for single layer graphene circular patch antenna using Polyimide as Substrate.....	74
Figure 73: VSWR for single layer graphene circular patch antenna using Polyimide as Substrate.....	74
Figure 74: Radiation Pattern of single layer graphene circular patch antenna using Polyimide as Substrate.....	75
Figure 75: Polar Plot of Directivity of single layer graphene circular patch antenna using Polyimide as Substrate.....	75
Figure 76: S Parameter for single layer graphene circular patch antenna using FR-4 as Substrate.....	76
Figure 77: VSWR for single layer graphene circular patch antenna using FR-4 as Substrate.....	76
Figure 78: Radiation Pattern of single layer graphene circular patch antenna using FR-4 as Substrate.....	77
Figure 79: Polar Plot of Directivity of single layer graphene circular patch antenna using FR-4 as Substrate.....	77
Figure 80: S Parameter for single layer graphene circular patch antenna using Alumina as Substrate.....	78
Figure 81: VSWR for single layer graphene circular patch antenna using Alumina as Substrate.....	78
Figure 82: Radiation Pattern of single layer graphene circular patch antenna using Alumina as Substrate.....	79
Figure 83: Polar Plot of Directivity of single layer graphene circular patch antenna using Alumina as Substrate.....	79
Figure 84: Comparison of s-parameter of circular patch antenna for different substrates.....	80
Figure 85: Polar plot of circular patch antenna for different substrates.....	80
Figure 86: Single Layer Graphene Triangular Patch Antenna.....	82

Figure 87: S Parameter for single layer graphene triangular patch antenna using Teflon as Substrate.....	83
Figure 88: VSWR for single layer graphene triangular patch antenna using Teflon as Substrate.....	83
Figure 89: Radiation Pattern of single layer graphene triangular patch antenna using Teflon as Substrate.....	84
Figure 90: Polar Plot of Directivity of single layer graphene triangular patch antenna using Teflon as Substrate.....	84
Figure 91: S Parameter for single layer graphene triangular patch antenna using Polyimide as Substrate.....	85
Figure 92: VSWR for single layer graphene triangular patch antenna using Polyimide as Substrate.....	85
Figure 93: Radiation Pattern of single layer graphene triangular patch antenna using Polyimide as Substrate.....	86
Figure 94: Polar Plot of Directivity of single layer graphene triangular patch antenna using Polyimide as Substrate.....	86
Figure 95: S Parameter for single layer graphene triangular patch antenna using FR-4 as Substrate.....	87
Figure 96: VSWR for single layer graphene triangular patch antenna using FR-4 as Substrate.....	87
Figure 97: Radiation Pattern of single layer graphene triangular patch antenna using FR-4 as Substrate.....	88
Figure 98: Polar Plot of Directivity of single layer graphene triangular patch antenna using FR-4 as Substrate.....	88
Figure 99: S Parameter for single layer graphene triangular patch antenna using Alumina as Substrate.....	89
Figure 100: VSWR for single layer graphene triangular patch antenna using Alumina as Substrate.....	89

Figure 101: Radiation Pattern of single layer graphene triangular patch antenna using Alumina as Substrate.....	90
Figure 102: Polar Plot of Directivity of single layer graphene triangular patch antenna using Alumina as Substrate.....	90
Figure 103: Comparison of s-parameter of triangular patch antenna for different substrates.....	91
Figure 104: Polar plot of triangular patch antenna for different substrates.....	91
Figure 105: S-Parameters of different patch antennas for Dielectric Substrate Teflon.....	93
Figure 106: Polar plot of different patch antenna for Dielectric Substrate Teflon.....	93
Figure 107: S-Parameters of different patch antenna for Dielectric Substrate Polyimide.....	95
Figure 108: Polar plot of different patch antenna for Dielectric Substrate Polyimide.....	95
Figure 109: S-Parameters of different patch antenna for Dielectric Substrate FR-4.....	97
Figure 110: Polar plot of different patch antenna for Dielectric Substrate FR-4.....	97
Figure 111: S-Parameters of different patch antenna for Dielectric Substrate Alumina (96%).....	99
Figure 112: Polar plot of different patch antenna for Dielectric Substrate Alumina (96%).....	99

List of Tables

Table 1: Effect of chemical potential on Resonant Frequencies taking length and width of $5\mu\text{m}$ and $0.5\ 5\mu\text{m}$ respectively	50
Table 2: Parameters of Single Layer Graphene Rectangular Patch Antenna.....	59
Table 3: Comparison of rectangular patch antenna parameters for different substrates.....	70
Table 4: Parameters of Single Layer Graphene Circular Patch Antenna.....	71
Table 5: Comparison of circular patch antenna parameters for different substrates.....	81
Table 6: Parameters of Single Layer Graphene Triangular Patch Antenna.....	82
Table 7: Comparison of triangular patch antenna parameters for different substrates.....	92
Table 8: Comparison among the different patch antenna for Dielectric Substrate Teflon.....	94
Table 9: Comparison among the different patch antenna for Dielectric Substrate Polyimide.....	96
Table 10: Comparison among the different patch antenna for Dielectric Substrate FR-4.....	98
Table 11: Comparison among the different patch antenna for Dielectric Substrate Alumina (96%).....	100

Chapter 1

Antenna Overview and Basics

1.1 Antenna Overview

Antenna the most widely used electrical equipment in the field of digital communication. Antennas began to be used extensively after the second world war when. The IEEE Standard Definitions of Terms for Antennas (IEEE Std 145–1983) defines the antenna or aerial as “a means for radiating or receiving radio waves.” An antenna is basically an element associated with the transmission and receiving of guided waves. Antennas of different sizes and shapes are used today for transmitting and receiving of waves for various purposes. The entire digital communication and radio industry are relying heavily on extensive usage of different types of antennas. Other than that, antennas are finding its usage in various other industries and gaining more popularity day by day.

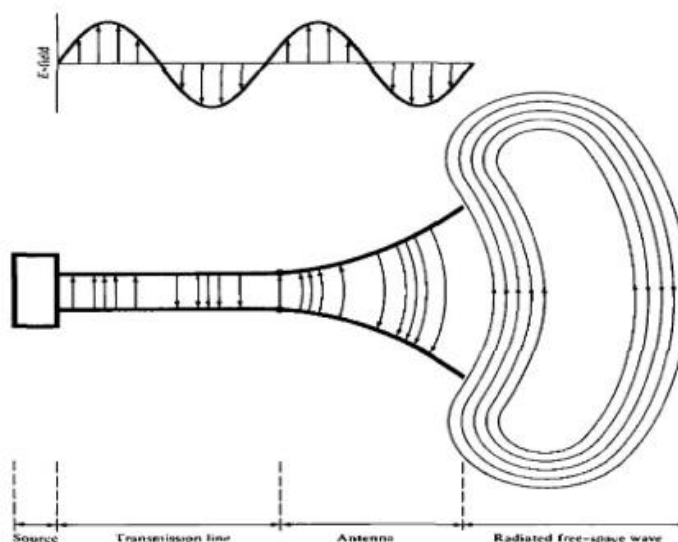


Figure 1: Antenna as transition device [17]

1.2 Types of Antenna

1.2.1 Wire Antenna

The type of antennas that we see in our everyday life are wire antennas. These types of antenna may be of varied shapes and sizes depending on their usage.

1.2.1(a) Dipole Antenna

The simplest form of wired antennas are the dipole antennas. A dipole antenna is constructed with two metallic rods on the either side of the antenna. In these types of antennas, the voltage and current ratios generally vary along the length of the dipole. There are different types of dipole antennas depending on different factors. The length of the antenna in this case is a very important as it determines many parameters that affect the impedance, frequency and the other factors. The contrasting type of antennas are the monopole antennas which contains only one pole mounted over a ground plane. This type of antennas is fed by connecting one end to the lower end of the antenna and the other to the ground plane. [2]

1.2.1(b) Half Wave Dipole Antenna

A special kind of dipole antenna would be the half wave dipole antenna. The term half wave length is used because in this type of antennas the size of the antenna is equal to half the wavelength or in mane case two quarter wavelengths. In this type of antennas, the feeding is done from the middle as a result the impedance falls maximum at the centre. Due to this at the centre the current remains maximum and voltage minimum. [2]

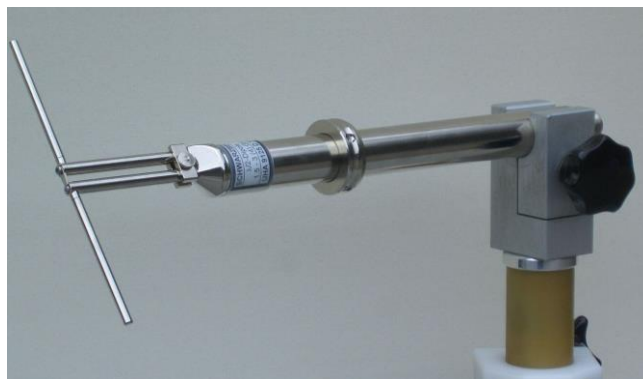


Figure 2: Half-Wave Dipole Antenna [18]

1.2.1(c) Folded Dipole Antenna

In case of a folded dipole antenna the difference here is the along with the general dipole antenna there is a conductor connecting the two ends of the conductor together. The additional dipole is usually made of wire or rod usually the size of the original dipole antenna. This type of antennas is mainly used in case of array antennas to increase feed resistance. It also has a flatter frequency response as a result it can be used for a wider range of bandwidth. [1]



Figure 3: Folded Dipole Antenna [19]

1.2.2 Travelling Wave Antennas

A travelling wave generally uses a travelling wave as the main transmitting component. This type of antennas usually is non-resonant therefore they can also manage to provide a wider bandwidth than resonant antennas.

1.2.2(a) Helical Antennas

Helix antennas are the most common type of travelling wave antennas. They generally bear a corkscrew type shape and radiates along the axis of the antenna that is in the positive z direction. This type of antennas is fed by connecting the feedline with the bottom of the helix and the ground plane. The helix antennas radiate in two modes namely normal and axial. [2]

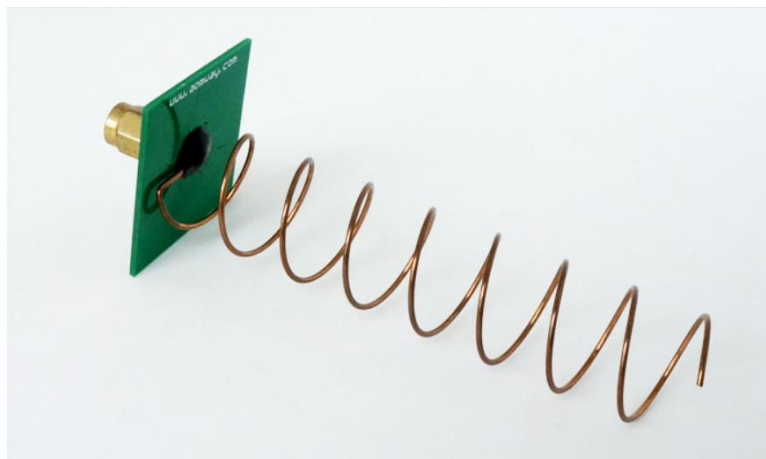


Figure 4: Helical Antenna [20]

1.2.2(b) Yagi-Uda Antennas

Yagi-Uda Antennas or commonly known as Yagi antennas are a unique and widely used type of antenna. This type of antennas is mostly used in case of television or commercial purpose. The feeding technique in case of this type of antennas is that there exists a dipole as main radiating element where the feeding is done. This type of antenna consists of a directional main lobe due to the reflector and a few side lobes. This type of antenna works very well for small gain but in case of high gain the size of the antenna becomes very long. [2]



Figure 5: Yagi-Uda Antenna [21]

1.2.3 Microwave Antennas

Microwave antennas are those antennas which are operational in microwave frequencies. This type of antennas is widely used in the industry for different types of communication. This type of antennas is very robust and versatile when it comes to use.

1.2.3(a) Microstrip Antennas

Microstrip antennas are generally constructed by fabricating a patch or strip over a ground plane. The strip here is mounted over a dielectric layer or substrate. For different sort of antennas different substrates are used. Each of them has different properties. On the other hand, patches can be of different shapes namely rectangular, dipole, circular, square etc. Rectangular and Circular shapes that are dominating in widespread use. The rectangular patch antennas are very simple to analyse, and the circular ones have a symmetric radiation pattern. Microstrip antennas are widely used for spacecraft or aircraft applications because of their simplicity and ease of use. Microstrip antennas are also used in case of military purposes and commercial purposes. A very common use of microstrip antennas are in case of GPS or Global Positioning System.

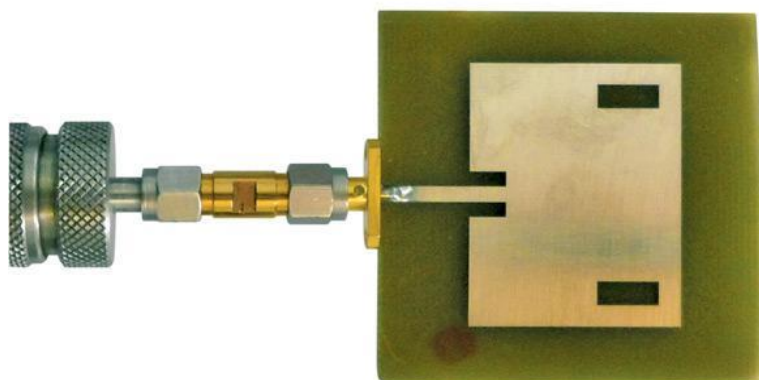


Figure 6: Rectangular Microstrip Patch Antenna [22]

1.2.3(b) Planar Inverted-F Antennas

This type of antenna is constructed using shorting pins on various locations. This type of antennas is very popular in the telecom industry. The shape of the antenna is like an inverted F from which the name Planar Inverted-F antenna has come into existence. There is another type of antenna that can be constructed like this that is inverted L antenna. As a result of the size

being very compact and the manufacturing cost being low, this type of antennas make the perfect fit for different wireless communications. In addition to that this type of antennas the rate of spurious emission is low.

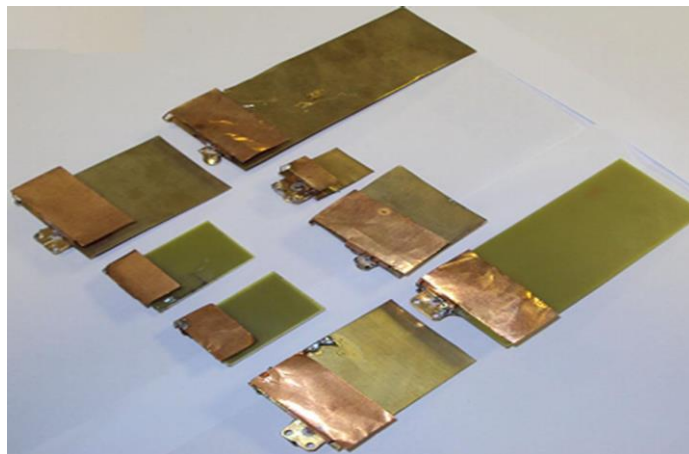


Figure 7: Planar Inverted-F Antenna [23]

1.2.4 Reflector Antennas

Reflector antennas are simple feed antennas that have a reflecting dish integrated in to its design. This type of antennas has operating frequency range of Ultra High Frequency (UHF) and microwave and are usually used for long distance applications such as radio astronomy, high resolution radars and satellite communication. Since these applications take place over very long distances, the waves travelling from and to the antennas are almost parallel to each other and is spread over a big area. Regular dipole or array antennas are far too small or inefficient to intercept these waves. So, large reflectors are used to capture them without sufficient loss in gain.

Several types of reflector designs are implemented now a days, notably: front feed, offset feed, cassegrain and gregorian. All these types have the same principle: they reflect the incoming waves and focus them on a single point or spread them parallel. For a receiving antenna, the incoming waves coming from long distances are parallel to each other. The reflecting dish is designed in such a way that the intercepted waves are reflected and focused on a single point, where the antenna is usually placed. For a transmitting one, the antenna placed at the focal

point of the dish radiates high powered radiations towards it. The dish then spreads out the waves parallel so that they can be transmitted over long distances. [10]

For both transmitting and receiving cases, the antenna reflector is designed in such a way that the reflected waves are all in phase with each other. If the wave fronts on the same plane meet at different phases, they would cancel each other and result in loss of information. To make sure of it, the shape of the reflector is usually a paraboloid of revolution, with a rotationally symmetric surface about its axis. This ensures maximum reflection and focusing of waves and keeps all waves of the same plane in phase. [9]



Figure 8: A Cassegrain Antenna used for Large Satellite Communication [24]



Figure 9 : A VSAT (Very Small Aperture Terminal) antenna used for home or business satellite communications [25]

1.2.5 Log Periodic Antenna

Log periodic antennas have impedance that is a logarithmically periodic function of the operating frequency. There are several types of such antenna that operates over a wide range of frequencies, around 30 MHz to 3 GHz. The most widely used is the LPDA - Log Periodic Dipole Antenna. This type of antenna can provide a good amount of gain and directivity along with a wide bandwidth, making it perfect to be used as rooftop television antennas. [4]

There are few different types of log periodic antennas, of which the Log Periodic Dipole Antenna (LPDA) is the most popular. The construction is similar to the Yagi-Uda antenna, but their working principles are different. They both have dipole rods, which decrease in size from the base to the tip, mounted on a main supporting beam. Increasing the number of dipole rods increases its frequency response, consequently increasing its bandwidth. [11] All the dipole rods will not be active at the same time for a single frequency and the active region shifts among them. The radiation pattern changes depending on the structure and can be used as uni-directional or bi-directional according to the need. [12]

LPDA has a wide range of uses for its high bandwidth. Since its gain and radiation pattern can be varied, it is extensively used for high-frequency communications and television receptions. [4]



Figure 10: Log Periodic Dipole Antenna [26]

1.2.6 Aperture Antenna

These are the type of antennas used in microwave frequencies. Their structure consists of a small antenna, specially a small dipole or loop antenna, with an aperture or opening at the end

of the transmission line. This open end radiates energy and hence works as an antenna. The working of the aperture antenna depends on how it is used and analysed, rather than depending on the actual form of it.

Three of the main types of aperture antenna are: waveguide antenna, horn antenna, and slot antenna.

1.2.6(a) Waveguide

The waveguide has an Omni-directional radiation pattern and has more radiation than a two-wire transmission line. The shape of the waveguide can be changed depending on the uses. Its operational frequency range is around 300 MHz to 300 GHz. [14]



Figure 11: Waveguide Antenna [27]

1.2.6(b) Horn Antenna

By attaching a horn type structure at the open end of the waveguide, a horn antenna can be made. It improves the radiation efficiency and directivity by gradually spreading out the wave, rather than a sudden discontinuity. It operates around a frequency range of 300 MHz to 30 GHz.[15]

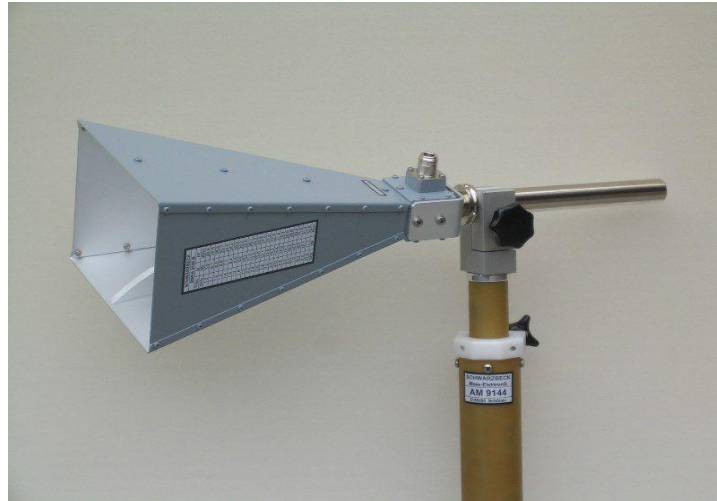


Figure 12: Horn Antenna [28]

1.2.6(c) Slot Antenna

A slot antenna can be made by cutting a slit or opening at sides of the waveguide. It operates in the same frequency range as the horn antenna and is used in secret and concealed communications over short distances. [16]



Figure 13: Slot Antenna [29]

1.3 Antenna Parameters

1.3.1 Bandwidth

Bandwidth is a very important concept when it comes to the usage of different types of antennas that are available in the market. Basing on the Bandwidth different antennas are used in different sectors. The range of frequencies where an antenna can radiate and operate efficiently is known as bandwidth. This is generally obtained from the difference between the lower cut off frequencies and the upper cut-off frequencies.[5] This is calculated in hertz. There are also two common terms that are used which are related to Bandwidth. These are narrowband and wideband. A narrowband is the range of frequencies which has smaller bandwidth than the coherence bandwidth and wideband conversely has a wide band in comparison with the coherence bandwidth.

1.3.2 Radiation Pattern

The radiation pattern is a relative pattern which is used to represent the power distribution that is flowing out from the antenna. [7] The radiation pattern determines the field intensity spatially distributed across the far field. The radiation pattern can be expressed by help of two different planes, one is E field and the other is H field in a two-dimensional diagram. Compared to 3D structure 2D structures are easier to analyse. That is why many times a 2D structure is used for understanding the radiation patterns.

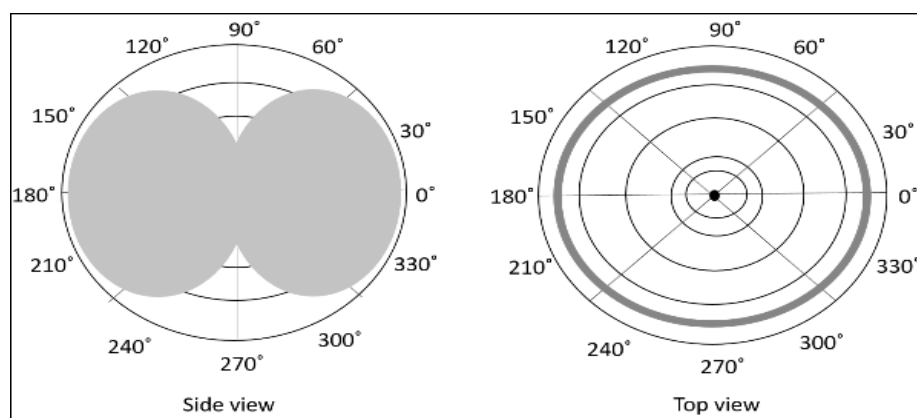


Figure 14: Radiation Pattern in 2D [30]

In the above picture two different views are shown one is the side view and the other is the top view. The above radiation pattern is for an omnidirectional antenna. Antennas with omnidirectional radiation patterns form a more donut like 3D structure. A 3D spatial representation of the radiation pattern of an omnidirectional with high gain might look something similar to the one shown below.

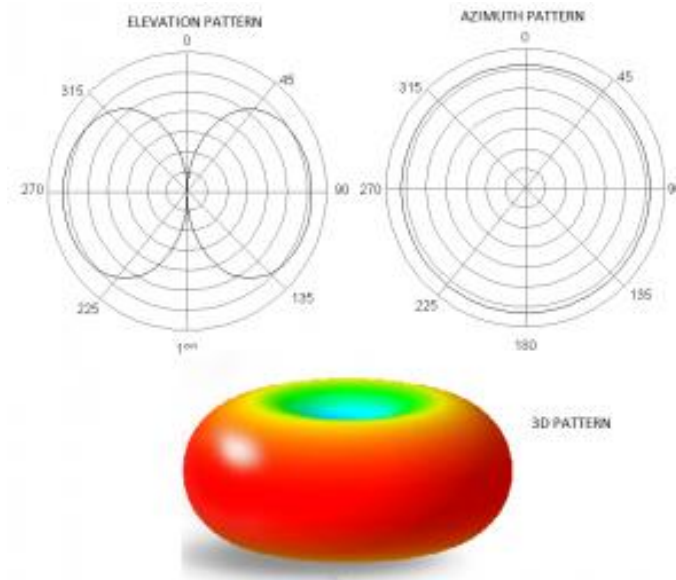


Figure 15: Omnidirectional Antenna Radiation Pattern [31]

Radiation pattern is very closely related to the gain of the antenna and the field strength of the antenna which influences the diagrams heavily. The other common type of radiation pattern is known as 'isotropic' portrays similar radiations in all directions and forms a spherical shape. The 2D structure of an isotropic type of radiation pattern may look something like the one shown below

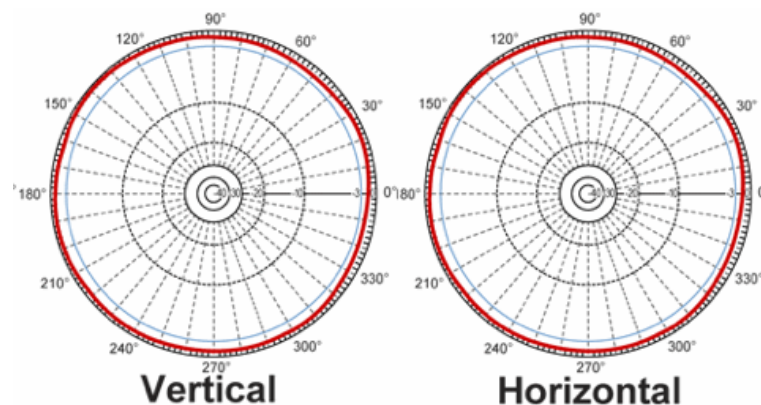


Figure 16: Isotropic Antenna Radiation Pattern [32]

If we closely notice both the figure, we see it forms a circular shape at both horizontal and vertical views. The radiation is equal in all directions in this case. So evidently it forms a spherical structure when visualized in 3D view.

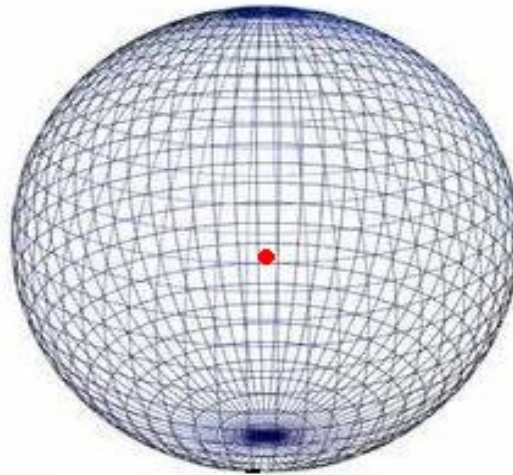


Figure 17: 3D Radiation Pattern of Isotropic Antenna [33]

On the other hand, another common type of patterns are directional radiation patterns. It may contain several lobes. There is a major lobe at the centre and couple of minor lobes and back lobes. A 2D directional antenna might be pictured something like the one given below.

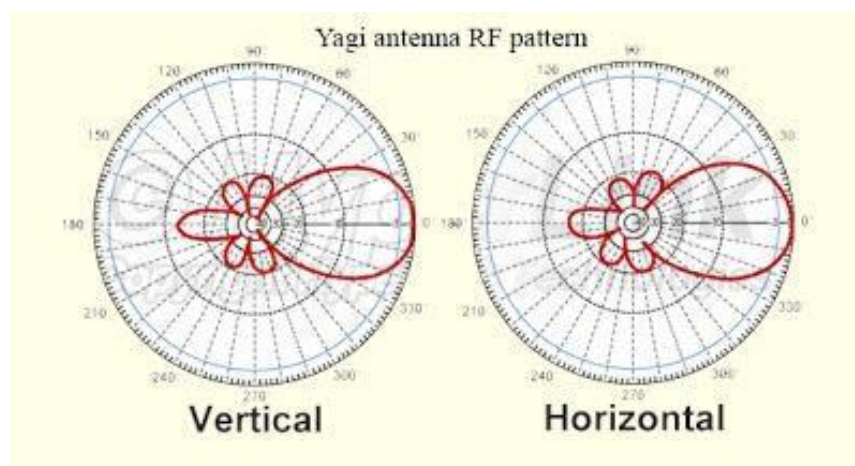


Figure 18: Yagi Antenna Directional Pattern [34]

Whereas a 3D representation maybe portrayed something like the below mentioned one.

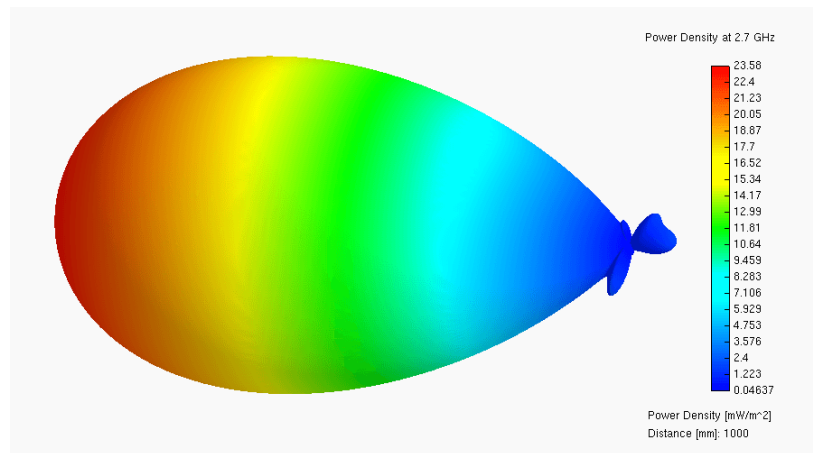


Figure 19: 3D Representation of Gain [35]

1.3.3 Directivity

Directivity is defined as the ratio between radiation intensity in a definite direction by the intensity of isotropic radiation. Directivity is one of the most important parameters when it comes to antenna parameters. In simpler words directivity is used to define how concentrated the radiation pattern of the antenna is. The antennas having higher degrees of directivity tend to be more concentrated towards a definite direction than antennas with a lower degree of directivity. The value of concentration depends on the implementation and type of antenna therefore a higher value might not always correspond to a better version. [1]

$$Directivity = \frac{Radiation\ Intensity\ in\ definite\ direction}{Isotropic\ radiation\ intensity}$$

In mathematical form directivity can be expressed as:

$$D_{Max} = \frac{U_{max}}{U_{av}} = (dimensionless)$$

where, D_{max} = Maximum Directivity, U_{max} = Maximum Radiation Intensity, U_{av} = Average Radiation Intensity.

$$D = \frac{4\pi U_{\max}}{P_r} \text{ (dimensionless)}$$

where, D = Directivity, U_{\max} = Maximum Radiation Intensity,

P_r = Total Radiated Power

The general expression for directivity can be expressed as

$$D(\theta, \phi) = 4\pi \frac{F(\theta, \phi)}{\int_0^{2\pi} \int_0^{\pi} F(\theta, \phi) \sin \theta \, d\theta \, d\phi}$$

$$D_0 = 4\pi \frac{F(\theta, \phi)|_{\max}}{\int_0^{2\pi} \int_0^{\pi} F(\theta, \phi) \sin \theta \, d\theta \, d\phi}$$

1.3.4 S-Parameters

The S-Parameters or scattering parameters is one of the most commonly used parameters. The S-Parameters or the scattering parameters is the mathematical representation of the input-output relation of the multi-port network. A port is any area through which we can exchange voltage and current. The S-Parameters are complex numbers which are a function of frequency [1]. The impedance and admittance matrices are for the total voltage while the scattering parameters denote the voltages incident and reflected from the port. Conversion to the other parameters is also very easy once the scattering parameters are known [8]. Suppose there is a system with 2 ports namely 1 and 2. The power when transmitted from the port 1 to the port 2, it is represented as S12. Conversely, the power when transmitted from port 2 to port 1 this is represented as S21. The parameter S12 is known as the reverse voltage gain and the parameter S21 is commonly known as the forward voltage gain.

In case of construction of antennas, the most noteworthy is S11 that is the power reflected to the antenna. This is also known as the return loss of an antenna or reflection coefficient. It is denoted by Γ :

$$\Gamma = \frac{Z_l}{Z_s}$$

If the power radiated from the antenna is completely reflected, then the value of reflection coefficient is equal to zero. If $S_{11} = -8\text{dB}$ and 2dB power is radiated, then the amount of power reflected from the antenna is -6dB .

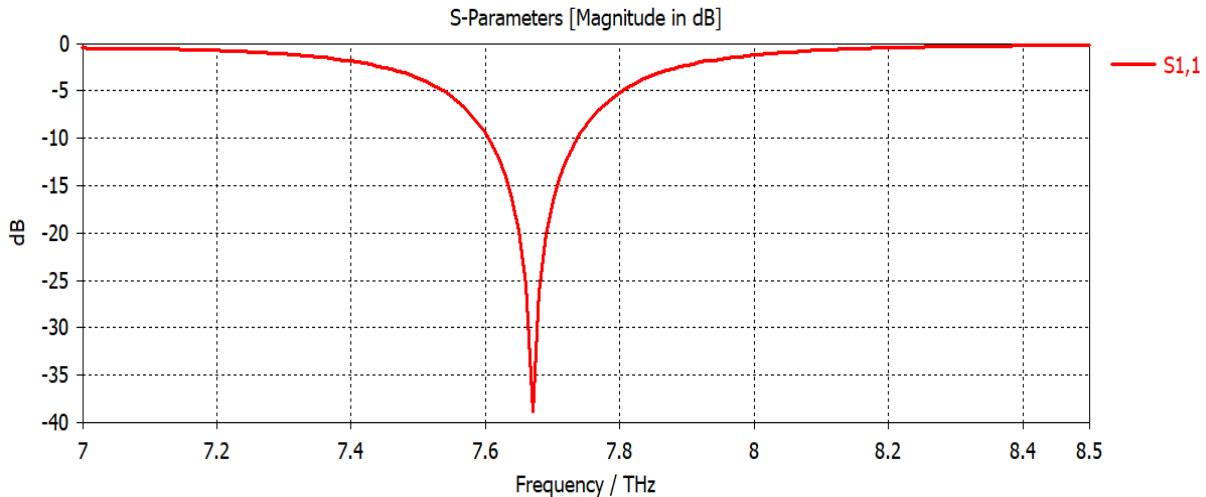


Figure 20: S-Parameter of Antenna

1.3.5 Antenna Efficiency

Antenna efficiency is another fundamental characteristic of antenna. This is defined as the ratio of the power delivered to the antenna to the power radiated from the antenna. An antenna having a high efficiency radiates most of the power that is supplied to it while an antenna having a low efficiency reflects most of the power that is delivered to it. The mathematical expression of antenna efficiency can be expressed as

$$\epsilon = \frac{P_{rad}}{P_{inp}}$$

The higher the efficiency the better it is for use. In real life it is impossible to make an antenna which is fully efficient, but a few types of antennas can reach a stage which is very near to it. Such a scenario occurs due to the antennas having minimal or no lossy materials around it. An antenna having an efficiency of 0.06 means the antenna is 60% efficient. It is expressed in dB. This is different from the total efficiency of an antenna which is the product of the radiation efficiency and the impedance mismatch loss of antenna. [1]

1.3.6 Antenna Gain

The gain of an antenna is the expression that expresses how much power is radiated by the antenna in the direction like that of an isotropic antenna (Antenna having unit gain in all directions). Mathematically antenna gain can be expressed as the ratio of the power radiated by antenna in a definite direction by the power radiated by an isotropic lossless antenna in that direction with the input power.

$$G = \epsilon_R + jX_A$$

An antenna having a gain of 5 dB means that the power which is radiated will be 5 dB higher than the power radiated by an isotropic lossless antenna with same input power.[1]

1.3.7 VSWR

VSWR is the short form for voltage standing wave ratio which is a mathematical expression that expresses how well impedance is matched to the radio or transmission line it is connected to. [1]

The VSWR of an antenna can be measured from the equation of the reflection coefficient. If the reflection coefficient is expressed in Γ

$$VSWR = \frac{1 + \Gamma}{1 - \Gamma}$$

1.3.8 Input Impedance

The voltage current relationship at the input of the antenna is known as the input impedance. The input impedance is denoted by Z_{in} . Its mathematical form it can be written as follows

$$Z_{in} = R_A + jX_A$$

In the above equation the real part denotes the power that is radiated from or absorbed by the antenna, whereas the imaginary part of the equation expresses the power stored or absorbed in the near field by the antenna. For example, if we take an antenna with an input impedance of 50 ohm and supply it with a sine wave of 1 V. The current in this case will be $1/50=0.02$ amps which is in phase with the voltage. This is because the impedance is a real number. On the

other hand if the input impedance is a complex number like $50 + j50$, then the impedance would have a magnitude of $\sqrt{50^2 + 50^2} = 70.71$ and a phase angle of $\tan^{-1}\frac{50}{50} = 45^\circ$. Therefore, we can see that in case of the complex value of the impedance the current is lagging the voltage by 45 degrees.

Chapter 2

Introduction to Microstrip Patch Antenna

2.1 Microstrip Antenna

Microstrip antenna was founded in 1950s, but its importance started to rise around 1970 as the printed circuit board (PCB) technology gradually became more developed. The antenna consists of a very thin patch of metal placed over a ground plane. The thickness (t) of the patch and the distance (h) between the patch and the ground plane is very small, much less than the free-space wavelength (λ_0) ($t \ll \lambda_0$, $0.003\lambda_0 \leq h \leq 0.05\lambda_0$) [17]. The position of the patch is designed in such a way so that the radiation pattern is normal to it. This can be achieved by the appropriate choice of excitation under the patch. End-fire radiation can also be attained in the same way.

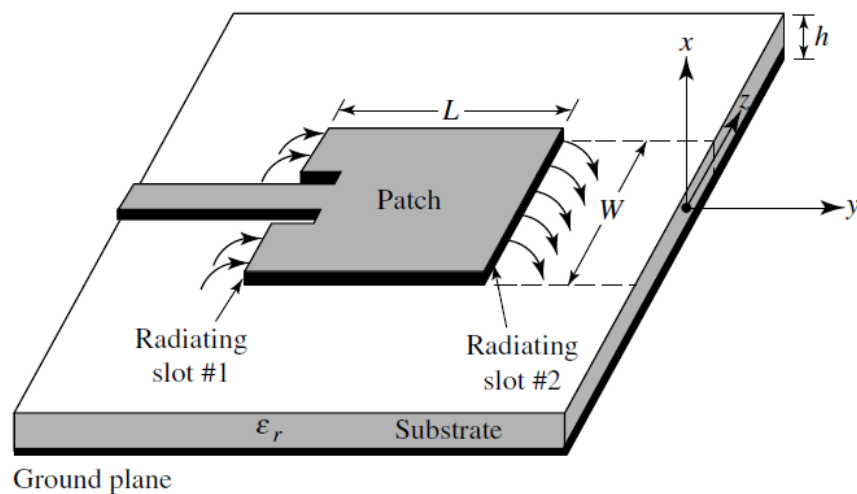


Figure 21: A microstrip patch antenna [17]

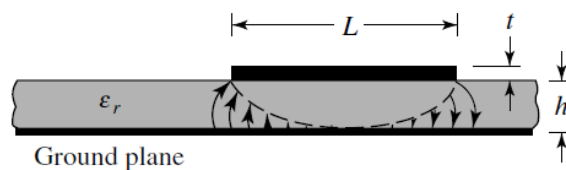


Figure 22: Side-view of a microstrip patch antenna [17]

The space between the patch and the ground plane contains a substrate, usually with a dielectric constant (ϵ_r) between 2.2 to 12 [17]. For microstrip antennas, thicker substrates with lower dielectric constants are more preferred because they give a better efficiency, wider bandwidth and less limited field of radiation. However, the antenna size becomes larger, which is not desired for this type of antenna. In order to make the microwave circuits small, thinner substrates with higher dielectric constants are used. They need limited field boundaries, causing less loss in radiation and coupling. Still, they are not that much efficient because of the increased amount of losses and smaller bandwidths. Therefore, for designing an overall good microstrip antenna, a balance between the circuit design and antenna performance must be achieved.

2.1.1 Applications

Microstrip antennas have various applications, specially where the size, cost, performance and ease of installation matters a lot [17]. Their characteristics make them suitable for uses in high performance aircrafts, spacecrafts, satellites and missile applications [17]. They can be used in government security systems, that require narrow bandwidth. Moreover, they are being considered for uses in wearable technologies.

2.1.2 Advantages

Microstrip antennas have several advantages over other types of antenna, which makes them a suitable choice for a diverse range of applications. They are low profile antennas, and simple and inexpensive to print using modern printed-circuit technologies. They can be easily formed over planar and nonplanar surfaces and are mechanically robust when attached to hard, rigid surfaces. They are compatible with current Monolithic Microwave Integrated Circuit (MMIC) designs and can be used in a wide range of applications. When a particular patch shape and mode are selected, they are very versatile in terms of resonant frequency, polarization, pattern, and impedance. Along with that, when loads such as pins and varactor diodes are added between the patch and the ground plane, elements with variable resonant frequency, impedance, polarization, and pattern can be designed. These elements are adaptive and can be used in applications that requires constant changes [17].

2.1.3 Disadvantages

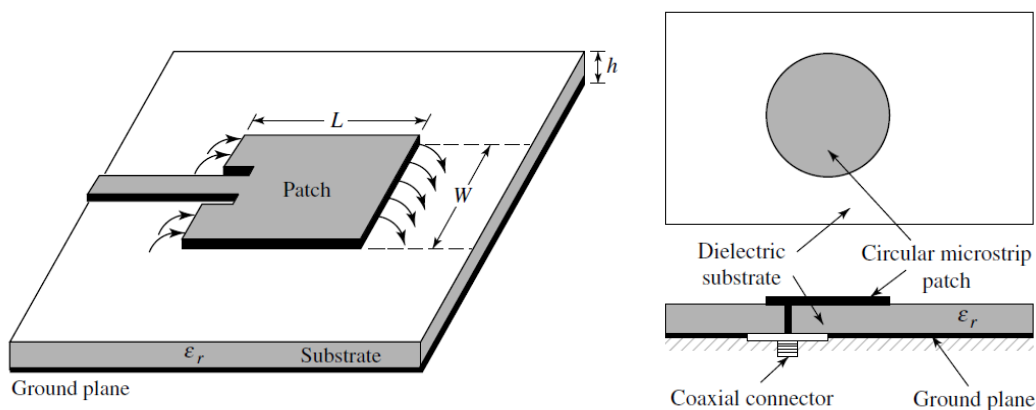
Despite their invaluable advantages and benefits, microstrip antennas have few major drawbacks. They have low efficiency, low power, high Q , poor polarization purity, poor scan performance, false feed radiation and very narrow frequency bandwidth, which is usually a fraction of a percent, and a few percent at best. There are some methods that can be used to increase the efficiency, such as increasing the substrate height. Nonetheless, as the height of the substrate is increased, surface waves are introduced which are not desirable at all. These waves withdraw power from the total power available for direct radiations. The surface waves remain within the substrate and travels around, getting scattered at bends and surface discontinuities, degrading the antenna pattern and polarization characteristics. Using cavities and other methods of stacking, surface waves can be removed, while maintaining high bandwidths. But in large arrays, the antenna size becomes very large, and a trade-off has to be made between bandwidth and scan volume [17].

2.1.4 Types

Microstrip antennas are of many different types, and are classified on different parameters such as shapes, feeding mechanisms, operating frequencies, band of operations, and so on. Depending on the use and other factors, microstrip antennas can be various shapes. Usually referred to as patch antennas, since the radiating surface and feed lines are engraved on the surface of the dielectric substrate, the radiating patch is made into different shapes. The most common shapes are square, rectangular, circular, and dipole strip, because they are the easiest to fabricate and analyse and has very good radiation characteristics [17]. These shapes have low cross-polarization radiation, which makes them very attractive for a lot of applications. Other shapes include elliptical, triangular, disc sector, circular ring, ring sector, and many more, depending on the use [17]. These antennas can be used as a single element or in arrays to achieve linear and circular polarization. Microstrip antennas can also be differentiated in terms of feeding mechanisms, operating frequency, bands of operations (wideband, narrowband, single band, multiband, etc.), and so on. Different types of feeding mechanisms are discussed below.

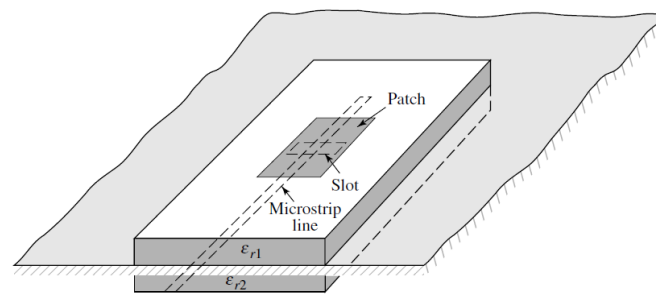
2.1.5 Feeding Techniques

There are many configurations that can be used to feed microstrip antennas. Four of the most popular techniques are the microstrip line, coaxial probe, aperture coupling, and proximity coupling [17]. In a patch antenna, the microstrip-line feed also acts as a conducting strip along with the patch, though it is much smaller in width compared to the patch. It is easy to fabricate and model and can be matched easily by controlling the inset positions. However, surface waves and false feed radiations increase as the substrate thickness increases, limiting the bandwidth for practical designs (typically 2-5%) [17].

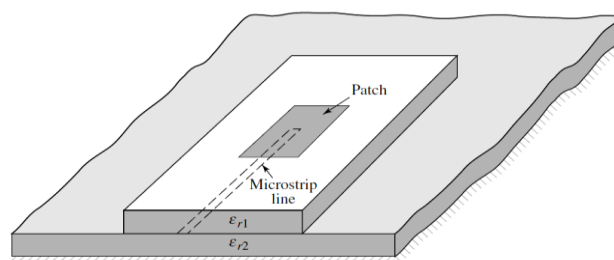


(a) Microstrip line feed

(b) Probe feed



(c) Aperture-coupled feed



(d) Proximity-coupled feed

Figure 23: Typical feeds for microstrip antennas [17]

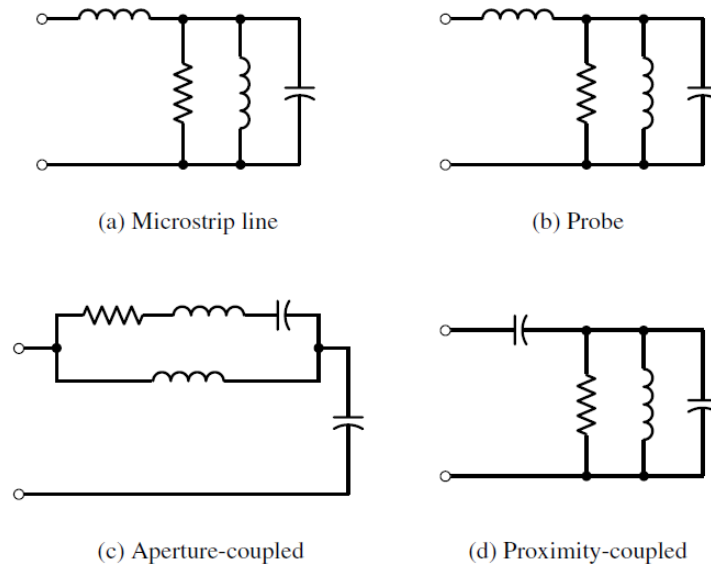


Figure 24: Equivalent circuits for typical feeds [17]

Coaxial-line feeds are constructed like a coaxial cable. The outer conductor is connected to the ground plane while the inner conductor is attached to the radiating patch. It has low false radiation and is easy to fabricate and match. Still, it also has a narrow bandwidth, and is more difficult to model, especially for thicker substrates ($h > 0.02\lambda_0$) [17].

To overcome the cross polarized radiation problems caused due to inherent asymmetries of the microstrip feed line and coaxial probe, noncontacting aperture-coupled feeds are used. The aperture coupled feed line is the most difficult to fabricate and has a narrow bandwidth. But it is easier to model than the others and has moderate spurious radiation. It consists of two substrates separated by a ground plane. The bottom side of the lower substrate has a microstrip feed line whose energy is coupled to the patch through a slot on the ground plane that separates the two substrates. This allows an independent optimization of the feed mechanism and the radiating element. The substrate's electrical parameters, feed line width, and slot size and position can be used to optimize the feed line's design [17].

The proximity coupling feed has the largest bandwidth between these four. Though it is easy to model and has low false radiation, its fabrication is difficult. The length of the feeding stub and the width-to-line ratio of the patch can be used to control the match [17].

In all our designs, we have used the microstrip feed line as the feeding technique.

2.1.6 Method of Analysis

Operation principals of microstrip patch antennas can be easily analysed using the transmission line theory and the cavity model [17]. The transmission line model is the easiest of the two as it gives a good physical insight but is less accurate. The cavity model is more accurate but is more complex at the same time. Since we are working on the rectangular, circular and triangular patch shape, we have provided a few analyses of the parameters of them.

2.2 Rectangular Patch

It is the most common patch antenna that is being used all over the world. It is very easy to configure, model and analyse.

2.2.1 Transmission Line Model

The transmission line model will allow a good physical insight into the rectangular patch antenna. It basically represents the microstrip antenna by two slots, separated by a low-impedance (Z_c) transmission line of length L .

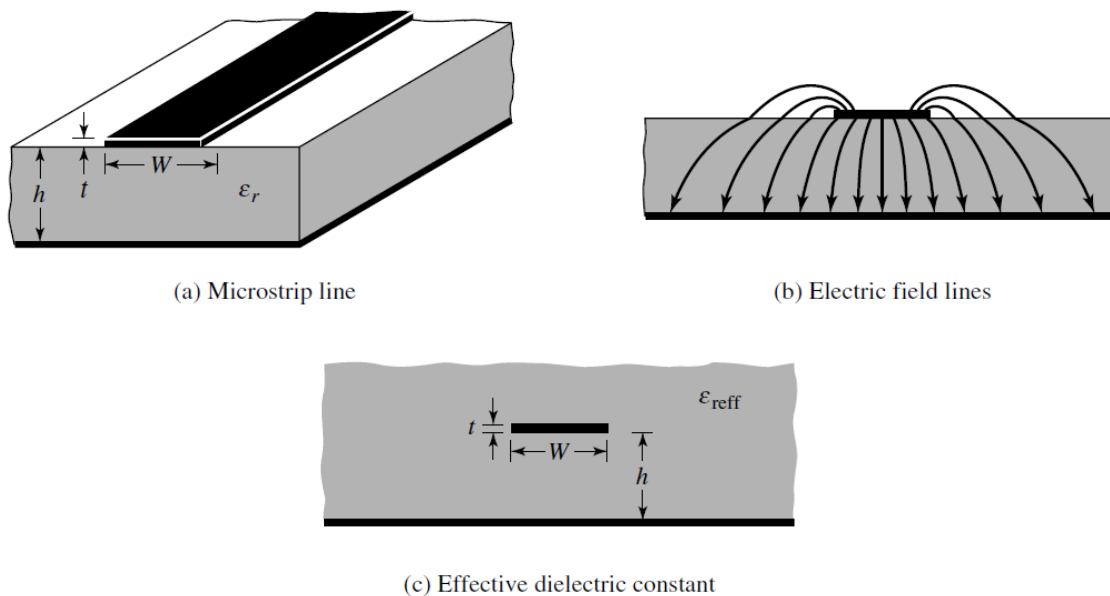


Figure 25: Microstrip line and its electric field lines, and effective dielectric constant geometry [17]

While analyzing a rectangular microstrip patch antenna using transmission line model, fringing effect plays a vital role. The fields at the edges of the patch undergo fringing effects because of the finite length and width dimensions [17]. The amount of fringing is a function of the height of the substrate and the dimensions of the patch. For the principle E-plane (xy -plane), fringing is a function of the length of the patch L to the height h of the substrate (L/h) and the dielectric constant ϵ_r of the substrate. For a microstrip line as shown in 25(a), the typical electric field lines around it are shown in 25(b). Most of the field lines remain in the substrate, while some of them exist in air. In this case, the microstrip line look wider in terms of electrical dimensions compared to the physical dimensions. Since the wave travels both in air and the substrate, an effective dielectric constant ϵ_{reff} is introduced to account for the fringing and the wave propagation in the line, shown in 25 (c). For low frequencies, the effective dielectric constant is more or less a constant value. But in higher frequencies, the value increases, and eventually approaches the value of the dielectric constant of the substrate [17]. For all cases, the value is in the range of $1 < \epsilon_{\text{reff}} < \epsilon_r$. The formula for the effective dielectric constant is:

$$\epsilon_{\text{reff}} = \frac{\epsilon_r + 1}{2} + \frac{\epsilon_r - 1}{2} \left[1 + 12 \frac{h}{W} \right]^{-1/2},$$

where h is the height of the substrate and W is the width of the patch, and $W/h > 1$.

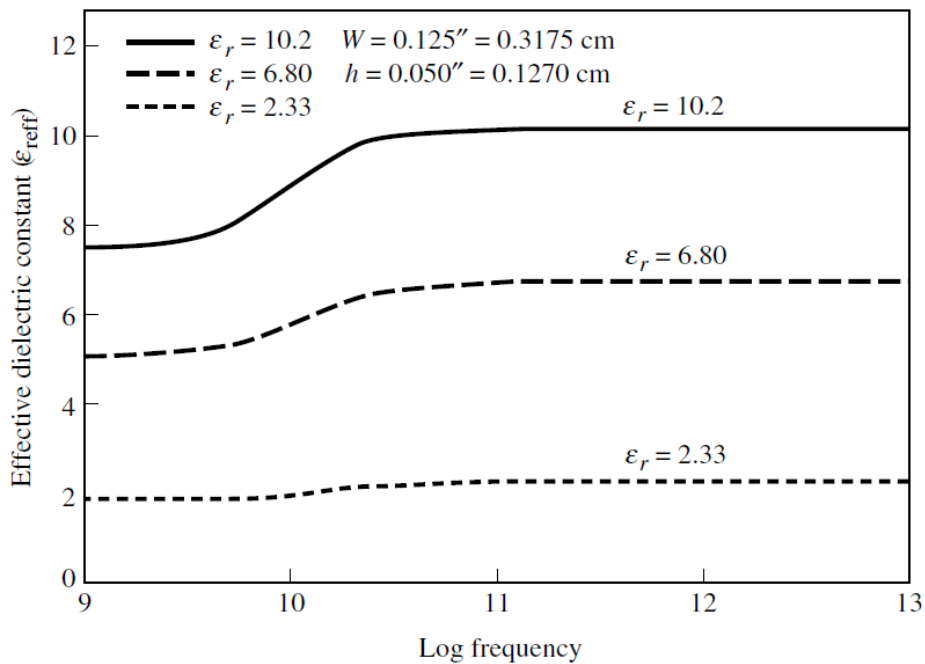


Figure 26: Effective dielectric constant vs frequency for typical substrates

Figure 26 shows the change in the effective dielectric constant with the change in frequencies for typical substrates.

Because of the fringing effects, the patch looks bigger in electrical dimensions than its physical dimensions. For the principle E -plane (xy -plane), the physical dimensions of the patch along its length is extended on each end by ΔL , which is a function of the effective dielectric constant ϵ_{reff} and width-to-height ratio (W/h):

$$\frac{\Delta L}{h} = 0.412 \frac{(\epsilon_{reff} + 0.3) \left(\frac{W}{h} + 0.264\right)}{(\epsilon_{reff} - 0.258) \left(\frac{W}{h} + 0.8\right)}$$

The effective length of the patch is now:

$$L_{eff} = L + 2 \Delta L$$

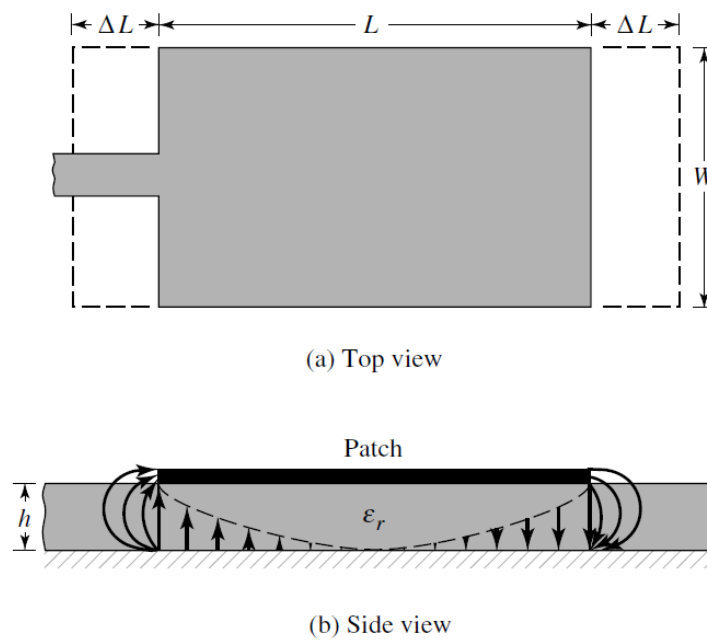


Figure 27: Physical and effective lengths of the rectangular microstrip patch

Figure 27 shows how the effective length affects the physical length of the patch.

Taking the fringing effects into accounts, the modified resonant frequency equation for the dominant TM_{010} mode is:

$$(f_{rc})_{010} = q \frac{v_0}{2L\sqrt{\epsilon_r}}$$

where v_0 is the speed of light in free space, and q is the fringe factor (length reduction factor).

For design parameters, i.e. the physical dimensions of the patch are calculated using the following formulas:

$$\text{Width, } W = \frac{v_0}{2f_r} \sqrt{\frac{2}{\epsilon_r + 1}}$$

$$\text{Length, } L = \frac{1}{2f_r \sqrt{\epsilon_{reff}} \sqrt{\mu_0 \epsilon_0}} - 2\Delta L$$

The resonant input resistance R_{in} for a normal rectangular patch, as shown in fig 14.9a is:

$$R_{in} = \frac{1}{2(G_1 \pm G_{12})}$$

where G_1 is the conductance of the patch, and G_{12} is the mutual conductance.

For rectangular patches that have a recessed distance y_0 as shown in the figure 14.11a, the input resistance $R_{in}(y_0)$ is modified to be:

$$R_{in}(y_0) = \frac{1}{2(G_1 \pm G_{12})} \cos^2\left(\frac{\pi}{L} y_0\right)$$

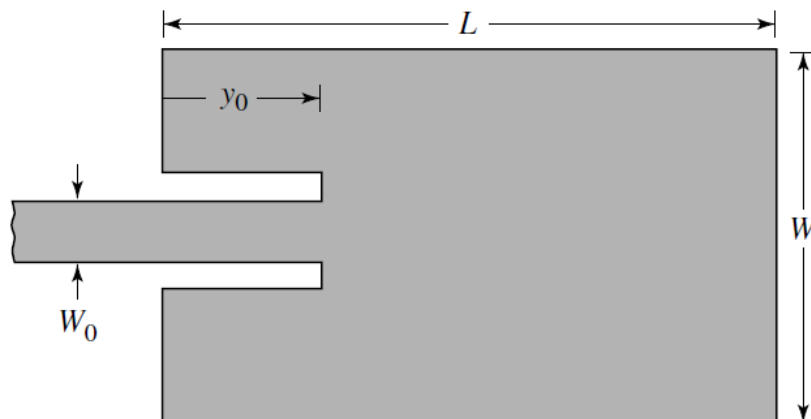


Figure 28: Recessed microstrip-line feed

Figure 28 shows the length y_0 in the rectangular patch.

2.2.2 Cavity Model

Due to some drawbacks of the transmission line model, we can use the cavity model. The cavity model is a very useful model for calculating input impedance and radiation pattern for antennas, specially patch antennas. Cavity means an empty space within a solid object. The electric fields and magnetic fields within the substrate of a patch antenna can be calculated accurately if it is considered as a cavity that is bounded by electric conductors and magnetic walls. This is an accepted and effective approach. A study of the formation of fields within the cavity and radiation through its side walls are done to understand the model better.

When energy is supplied to the microstrip patch, the charge distribution on the upper and lower surface of the patch, and on the ground plane's surface is shown in figure 29. The opposite charges located on the bottom of the patch and above the ground plane acts according to the attractive mechanism, thus maintain the charge concentration on the bottom of the patch. Another mechanism called the repulsive mechanism pushes some charges from the bottom of the patch around its edges and forces them to move to the upper side surface. Current densities \mathbf{J}_b and \mathbf{J}_t at the top and bottom surfaces of the patch is created because of the movement of these charges, as shown in the figure 29. As the height-to-width ratio of patch antennas is very small, the current \mathbf{J}_b dominates, and most of the current flows below the patch. As the current flow \mathbf{J}_t on the top of the patch remains almost zero, negligible magnetic field will be created along the edges of the patch. This results in an easy modelling of the rectangular patch antenna that represents a four sided perfectly conducting magnetic wall. This will not create any disturbance to the electric field and magnetic field beneath the patch [17].

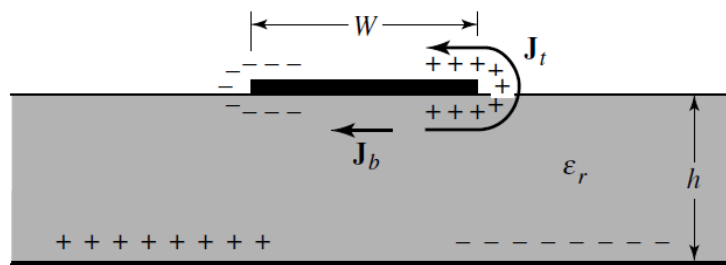


Figure 29: Charge distribution and current density creation on microstrip patch

The antenna efficiency decreases a lot since the waves generated within the dielectric substrate undergoes considerable reflections when they arrive at the edge of the patch. Standing waves are formed in the fields beneath the patch. Since the height of the substrate is very small, the

field variations along the height is considered to be constant, and fringing effects are also neglected. Therefore, only the TM^x field configurations are considered within the cavity [17].

The volume under the patch is considered as a rectangular cavity filled with a dielectric material with dielectric constant ϵ_r and is assumed that the dielectric material does not extend beyond the edges of the patch.

The vector potential A_x within the cavity is:

$$A_x = A_{mnp} \cos(k_x x') \cos(k_y y') \cos(k_z z')$$

where k_x , k_y and k_z are the wavenumbers m , n , p represents the number of half-cycle field variations respectively along the x , y , and z directions.

The resonant frequency for the cavity is:

$$(f_r)_{mnp} = \frac{1}{2\pi\sqrt{\mu\epsilon}} \sqrt{\left(\frac{m\pi}{h}\right)^2 + \left(\frac{n\pi}{L}\right)^2 + \left(\frac{p\pi}{W}\right)^2}$$

Figure 30 shows the geometry of the rectangular patch along the x , y and z directions.

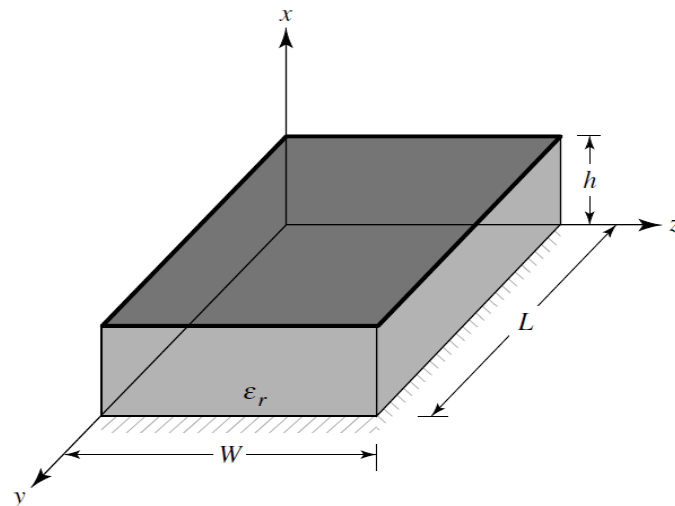


Figure 30: Rectangular microstrip patch geometry

The electric and magnetic fields within the cavity can be written as:

$$E_x = -j \frac{(k^2 - k_x^2)}{\omega \mu \epsilon} A_{mnp} \cos(k_x x') \cos(k_y y') \cos(k_z z')$$

$$E_y = -j \frac{k_x k_y}{\omega \mu \epsilon} A_{mnp} \cos(k_x x') \cos(k_y y') \cos(k_z z')$$

$$E_z = -j \frac{k_x k_z}{\omega \mu \epsilon} A_{mnp} \cos(k_x x') \cos(k_y y') \cos(k_z z')$$

$$H_x = 0$$

$$H_y = -\frac{k_z}{\mu} A_{mnp} \cos(k_x x') \cos(k_y y') \cos(k_z z')$$

$$H_z = \frac{k_y}{\mu} A_{mnp} \cos(k_x x') \cos(k_y y') \cos(k_z z')$$

Based on these equations, the distribution of tangential electric field along the side walls of the cavity for the TM_{010}^x , TM_{001}^x , TM_{020}^x and TM_{002}^x is as shown, respectively, in figure 31.

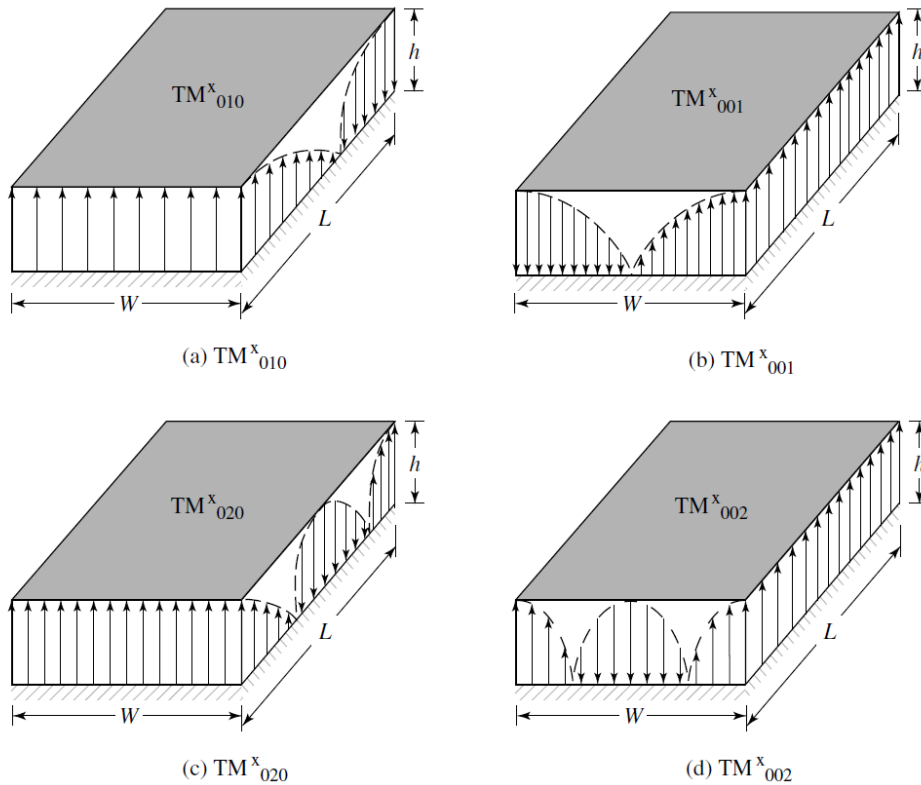


Figure 31: Field configurations (modes) for rectangular microstrip patch

2.2.3 Directivity

Directivity is one of the most important and fundamental parameters that shows how much better an antenna is. It is the ratio of radiation intensity in a definite direction to the intensity of isotropic radiation [36]. It is a measure of how directional the radiation pattern of the antenna is in a certain direction. The equation to find out the directivity is:

$$D_0 = \frac{4\pi U_{max}}{P_{rad}}$$

where, U_{max} is the maximum radiation intensity, and P_{rad} is the total radiated power.

2.3 Circular Patch

After the rectangular patch, the next most popular shape of the patch antenna is the circular, or the disc shaped one. The design takes the patch, ground plane, and the substrate material between the two as a circular cavity. As in the rectangular patch, the modes could be controlled by changing the dimensions, i.e. the length and the width of the patch. However, for the circular patch, the only dimension that can be changed is the radius of the patch. Changing the radius does not bring any change to the order of the modes but can change the absolute value of the resonant frequency of each mode [17].

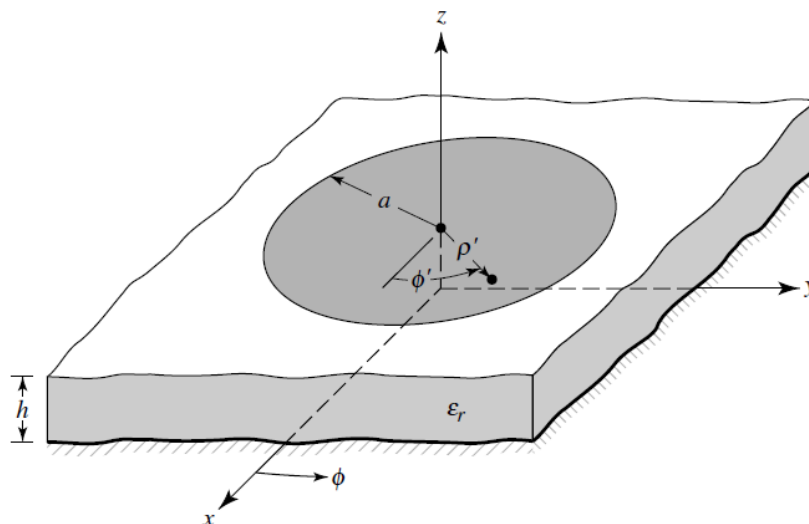


Figure 32: Geometry for circular microstrip patch antenna

2.3.1 Cavity Model

Analysis of the circular patch using the transmission line model does not produce any results and can be only analysed conveniently using the cavity model. Since radius is the only changeable dimension, we must use cylindrical coordinates in the cavity model analysis [17].

Using the vector potential approach, and applying necessary boundary conditions to the electric and magnetic fields, the magnetic vector potential, A_z is found to be:

$$A_z = B_{mnp} J_m(k_\rho \rho') [A_2 \cos(m\phi') + B_2 \sin(m\phi')] \cos(k_z z')$$

with the constraint equation of:

$$(k_\rho)^2 + (k_z)^2 = k_r^2 = \omega_r^2 \mu \epsilon$$

The primed coordinated ρ', ϕ', z' are used to represent the fields within the cavity while $J_m(x)$ is the Bessel function of the first kind of order m . The variables k_ρ, k_z and k_r are wave-numbers along the cylindrical coordinates.

Based on the cavity model formulation, a design procedure is formulated which leads to practical designs of the circular microstrip antenna for the dominant TM_{110}^z mode. Assuming that the dielectric constant of the substrate ϵ_r , the resonant frequency f_r (in Hz) and the height of the substrate h (in cm) is given, the equation for the radius of the patch is:

$$a = \frac{F}{\left\{ 1 + \frac{2h}{\pi \epsilon_r F} \left[\ln \left(\frac{\pi F}{2h} \right) + 1.7726 \right] \right\}}$$

where

$$F = \frac{8.791 \times 10^9}{f_r \sqrt{\epsilon_r}}$$

Taking the effects of fringing along the circumference of the circular patch into account, the effective radius of the patch is:

$$a_e = a \left\{ 1 + \frac{2h}{\pi a \epsilon_r} \left[\ln \left(\frac{\pi a}{2h} \right) + 1.7726 \right] \right\}^{\frac{1}{2}}$$

Since the height of the substrate is very small (typically $< 0.05 \lambda_0$), the fields along z axis are essentially constant. Therefore, the resonant frequencies for the TM_{mn0}^z modes can be written as:

$$(f_r)_{mn0} = \frac{1}{2\pi\sqrt{\mu\epsilon}} \left(\frac{X'_{mn}}{a} \right)$$

The input impedance of the circular patch is real, just like the rectangular one. The input power is independent of the feed-point position along the circumference [17]. The input resistance (R_{in}) at any radial distance $\rho' = \rho_0$ from the centre of the patch, for the dominant TM_{11} mode, can be written as:

$$R_{in}(\rho' = \rho_0) = \frac{1}{G_t} \frac{J_1^2(k\rho_0)}{J_1^2(ka_e)}$$

where G_t is the total conductance due to radiation, conduction (ohmic) and dielectric losses.

With a circular patch with an inset feed, the resonant input resistance is:

$$R_{in}(\rho' = \rho_0) = R_{in}(\rho' = a_e) \frac{J_1^2(k\rho_0)}{J_1^2(ka_e)}$$

$$R_{in}(\rho' = a_e) = \frac{1}{G_t}$$

Directivity of the circular patch is given by:

$$D_0 = \frac{(k_0 a_e)^2}{120 G_{rad}}$$

where G_{rad} is the conductance due to radiation.

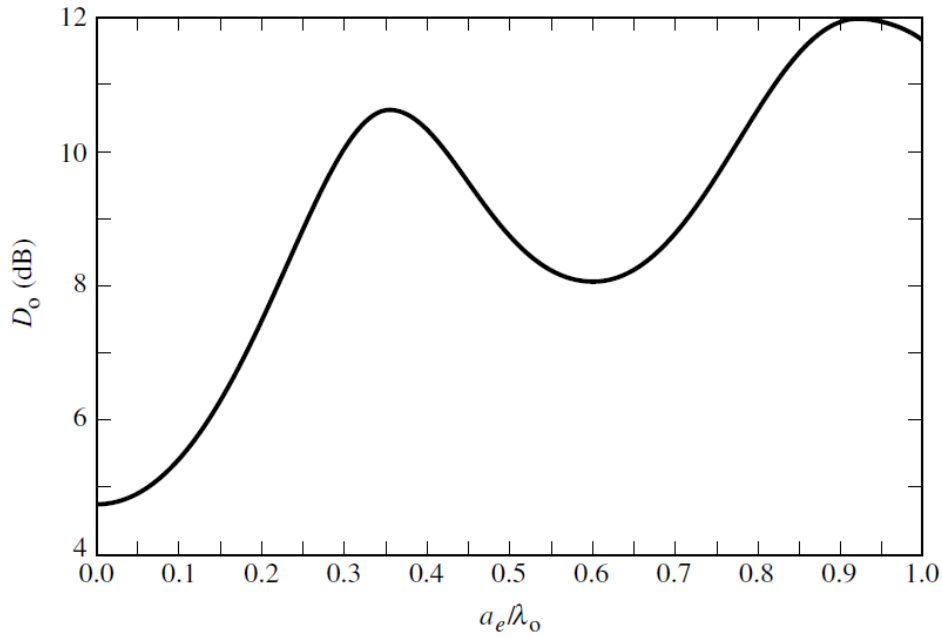


Figure 33: Directivity vs effective radius for circular microstrip patch antenna operating in dominant TM_{110}^x mode

The figure 33 shows the variation of directivity with the effective radius of the circular patch.

2.4 Triangular Patch

Studies of the triangular patch shows that it has similar radiation characteristics to rectangular patches, but smaller in size. The simplest of the triangular shapes comprises of an equilateral triangle patch has circular polarization like that in a nearly square patch antenna [37].

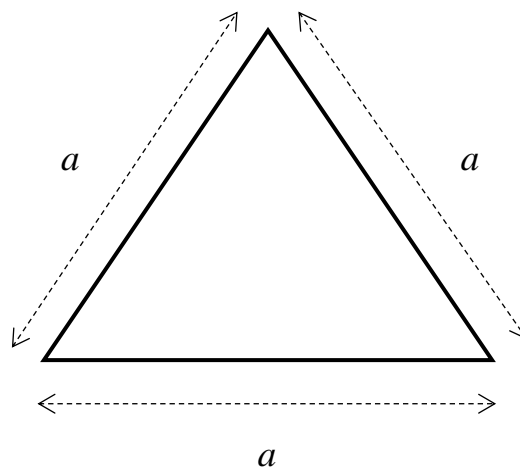


Figure 34: Triangular microstrip patch antenna design

The field distribution in a triangular patch can be found using the cavity model, in which the triangle is surrounded by a magnetic wall along the periphery, as was done for the rectangular and circular configurations. Since the thickness of the dielectric substrate, h is much less than λ_0 , there is no variation of the field along the z direction. So, the structure supports TM to z modes [37].

The resonant frequency corresponding to the various modes described by k_{mn} is:

$$f_r = \frac{2c}{3a\sqrt{\epsilon_r}} \sqrt{m^2 + mn + n^2}$$

where c is the speed of light in free space, and a is the length of one side of the equilateral triangular patch, and k_{mn} is the wave number.

The value of k_{mn} is given by:

$$k_{mn} = \frac{4\sqrt{m^2 + mn + n^2}}{3a}$$

The length of the side, a , of the equilateral triangular patch can be calculated by the following formula:

$$a = \frac{2c}{3f_r\sqrt{\epsilon_r}}$$

2.5 Quality Factor, Bandwidth, And Efficiency

The quality factor, bandwidth, and efficiency are antenna figures-of-merit, which are interrelated, and there is no complete freedom to independently optimize each one. Therefore, there is always a trade-off between them in arriving at an optimum antenna performance [17].

The quality factor is a figure-of-merit that represents the antenna losses. The total quality factor Q_t has effects of the radiation, conduction (ohmic), dielectric and surface wave losses:

$$\frac{1}{Q_t} = \frac{1}{Q_{rad}} + \frac{1}{Q_c} + \frac{1}{Q_d} + \frac{1}{Q_{sw}}$$

The fractional bandwidth of the antenna is inversely proportional to the Q_t , and is also related to the VSWR of the antenna:

$$\frac{\Delta f}{f_0} = \frac{VSWR - 1}{Q_t \sqrt{VSWR}}$$

The radiation efficiency is defined as the power radiated over the input power. It can also be expressed in terms of quality factors, which for a microstrip antenna can be written as:

$$e_{cdsw} = \frac{Q_t}{Q_{rad}}$$

Chapter 3

Introduction to Graphene

3.1 What Is Graphene

As an allotrope of carbon, graphene is a new addition in the world of material science and condensed matter physics [45]. At present, Graphene is considered as the thinnest elastic material. In addition, it has created a lot of buzz due to its exceptional electrical, mechanical, optical, and thermal properties [38-44]. At room temperature carrier mobility of graphene is high up to $200,000 \text{ cm}^2/\text{V}\cdot\text{s}$ [39] as well as low resistivity which is up to $30 \text{ }\Omega/\text{m}$). Moreover, graphene possesses intrinsic strength of 130 GPa, Young's modulus of 1 TPa, immense thermal conductivity of about $3,000 \text{ W/mK}$ and optical absorption of exactly $\alpha < 2.3\%$ along with complete impermeability to any gases. It also has the ability to sustain extremely high densities of electric current almost a million times higher than copper [42]. Such characteristics and properties prove that graphene can perform better than existing established inorganic materials for certain applications that require high-speed transistors and transparent conductive films, respectively. Moreover, large availability of carbon in nature, graphene can substitute elements such as Si, Cu etc.

A flat single layer of carbon atoms is rigidly arranged into a two-dimensional (2D) honeycomb lattice is called graphene. Graphitic materials of all other dimensionalities are built from stacked layers of graphene. In addition, 3D graphite can be represented by wrapping 0D fullerenes or 1D rolled carbon nano tubes (CNT) [45]. In Figure 35, it is shown that in graphene the 2s orbital combines with the 2p_x and 2p_y orbitals to form three sp² hybrid orbitals. Such hybridization of carbon atoms forms three bonds which are also known as σ -bonds. These σ -bonds show the strongest covalent bonds. The source of strength, robustness, elasticity and other electrical properties of graphene and carbon nano tubes (CNTs) come from the electrons of σ -bonds located along the plane connecting carbon atoms. The 2p_z electrons forms covalent bonds called π -bonds, where the electron cloud is distributed normal to the plane connecting carbon atoms. On the other hand, the 2p_z electrons are weakly bound to the nuclei and thus become delocalized. These delocalized electrons are responsible for the electronic properties of graphene and CNTs [46].

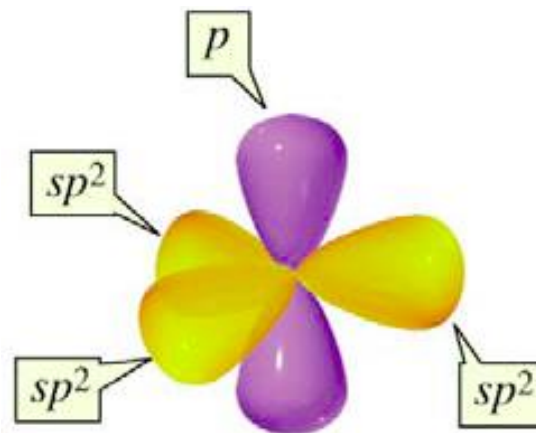


Figure 35: Illustration of Orbitals [96]

3.2 A Brief History of Graphene

In 1947 Wallace first initiated the theory 2D graphene in order to investigate the electronic properties of 3D graphite. Semenoff et al first deduced the emergent massless Dirac equation. Moreover, at Dirac point electronic Landau level occurs in a magnetic field. Therefore, anomalous integer quantum Hall Effect is observed due to this level. It is seen that electronic structure of graphite evolves rapidly by increasing the number of layers until the 3D limit i.e. 10 layers. Graphene even with two layers shows simple electronic spectra as well as being zero-gap semiconductor. The spectra get complicated for layers greater than three in addition to it, more charge carriers appear, and the conduction and valence bands starts to overlap. In case of graphite the screening length is only $\approx 5\text{\AA}$. Until 2004 graphene planes were separated through intercalating bulk graphite Thus graphene became layers of intervening atoms or molecules. Graphene can also be cultivated epitaxially by chemical vapor deposition of hydrocarbons on metal substrate, thermal decomposition of SiC etc [47].

In 2004, when Professor Sir Andre Geim and Professor Sir Kostya Novoselov of the University of Manchester successfully isolated a single atomic layer of carbon for the first time. The ‘Scotch tape method’ also known as micromechanical cleavage technique used at Manchester was so simple and effective that this area of science grew extremely quickly, and now hundreds of laboratories around the world deal with different aspects of graphene research [48].

3.3 The Graphene Lattice

Graphene, an infinitely large 2-dimensional layer of carbon can be considered as infinitesimal thickness. The carbon atoms inside graphene exist as sp^2 hybrid form where each orbital is 120° apart. Every carbon atom constitutes a symmetrical lattice along with their three other neighbouring atoms. This formation can also be defined as honeycomb lattice. Although this honeycomb lattice structure cannot be considered as a 2-dimensional Bravais lattice. On the contrary the honeycomb structure shows 2-dimensional hexagonal lattice with a 2-atom-basis which can also be described the Bravais lattice due to the 2-dimension crystal [49].

We assume \vec{a}_1 and \vec{a}_2 be two Bravais Lattice which can be defined as $\vec{a}_1 = a \left(\frac{1}{2}, \frac{\sqrt{3}}{2} \right)$ and $\vec{a}_2 = a \left(-\frac{1}{2}, \frac{\sqrt{3}}{2} \right)$ where \vec{a}_1 and \vec{a}_2 are lattice vectors and a is the constant. Figure 3 shows the graphene's honeycomb structure in addition to its other two sub lattices. Let \vec{b}_1, \vec{b}_2 and \vec{b}_3 are the three closest neighbor vectors. These neighbor vectors are defined as follows. $\vec{b}_1 = \left(0, \frac{1}{\sqrt{3}} \right), \vec{b}_2 = \left(\frac{1}{2}, \frac{-1}{2\sqrt{3}} \right)$ and $\vec{b}_3 = \left(\frac{-1}{2}, \frac{-1}{2\sqrt{3}} \right)$ [50,51].

From the Fig. (36) given below it is evident that the Brillion zone of graphene is nothing but a hexagon in the form of honeycombs. Hence, reciprocal lattice's basis vectors are defined in terms of $\vec{G}_1 = 2\pi a^{-1} \left(1, \frac{1}{\sqrt{3}} \right)$ and $\vec{G}_2 = 2\pi a^{-1} \left(1, \frac{-1}{\sqrt{3}} \right)$. Therefore, every second corner of the hexagon is equivalent. The only difference is found either in addition or subtraction of the basis vectors [52]. The first Brillouin zone of graphene is shown in Fig. (37). Each equivalent corner can be defined as K and K' where charge carrier density as well as state density is same.

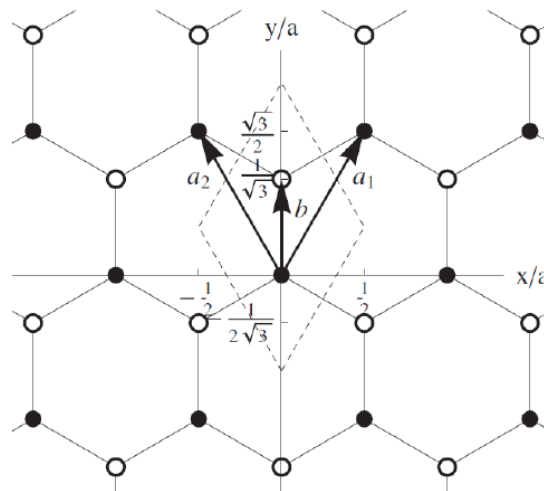


Figure 36: The honeycomb lattice of graphene.

Two Bravais sub lattices can be identified. All points of the sub lattice A (black circles) are given by $n_1\vec{a}_1 + n_2\vec{a}_2$ with n being integers and \vec{a} being the lattice vectors. All points of the sub lattice B (open circles) are given by $n_1\vec{a}_1 + n_2\vec{a}_2 + \vec{b}$ with \vec{b} being the one vector to a closest neighbour atom of which every atom in a honeycomb lattice has three in total. Dashed lines show the boundaries of the elementary cell. a is the lattice constant [53].

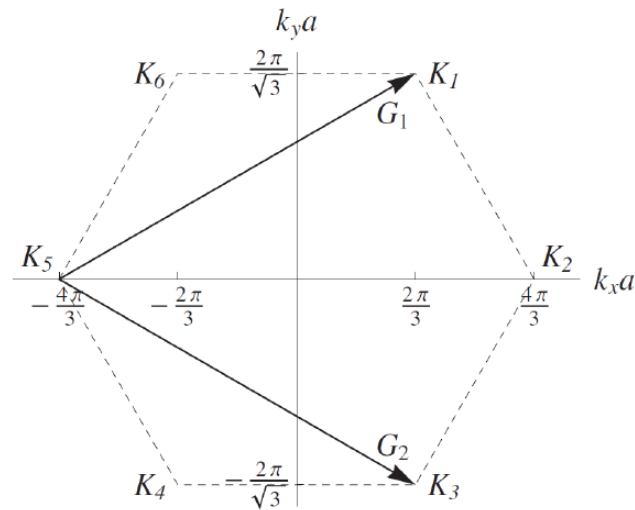


Figure 37: The Brillouin zone of graphene.

\vec{G}_1 and \vec{G}_2 are the basis vectors of the reciprocal lattice. The corners of the Brillouin zone are represented by vectors $K_j, j = 1, \dots, 6$. These corner points are defined as the Dirac points [53].

3.4 Electronic Configuration of Graphene

The electronic band structure of graphene can now be explained in terms of tight binding model. Wallace et al in their paper described the relation for the energy Eigen values in dependence of the wave vector [50,51].

$$E(\vec{k}) = \pm \frac{2\hbar V}{a\sqrt{3}} \left| e^{i\vec{k}\cdot\vec{b}_1} + e^{i\vec{k}\cdot\vec{b}_2} + e^{i\vec{k}\cdot\vec{b}_3} \right| \dots \dots (1)$$

Let \vec{b}_1, \vec{b}_2 and \vec{b}_3 are the three closest neighbor vectors from previously discussed section. Fig. 38 represents both the conduction and valence band which is specified for the whole 1st Brillouin zone. It is evident that the two energy bands around energy 0 show symmetry. In this way the six corners of the 1st Brillouin zone is formed [51].

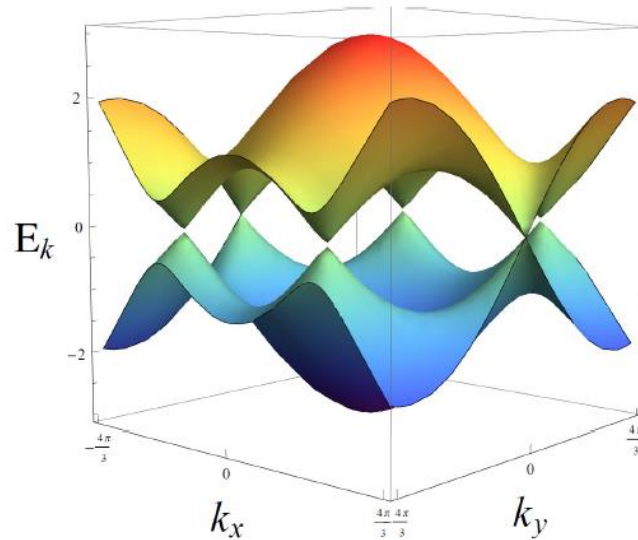


Figure 38: Energy band structure of graphene for whole 1st Brillouin zone.

k is given in units of $1/a$. Valence band and conduction band are symmetrical around zero-energy and the band gap are zero. Touching points are the six corners K and K' of the 1st Brillouin zone. For $\tau = 0$ and $T = 0$ all negative energy states are filled, all positive energy states are empty [49].

The 1st approximation cones are actually the Dirac cones having feeble values of q . It is shown as an example for wave vectors similar to $\vec{K}' = \vec{K}_2$. The wave vector \vec{q} can be written as $\vec{q} = \vec{K} + \vec{k}$ and $\vec{k} = \vec{K}' + \vec{k}$ for the corners K and K' respectively. Here $\vec{k} \ll K$ and $\vec{k} \ll K'$. Now the energy band can be calculated as

$$\begin{aligned}
 e^{i((\vec{K}'+\vec{k})\cdot\vec{b}_1)} + e^{i((\vec{K}'+\vec{k})\cdot\vec{b}_2)} + e^{i((\vec{K}'+\vec{k})\cdot\vec{b}_3)} &\approx \\
 &= \left(1 + i\vec{k}\cdot\vec{b}_1\right) e^{i\vec{K}'\cdot\vec{b}_1} + \left(1 + i\vec{k}\cdot\vec{b}_2\right) e^{i\vec{K}'\cdot\vec{b}_2} + \left(1 + i\vec{k}\cdot\vec{b}_3\right) e^{i\vec{K}'\cdot\vec{b}_3} \\
 &= a \frac{\sqrt{3}}{2} (\vec{k}_x + i\vec{k}_y) \dots \dots (2)
 \end{aligned}$$

Energy Eigenvalue and relative wave vector produce linear relationship from the complex from $|z| = \sqrt{\Im(z)^2 + \Re(z)^2}$. Close vectors like $\vec{K} = \vec{K}_5$ similar results can be obtained [54].

$$e^{i((\vec{K}'+\vec{k})\cdot\vec{b}_1)} + e^{i((\vec{K}'+\vec{k})\cdot\vec{b}_2)} + e^{i((\vec{K}'+\vec{k})\cdot\vec{b}_3)} \approx = a \frac{\sqrt{3}}{2} (-\tilde{k}_x + i\tilde{k}_y) \dots \dots (3)$$

Finally, near Brillouin corner points the total energy relation can be simplified as:

$$E_{\pm}(\vec{k}) = \pm \hbar V \tilde{k} - \mathcal{O}\left(\left(\frac{\tilde{k}}{K}\right)^2\right) \dots \dots (4)$$

Hence around zero Fermi energy level the energy levels both happens to be linear rather than parabolic and simultaneously touch at six distinct points i.e. K and K' located in the corner [55]. Geim et al. in their paper showed that the Fermi velocity V found in graphene to be 10^8 cm/s or in other words, 1/300 of the speed of light [56]. The energy structure of the graphene lattice and band structure of relativistic particles exhibits similarity. So, the graphene electrons and the resulting corners of the Brillouin zone can be identified as quasi-relativistic electrons and Dirac points respectively [55]. In Fig. 39 the energy bands cone structure is portrayed.

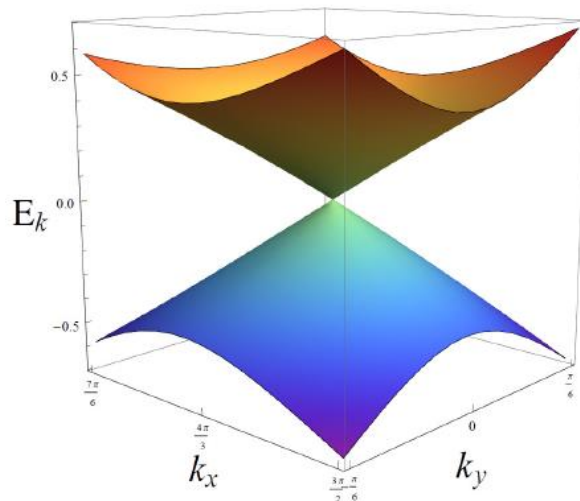


Figure 39: Energy band structure of graphene around Dirac point $K'=K_2$. K is given in units of $1/a$. Cone structure for low energies is clearly visible [49].

Chapter 4

Graphene Modelling

Conventional Micro-strip Patch antenna is generally comprised of patch primarily made of copper. Graphene has provided such promising properties and virtues which have enabled us to consider it as a replacement of copper. We believe Graphene can be a prime candidate in order to achieve next generation wireless communication. This wireless communication is specifically intended for nano communication systems operating in terahertz regime.

Graphene possesses extraordinary attributes for propagation of surface polaritons. Transverse EM wave coupled to a plasmon (wave of charges on a metal/dielectric interface) is called SPP (surface plasmon polariton). The wave must have the component of E transverse to the surface (be TM-polarized). Polariton can be defined any coupled oscillation of photons and dipoles in a medium.

4.1 Graphene Conductivity

We know that for the trivial metallic conductors, the electromagnetic fields are governed by Maxwell's equations. But in case of graphene a different approach is considered. In this case it is represented by means of surface conductivity derived from a semi classical intraband mode as well as quantum-dynamical interband mode [57]. Falkovsky et al. and Hanson et al. from their work deduced the surface conductivity of a graphene film of infinitesimal size with the help of the Kubo formalism [58,59]. By means of random-phase approximation, it is possible to represent the surface conductivity in a local form correspondingly to the Drude-like contribution [57]. The intraband contribution is defined as follows [68].

$$\sigma(\omega) = \frac{2e^2 k_B T}{\pi \hbar} \frac{1}{\hbar} \ln \left[2 \cosh \left[\frac{\mu_c}{2k_B T} \right] \right] \frac{i}{\omega + i\tau^{-1}} \dots \dots \dots (1)$$

Here T is the temperature at 300K; \hbar is defined as reduced Plank's constant; k_B is Boltzmann constant; $\tau = 10^{-13}$ sec is the relaxation time, μ_c is the chemical potential.

The interband form of the surface conductivity is also given by

$$\sigma_i(\omega) = \frac{e^2}{4\hbar} \left(H\left(\frac{\omega}{2}\right) + i \frac{4\omega}{\pi} \right) \int_0^\infty d\epsilon \frac{H(\epsilon) - H\left(\frac{\omega}{2}\right)}{\omega^2 - 4e^2} \dots \dots \dots (2)$$

$H(\epsilon)$ is defined as [57]

$$H(\epsilon) = \frac{\sin(\hbar \epsilon / k_B T)}{\cosh(\mu_c / k_B T) + \cosh(\hbar \epsilon / k_B T)}$$

In Eq. (1) and (2), the electron photon scattering process has been characterized along with interband electron transition respectively. The inter-band and intra-band transitions contribute for different conditions. Shorter wavelengths such as infrared and visible light, the optical conductivity is determined with the help of inter-band transitions. On the other hand, high frequency operations i.e. for long wavelengths intra-band transitions is considered. This model assumes the simplified model for graphene conductivity where the magnetic hall conductivity is ignored. Graphene is assumed only to be electrically biased [68].

Besides, the surface plasmon polariton of graphene can be tuned through material doping. Furthermore, it can be manipulated by means of external bias V_{DC} . This means, the external voltage V_{DC} also controls the conductivity σ of the graphene and therefore the surface impedance $Z = \frac{1}{\sigma}$ can also be controlled dynamically. We propose to use this property of graphene to design nano micro-strip patch antenna which can be tuned easily externally. The key advantage is that we will be able to increase its chemical potential therefore, decreasing losses by making the graphene sheet more inductive in order to design a graphene radiating at THz regime [68].

From Kubo formula it is not yet possible to achieve the solution accurate enough to represent graphene conductivity by changing the chemical potential via V_{DC} . Eq (3) simplifies the Kubo formula for intraband transition and a MATLAB code is generated in its correspondence. Here $\mu_c \neq 0$ is assumed, other parameters includes $k_B T = 0.0256 \text{ eV}$ where k_B is Boltzmann constant, $\hbar = 6.582 \times 10^{-16} \text{ eVs}$, $q_e = 1.6 \times 10^{-19} \text{ C}$ with Coulomb charge (C) = 6.25×10^{19} electrons, $\Gamma = 0.11 \text{ eV}$, $\omega = 2\pi f$ where f stands for frequency [68].

$$\sigma_{(intraband)} = \frac{3.009 \times 10^{10}}{6.28f + 0.22j} \left(\frac{\mu_c}{k_B T} + 2 \ln \left(e^{\frac{-\mu_c}{k_B T} + 1} \right) \right) \dots \dots (3)$$

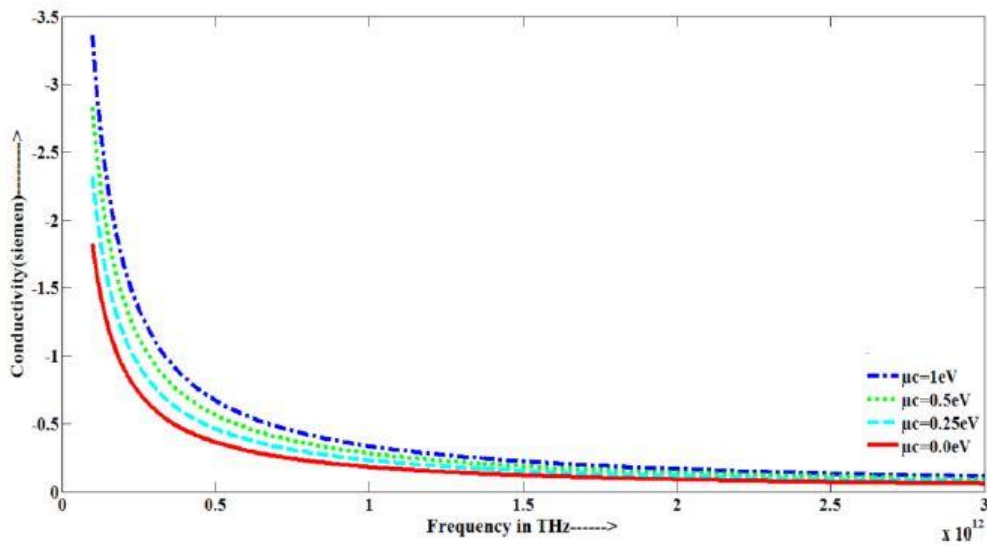


Figure 40: Real part of intraband conductivity at room temperature ($T = 300\text{k}$) for different values of chemical potential

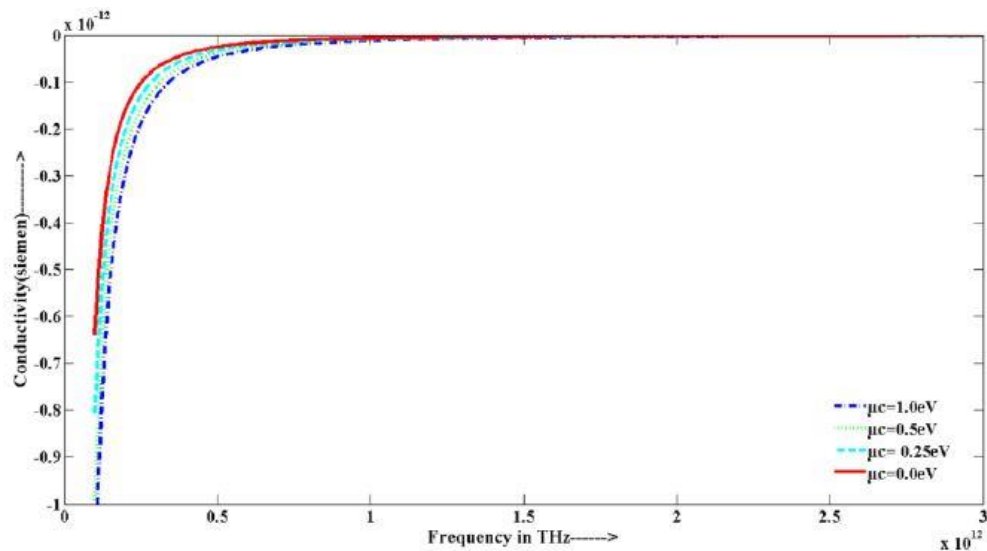


Figure 41: Imaginary part of intraband conductivity at room temperature ($T = 300\text{k}$) for different values of chemical potential

The intraband term of the graphene conductivity can be more minimized and simplified by taking $\mu_c = 0$. From Eq (4) we can clearly observe that the intraband term of the graphene conductivity resembles Drude-like form.

$$\sigma_{(intraband\ simplified)} = j \frac{q_e^2 \mu_c}{\Pi \hbar^2 (\omega + j\tau^{-1})} \dots \dots (4)$$

Thus, from Eq (4) we can conclude that the conductivity of graphene is a form of the Drude model for high frequency. Moreover, it also can be related that the electron conductivity of graphene at high frequency is directly proportional to the absorption of its free carrier. Hence with the increase of frequency the absorption of free carriers at lower frequency increases in case of intraband absorption transitions. Wang et al also proved in their spectroscopy measurements that the intraband transitions regulate the behaviour of graphene conductivity for high frequencies. [60,61].

4.2 Drude-Lorentz Model And Effective Permittivity

The antenna simulation tool used for designing the graphene patch antenna is CST (Computer Simulation Technology). Graphene here is simulated assuming an infinitesimal thickness and its in-plane effective permittivity is dependent on the volumetric conductivity (σ_s) [62].

$$\sigma_V^{intra} \triangleq \frac{\sigma_s^{intra}}{\Delta} = \frac{2e^2 k_B T}{\Delta \pi \hbar} \ln \left[2 \cosh \left[\frac{\mu_c}{2k_B T} \right] \right] \frac{i}{\omega + i\tau^{-1}} \dots \dots (5)$$

In order to determine the parameters of an antenna, it is essential to study its dielectric materials. Dielectric materials in its closed form can be represented by the Drude-Lorentz model. In case of metal the Drude -Lorentz classical model is reduced to Drude metal model with no resonance [62].

$$\sigma_{Drude}(\omega) \triangleq \frac{\sigma_0}{1 - j\omega\tau} \Rightarrow \times \frac{i}{j} \Rightarrow \frac{\sigma_0}{\omega\tau + j} \Rightarrow \sigma_{Drude}(\omega) = \frac{\frac{\sigma_0}{\tau}}{\omega + j\tau^{-1}} \dots \dots (6)$$

$$\sigma_V^{intra} = \frac{\frac{\sigma_0^{Gr}}{\tau}}{\omega + j\tau^{-1}} \dots \dots (7)$$

$$\sigma_0^{Gr} \triangleq \frac{2e^2 k_B T \tau}{\Delta \pi \hbar} \ln \left(2 \cosh \left(\frac{E_F}{k_B T} \right) \right) \dots \dots (8)$$

The equivalent effective permittivity for infinitesimal thickness of graphene is written as follows:

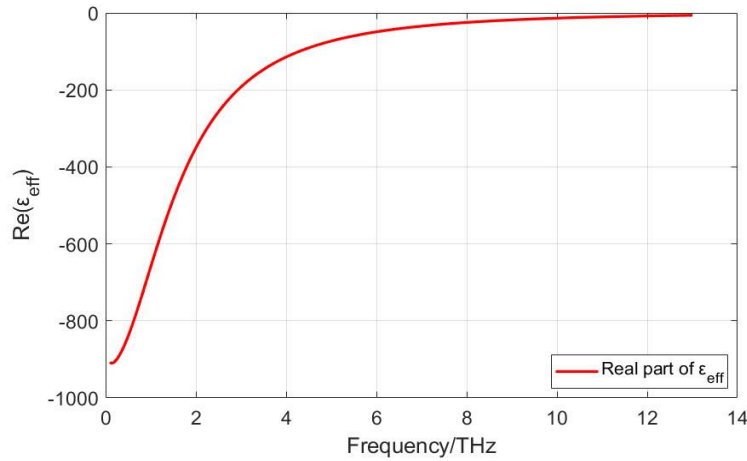
$$\varepsilon_{eff}^{Gr}(\omega) = \varepsilon_0 + j \frac{\sigma_V^{intra}(\omega)}{\omega} = \varepsilon_0 + \frac{j\sigma_0^{Gr}}{\omega(1 - j\tau)} \dots \dots (9)$$

Furthermore, it can also be shown in Eq (10) that the classical Drude-Lorentz representation based on dielectric where resonance carrier frequency is zero i.e. ($\omega_0=0$) and Plasma frequency (ω_p) is related [62] Real and imaginary part of effective permittivity is shown in Fig 42.

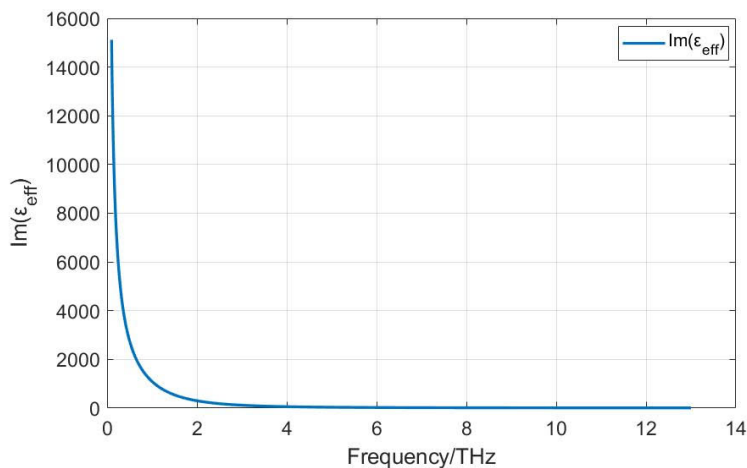
$$\epsilon_{eff} = \epsilon_0 \left(1 - \frac{\omega_p^2}{\omega(\omega + j\gamma)} \right), \quad \gamma = \tau^{-1} \dots \dots (10)$$

Relation between ω_0 and ω_p with Fermi level dependent can be written as follows.

$$\omega_p = \left[\frac{2e^2 k_B T}{\Delta \pi \epsilon_0 \hbar^2} \ln(2 \cosh(\frac{E_F}{2k_B T})) \right]^{\frac{1}{2}} \dots \dots (11)$$



(a) Real part



(b) Imaginary part

Figure 42: Real(a) and imaginary (b) part of effective permittivity at room temperature (300K) at $\mu_c = 0$ eV

4.3 Graphene Extinction

The absorption cross section can be defined as the measure of the fraction of power which is absorbed by the graphene antenna by the incident wave. Hence the graphene antenna's resonant frequency fits with the frequency where maximum value of the absorption cross section is obtained. In Fig.43 we have attempted to recreate the same plot of absorption cross section as discussed in paper [63].

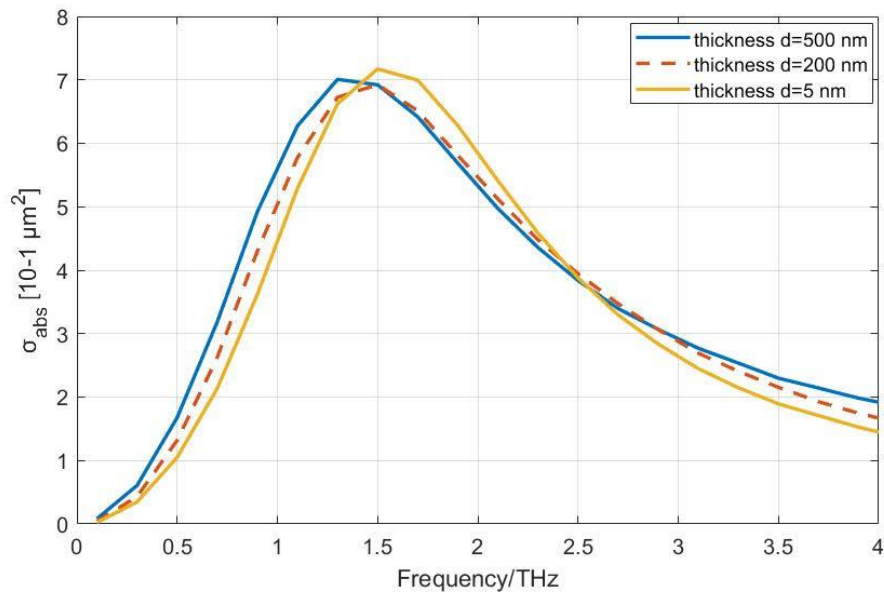


Figure 43: Dependence of the absorption cross section of a graphenna as a function of its width. The length of the graphenna is $L = 5 \mu\text{m}$. The plots correspond to 500 nm, 200 nm and 5 nm wide patches (right to left) [63].

From the above figure it is evident that if the dimensions of the graphene patch antenna (with a fixed length) are varied then we can easily tune the resonant frequency for wider spectrum [63].

4.4 Chemical Potential

Unlike conventional materials such as copper chemical potential plays an important role in graphene scattering leading to performance of the antenna, Chemical potential can be defined as the likelihood of quantum state whose probability is equal for both empty or occupied. The likelihood of quantum state depends on the electron energy distribution level [63].

Up to this we have assumed that the chemical potential to be zero for simplification purposes. On the contrary Eq. (5) unveils that the chemical potential impacts graphene conductivity. Therefore, radiation performance of graphene patch antennas is indirectly related to chemical potential. Several ways can be considered in order to control graphene's chemical potential. One of the ways is by doping of the material or application of external electrostatic bias voltage. Such arrangements can dynamically and effectively tune the antenna radiation. A comparative study is needed to observe how the chemical potential variations influence the resonant frequency of graphene patch [63].

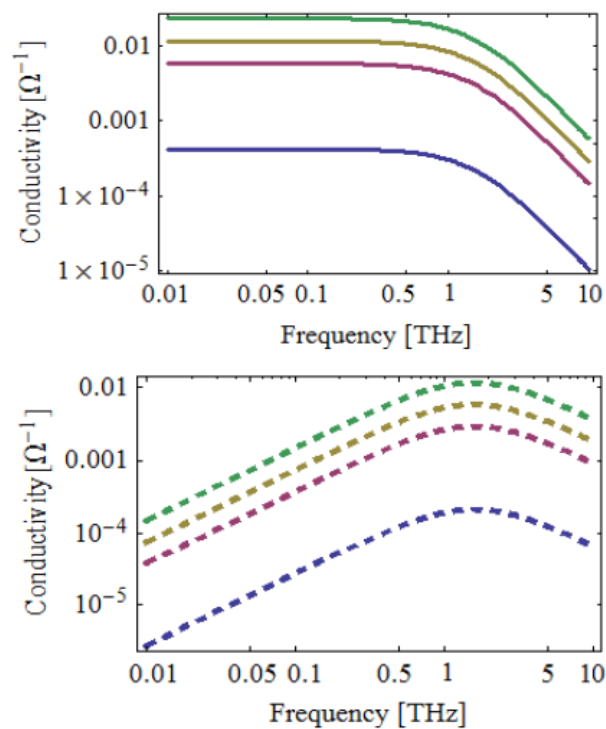


Figure 44: Log-log plots of the real (above) and imaginary (below) parts of the electrical conductivity of graphene as a function of the frequency, for different values of the chemical potential: 0 eV (blue line), 0.5 eV (purple line), 1 eV (yellow line) and 2 eV (green line) [63].

Fig 44. represents how chemical potential makes a significant difference in graphene conductivity. Here, it is observed that as the chemical potential increases the conductivity shifts upwards and increases almost 10 times. The power absorbed by the microstrip graphene patch is also affected by the chemical potential. As a result, resonant frequency of the antenna changes dynamically [63].

Table 1: Effect of chemical potential on Resonant Frequencies taking length and width of $5\mu\text{m}$ and $0.5\mu\text{m}$ respectively [63]

Chemical Potential (eV)	Resonant Frequency (f_r)
0.0 eV	0.918 THz
0.5 eV	3.356 THz
1.0 eV	4.704 THz
2.0 eV	6.541 THz

From Table 1, it is evident that the resonant frequency changes drastically with the change of the chemical potential. [63].

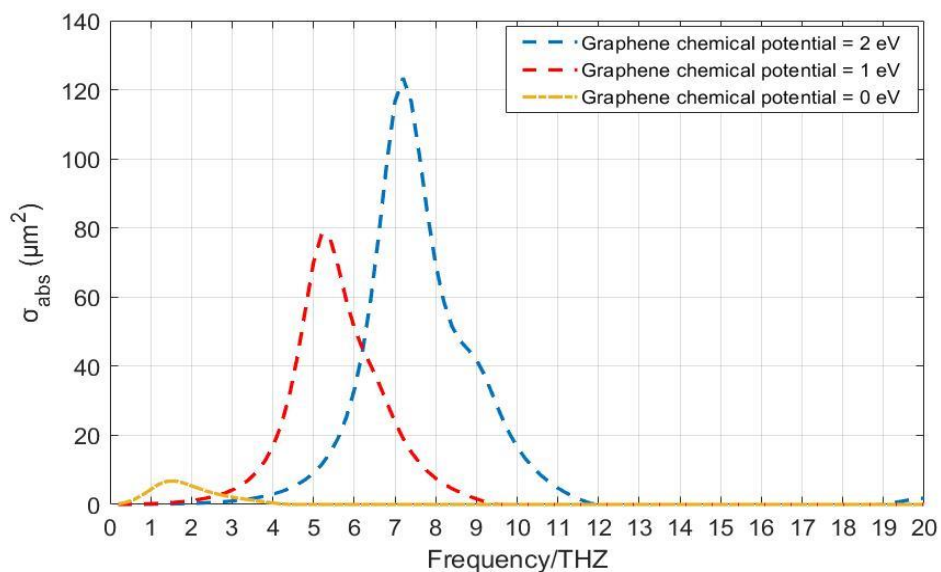


Fig 45: Absorption cross-section of graphene slab with respect to frequency for different values of chemical potential.

In a nutshell, the chemical potential view points to the power absorbed by graphene antenna and its transmission range cannot go hand in hand. Shown in Fig 45. In order to achieve one, other must be compromised. With zero chemical potential the graphene radiates at low frequency having small absorption cross section. Hence, the radiation efficiency gets limited.

High chemical potential represents antenna resonating at higher frequencies due to greater absorption ability but shaving its transmission range. Antenna designer should keep in mind about these two contradictions for future application of graphene-based antenna for nano wireless systems [63].

4.5 Relaxation Time

The relaxation time of a material can be defined as the time required for distortion of a charge due to fluctuations and becomes stable to a uniform charge density after being introduced to a material. Depending on quality of graphene relaxation time in graphene is considered as a key parameter also related to the conductivity of graphene shown in Eq (5). George et al, Trushin et al, Hu et al, Ryzhii et al in their respective papers have opted for different values form 10^{-14} s to 10^{-11} s in order to consider the relaxation time [64-68]. Since no conclusive arguments where found regarding the actual relaxation time, we seemed it will be logical to study the relaxation time in terms of resonant frequency i.e. how it affects radiation of the graphenna [63].

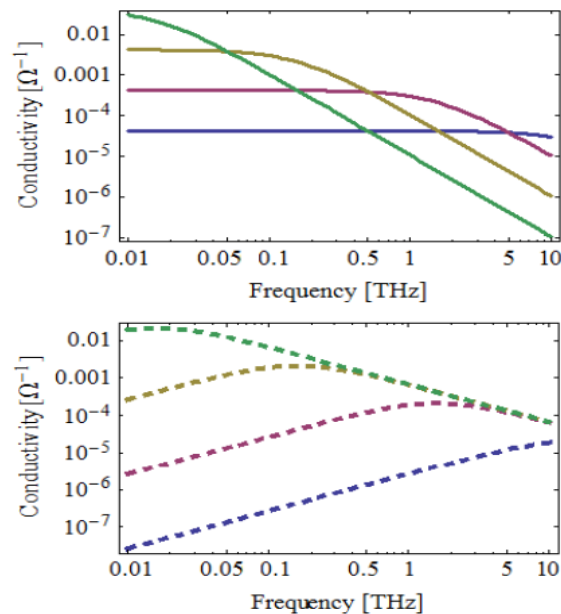


Figure 46: Log-log plots of the real (above) and imaginary (below) parts of the electrical conductivity of graphene as a function of the frequency [63].

Figure 46 represents graphene conductivity with respect to its frequency changing its relaxation time. In the above figure, for different values of the relaxation time: 10^{-14} s (blue line), 10^{-13} s

(purple line), 10^{-12} s (yellow line) and 10^{-11} s (green line), the plots are shown. We have analysed how relaxation time affects the conductivity taking values described in the literature [45-48]. From the figure it is evident that the relaxation time possesses strong dominance up to 3 orders for controlling the conductivity [63].

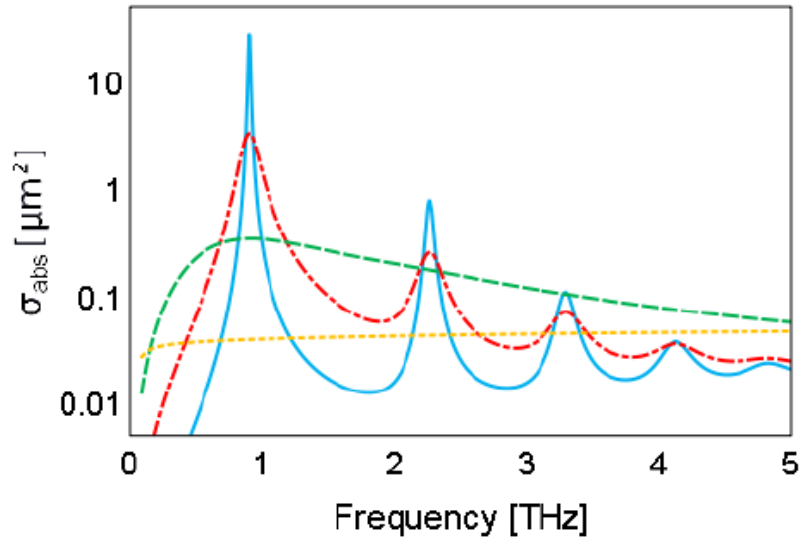


Figure 47: Absorption cross section (in logarithmic scale) of a graphenna as a function of frequency, for different values of the relaxation time: 10^{-14} s (yellow dotted line), 10^{-13} s (green dashed line), 10^{-12} s (red dot-dashed line) and 10^{-11} s (blue solid line) [63].

Figure 47 represents graphene absorption cross section with respect to its frequency varying its relaxation time. In this case also the relaxation time imposes a significant impact on the results such as bandwidth. It is evident from the results that the graphenna does not resonate for $\tau = 10^{-14}$ s. Increasing the relaxation time to $\tau = 10^{-13}$ s a wide resonance is recorded around 1 THz whose 3dB bandwidth is around 1.9 THz. Further increasing τ leads to higher order resonance with strong resonance characteristics. When $\tau = 10^{-12}$ s the 3dB bandwidth is shifted to 0.16 THz and $\tau = 10^{-11}$ s the 3dB bandwidth is 0.019 THz [63]. Higher bandwidth is indispensable in order to maximize the channel capacity. Therefore, we have decided to keep the relaxation time to $\tau = 10^{-12}$ s which ensures strong radiation behaviour as well as achieve maximum bandwidth as possible [63].

Chapter 5

Literature Review and Methodology

5.1 Literature Review

In today's communication system, an antenna plays a crucial role in our day to day life. An antenna is a metallic object that converts high frequency current into electromagnetic waves and vice versa. [69]. the behaviour and electronic properties of graphene proves that it is more attractive for EM applications such as antenna, waveguide etc. Graphene is the building block of carbon nano tubes (CNT). The proposed paper shows the radiation characteristics of nanoribbon based nano scale strip for both rectangular and circular patch antenna radiating between 2.45 to 2.98 THz band. The S-parameters and well as radiation pattern shows laudable results in gain and directivity from conventional antennas [70].

Yanfei Dong proposed antenna creates a patch resonance based on backing cavity. The backing cavity composed of graphene/Al₂O₃ stacks can perform dynamically dual-resonance frequency-tuned on large range at 1 THz through electrostatic gating on the graphene stack. The paper outlines reflection coefficient over 0.16–0.26 eV range of chemical potential which creates two resonant frequency bands over whole frequency range, namely 4–5 and 6.5–7.5 THz. Due to the variation of effective dielectric constant of cavity substrate is irregular and change occurs in upper frequency band. The maximum of first resonant frequency BW with 0.8 THz is obtained when $\mu_c = 0.2$ eV, When $\mu_c = 0.16$ eV, the maximum of the second resonant frequency BW with 1.2 THz. Moreover, the least return loss (RL) is found to be 42dB. Considering directivity at first resonance frequency with different chemical potential (μ_c) the magnitude of main lobe gradually rises as chemical potential μ_c rises. For $\mu_c = 0.26$ eV, the peak magnitude of main lobe of the antenna is 7.2 dBi. In addition, direction of main lobe can be varied from -15° to 25° due to the transformation of surface current distribution on the patch by changing chemical potential of graphene. Therefore, beam reconfiguration is achieved with a deflection range of 40° [71].

Jornet M.J et al proposed to create Nano-Antennas for Electromagnetic Nano communications in the Terahertz Band. It is found that for a maximum antenna size in the order of several hundred nanometres both a nano-dipole and a nano-patch antenna will be able to radiate electromagnetic waves in the terahertz band [72]. Carrasco.E proposed to use graphene for fixed beam reflects array antennas at terahertz frequency. The array was designed at 1.3

Terahertz and was analysed by using a full vertical approach. A very substantial reduction was seen in interelement spacing due to the plasmonic propagation supported by the elements. In the study positive performance in terms of bandwidth, cross-polar and grating lobes suppression, proving the feasibility of graphene-based reflect arrays and other similar spatially fed structures at Terahertz frequencies [73]. Llatser. I et al proposed for the scattering of terahertz radiation on a v-based nano-patch antenna. In the study dependence of the real and imaginary part of the intraband conductivity s and the total conductivity $\text{total} = \sigma_s + \sigma_{si}$ were compared at room temperature ($T = 300 \text{ K}$) and zero electrostatic bias ($\mu_c = 0 \text{ eV}$). In the study a vivid dependency on chemical potential was found which opened the possibility of tuning the resonant frequency. These antennas opened doors for wireless communications in the nanoscale [74].

Zhou. T et al proposed a miniaturized antenna using graphene. The antenna was constructed having dimensions of dipole $L=20 \mu\text{m}$ $W=5\mu\text{m}$ and thickness $50\mu\text{m}$. The value of μ_c was considered $0-0.5\text{eV}$ and operation frequencies 0.8 to 1.6THz . The radiation pattern is similar to metal antennas having an omnidirectional structure. The directivity is 1.8dBi in this case. The study concluded attractive properties of the graphene antenna to be used in nanoscale wireless communications and sensing system [75]. Walter Fuscaldo states in the proposed that a novel reconfigurable radiating device operating in the THz range for graphene based super substrate (SS) and leaky wave antenna (LWA). Dispersion and radiation properties of fundamental leaky modes are supported by electronic structure of graphene. Thus, by changing chemical potential of graphene beam scanning at a fixed frequency can be achieved. Due to reduced attenuation variations of fundamental TE/TM leaky mode pair, peak directivity can be achieved from proper positioning of graphene in the substrate. Beam scanning is obtained at fixed frequency by changing chemical potential of graphene through electronic bias. Furthermore, it is also evident that at different frequencies and biased scanned pointing angles shows improved half power beam width (HPBW) for graphene based planar waveguide than graphene-based substrate superstrate [76].

Tamagnone. M et al proposed on designing of terahertz antennas from plasmonic graphene sheets. The study showed higher the values of μ_c larger the radiation efficiencies which is a result of higher resonating size. Again, for maximization of (gr) small values for W was taken. The antenna performed better than typical Terahertz Antenna. The gm is less than 1% for the photo mixer despite the miniaturized size of proposed antennas. Two frequency working points was noticed for the antennas where input impedance for the first one is real with a low resistance value and the input impedance of the second one with a low resistance value. This

study showed further opportunities for design of terahertz antennas using graphene-based materials [77]. Wang, X.-C. et al suggested the implementation of a High-Impedance Surface (HIS) containing graphene and metal patches into designing a two-dimensional THz leaky-wave antenna, whose resonant frequency and beam angle can be reconfigured independently. By drawing transmission-line models of the 2-D LWA and making necessary calculations, the research shows that by changing the chemical potential of the graphene based HIS, the bandwidth of the antenna can be increased. Though the direction of can be changed as frequency increases, the width of it becomes narrower and sharp. Moreover, by decreasing μ_c , beam-steering is possible in both E and H-plane [78]. Li, J. et al proved with both theoretical and calculated results that beam sweeping is possible in a grating based dielectric antenna with a graphene sheet on top. By varying the chemical potential, and the working frequency, the results show that the beam scans over a broad angle due to the changes [79].

Dragoman, M. et al shows that a metallic antenna on a graphene layer can have different radiation pattern and efficiency when different gate voltages are applied. He used the low resistive property of graphene at high voltages to switch the antenna on and off. At terahertz region, the dipole antenna has higher gain and radiation efficiency. The paper also shows that an array of such antennas can have a more concentrated, less lobed radiation pattern when some of them are switched off, compared to keeping all of them on [80]. Tamagnone, M. et al demonstrates the idea of an antenna with more efficient radiation properties along with reformable resonant frequencies. By designing an antenna with graphene layered stacks and metal surfaces, the input impedance varies as the chemical potential is varied, which in turn allows the resonant frequency to be changed. Also, zero crossing of the imaginary part of the varying input impedance lets the antenna to have a good match with the THz source and detector. This leads to a better efficiency, as much as up to 9% with a 10 k Ω photo mixer, as simulated results show [81].

Huang, Y. et al shows that impurities on a single layer doped graphene can contribute to the switching of the HIS. At a density of charged impurity of around $2.0 \times 10^{13} \text{ cm}^{-2}$, the SLG conducts 180 times more when gate voltage (V_g) is zero than when V_g is high ($\approx 35\text{V}$), acting like a dielectric material in the later state. By designing a dual-looped antenna over a 6x6 array of HIS cells, and switching columns of cells on and off, they demonstrated the beam sweeping capability of it over an angle of $\pm 30^\circ$ at 860 GHz. Keeping HIS cell columns(m) ON from $m=0$ to $m=3$, the efficiency was pretty much stable over the different cases [82]. Esquiús-Morote, M. et al demonstrates how a graphene LWA is sinusoidally modulated to perform beam scanning at a fixed THz frequency. By effectively controlling the numerous gate voltages

applied, the graphene conductivity can be controlled. To have a constructive interference between the main and reflected beams over the calculated beam scanning range, specific value of the substrate thickness is chosen. The paper shows that the simulation results match the theoretical findings. It also exploits the practical limitations of such antenna, and how those can be minimized [83].

Due to the complexity and high expense of fabricating a graphene LWA, Cheng, Y. et al proposes a new design that will help to overcome such difficulties. Graphene ribbons are placed on top of a dielectric-polysilicon layer, where gaps between the ribbons are varied as if they represent a sinusoid. Connecting all the ribbons to a metal plate, a single source is needed to apply voltage to all the ribbons. The surface reactance varies sinusoidally with the change in gap width for different chemical potentials. Also, a higher gain and radiation efficiency is achieved with higher μ_c . Beam sweeping is also attained [84]. Tamagnone, M. et al shows how the propagation constant can be controlled to make the graphene-stacked antenna to resonate at different frequencies, making it an easy and effectively frequency reconfigurable. Changing the chemical potential by applying different bias voltage, the conductivity, and hence the plasmonic propagation constant of the graphene layer is varied. They verified with equations that the high input impedance at resonant frequency is independent of the working frequency and does not change when it is reconfigured. Analysing graphically, it is shown that the total efficiency, as well as the resonant frequency, increases as the graphene conductivity increases[85].Rodriguez, N. R. N. M., de Oliveira, R. M. S., & Dmitriev, V. proposed a parasitic graphene sheet inclusion to the design discussed in [31], and showed how it can be operated at three different states. By altering the parasitic sheets' chemical potentials, the radiation pattern of the antenna can be changed to point in opposite directions or acts as a dipole antenna. Though it is less efficient than the originally proposed antenna, it is more directive in the direction. The dipole state is more efficient and has more gain than the original design [86]. Zhang, H., et al implies the design of a graphene antenna which has certain advantages to conventional metal antennas at the UWB region. By increasing the chemical potential of the graphene patch on the antenna, the imaginary part of the surface impedance becomes much bigger than the real part, making it a high reactance surface. This results in less side lobes and higher front-to-back ratio, stable radiation pattern and more efficient radiation [87].

Exploring other areas of work in the field of antenna despite usage of graphene quite a few interesting research works was found. Sagor M. H, et al proposed a design of antenna fabricating on Liquid Crystal Polymer. This was done to make antennas applicable to wearable applications for broad spread use. The design did not rely on compromising of any of the factors

and its effectivity in different conditions was tested. The design showed quite interesting prospects of new research into the arena of wideband antenna applications. [88] Rahman S. et al dived into an investigation to design a transparent and flexible antenna which can be used for 5G communications at 28GHz frequency. The substrate here used was Polyethylene Terephthalate (PET) and was designed which had a transparency of near 70-80%. The designs however were not fabricated and AgHT-8 was used a conductive material here. The scope of further work could include designing a more transparent design. [89] Nahiyan S. A et al explored the use of metamaterial for modifying higher order resonances. The research showed amazing results with maximum radiation and radiation across different radiating bands. The metamaterial used in this case was DPS-ENG and the main lobe is more shifted than usual, but the side lobe shrank at loss. This opened prospects for further research and design of patch antennas arrays for making the beam steering process easier. [90] Callaghan, P. et al proposed a Double Layered- Grid filter design to allow transmission at specific wireless bands. The research showed insightful reading on the effect of incidence angle which was reduced considerably and transmitting properties were also improved. There are a few challenges in designing it in real life which could open arenas for further research into this topic. [91]

5.2 Methodology

Our research began with a view to incorporate graphene material with the terahertz spectrum as it opens the door for many exceptional applications such as wireless communication with higher data rate, miniaturized devices etc. At first, we investigated [92] work which consisted of a microstrip patch antenna using graphene as the conducting material operating at 0.7 THz frequency. In our research, we worked with an operating frequency range of 6-8 THz which is approximately ten times larger and analysed the antenna parameters for different antenna shapes and substrate materials. However, the research done in [1] introduced us with the tunable properties of graphene material which were crucial for our research work. The paper [57] proposed two different concepts to model a graphene patch: equivalent slab model and surface impedance model, of which we chose to model our graphene patch using the equivalent slab model. Additionally, this paper [63] analysed the tunability of graphene surface conductance as well as resonant properties in terms of chemical potential and relaxation time. In our research, we used chemical potential of 2eV and relaxation time of 0.1ps to obtain the desired operating frequency range of 6-8 THz. Moving on to the antenna design part, we designed microstrip patch antenna of rectangular, circular and triangular shapes as these are

the most popular antenna shapes using single layer graphene of thickness 0.345nm. The dielectric material used as a substrate in antenna design is an important element to consider as its dielectric properties determines the size of the patch, radiation pattern and the bandwidth [93]. In our research, we used Teflon, Polyimide, FR-4 and Alumina (96%) as dielectric substrate material and analysed the antenna parameters for different antenna shapes. Finally, we started our antenna simulation in CST Microwave Studio Software after contemplating all the books, papers and articles.

Chapter 6

Simulation and Results

6.1 Single Layer Graphene Rectangular Microstrip Antenna

The figure of single layer graphene rectangular microstrip antenna is given below:

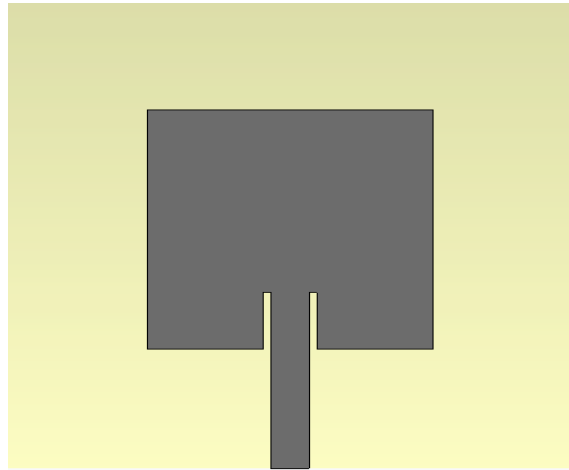


Figure 48: Single Layer Graphene Rectangular Patch Antenna

The parameters of single layer graphene rectangular microstrip antenna are given below:

Table 2: Parameters of Single Layer Graphene Rectangular Patch Antenna

Parameter	Values (in μm)
Substrate Length	56.24
Substrate Width	52.24
Substrate Height	1.5
Patch Length	28.12
Patch Width	26.12
Patch Thickness	0.000345
Inset Feed	9.25
Feed Line Width	4.79

6.1.1 Teflon As Dielectric Substrate

Teflon is one of the most used dielectric materials to design a microstrip patch antenna. It has a lower dielectric constant of 2.1. The unique properties such as lower dielectric constant, high dielectric strength, low dissipation factor makes it suitable to design microstrip antennas. This material maintains a stable electrical and chemical properties which makes it befit to operate in higher frequencies.

S-Parameter:

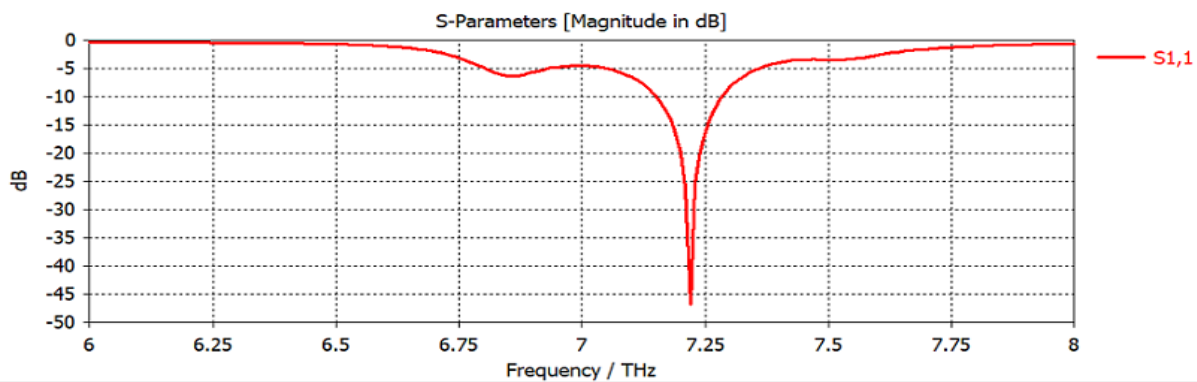


Figure 49: S Parameter for single layer graphene rectangular patch antenna using Teflon as Substrate

Here, the S parameter which represents the return loss of the antenna is -46.95dB at 7.22 THz which is in the desired resonant frequency range of 6-8 THz. The return loss is the measure of how much power is reflected from the antenna. Generally, a return loss with a value less than -10dB is considered optimum for antenna design as it means more than 90% of the power is delivered to the antenna.

VSWR:

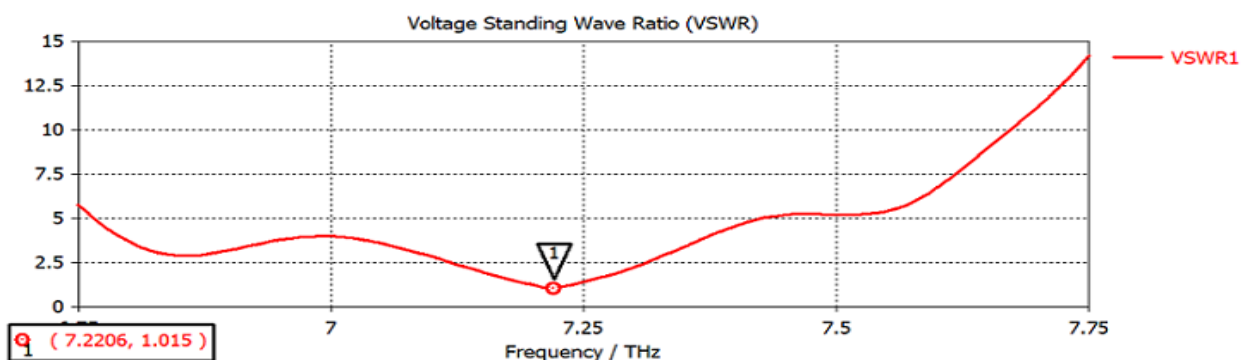


Figure 50: VSWR for single layer graphene rectangular patch antenna using Teflon as Substrate

For this design, we got a voltage standing wave ratio of around 1.015. VSWR demonstrates how well an antenna is matched impedance-wise with the feedline. The lower the VSWR, the better the antenna is matched with the feed line. For optimum result, the VSWR value should be close to 1. For Teflon substrate, we have almost an ideal voltage standing wave ratio.

Radiation Pattern:

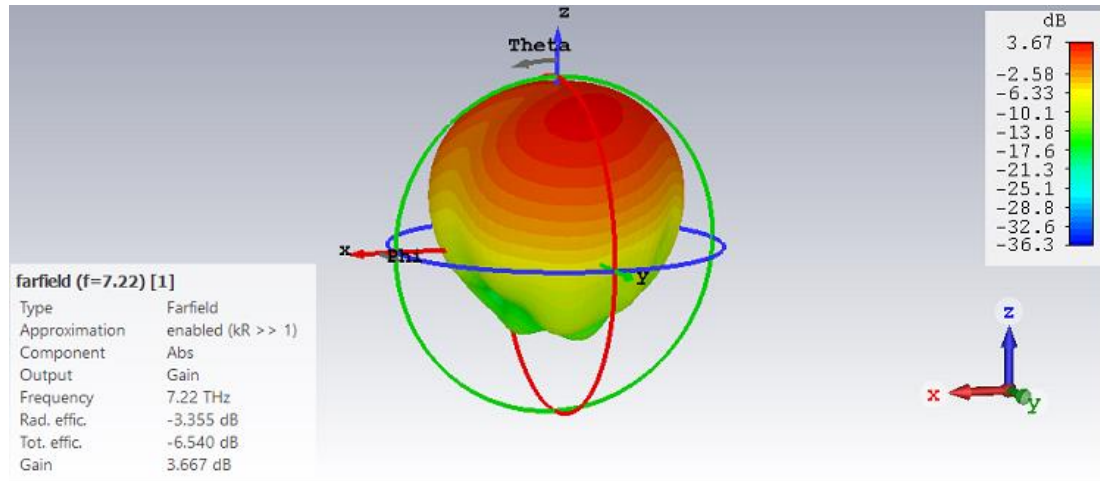


Figure 51: Radiation Pattern of single layer graphene rectangular patch antenna using Teflon as Substrate

The gain of the antenna is 3.67 dB at 7.22 THz which is quite good considering the thickness of the graphene material. The radiation efficiency of the antenna is -3.355 dB and the total efficiency is -6.540 dB.

Directivity:

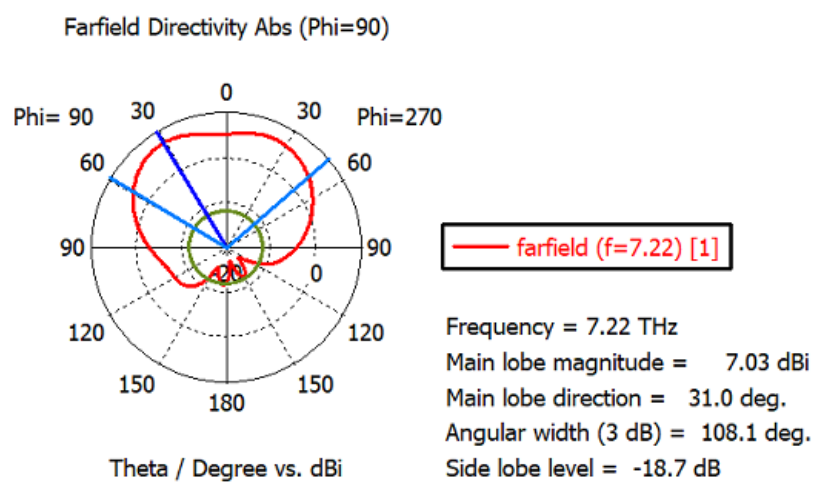


Figure 52: Polar Plot of Directivity of single layer graphene rectangular patch antenna using Teflon as Substrate

The directivity of the designed antenna is 7.03dBi. Directivity is a measure of how much power is radiated towards a particular direction. The direction of the main lobe of the antenna deviates by 31.0 degree and has a larger angular width of 108.1 degree which indicates the omnidirectional property of the antenna. Moreover, this design has a side lobe level of -18.7dB. The lower the side lobe level, the better performance is provided by the antenna as less power is radiated in unwanted direction.

6.1.2 Polyimide As Dielectric Substrate

Polyimide is a dielectric material with a dielectric constant of 3.5 which is commonly used in graphene antenna designs. This material shows good optical and electrical properties along with some remarkable attributes such as thermal stability, chemical resistance and high mechanical strength which makes it suited for graphene antenna design.

S-Parameter:

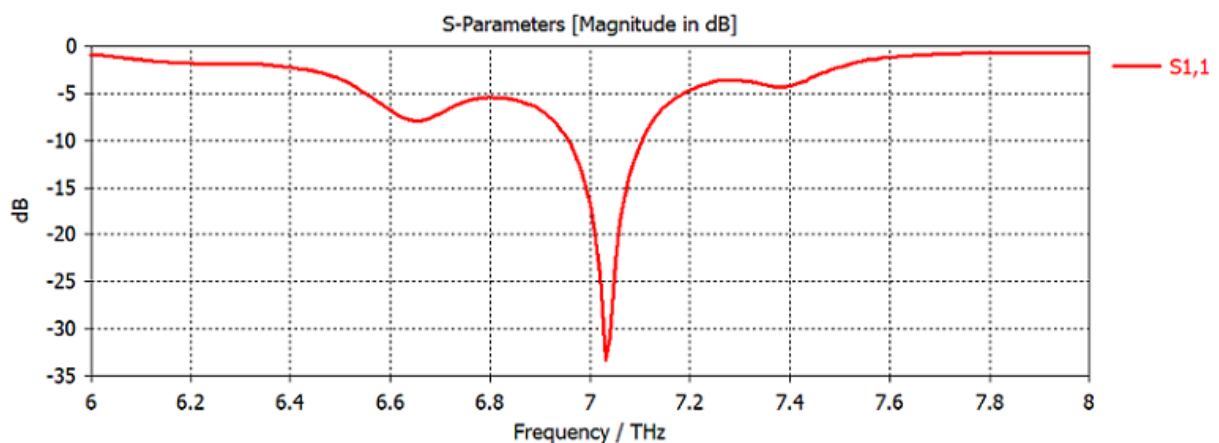


Figure 53: S Parameter for single layer graphene rectangular patch antenna using Polyimide as Substrate

For this design, we get a return loss of -33.41 dB at 7.03 THz which is in the desired frequency range. This design yields a very good return loss as it is way below the -10dB range.

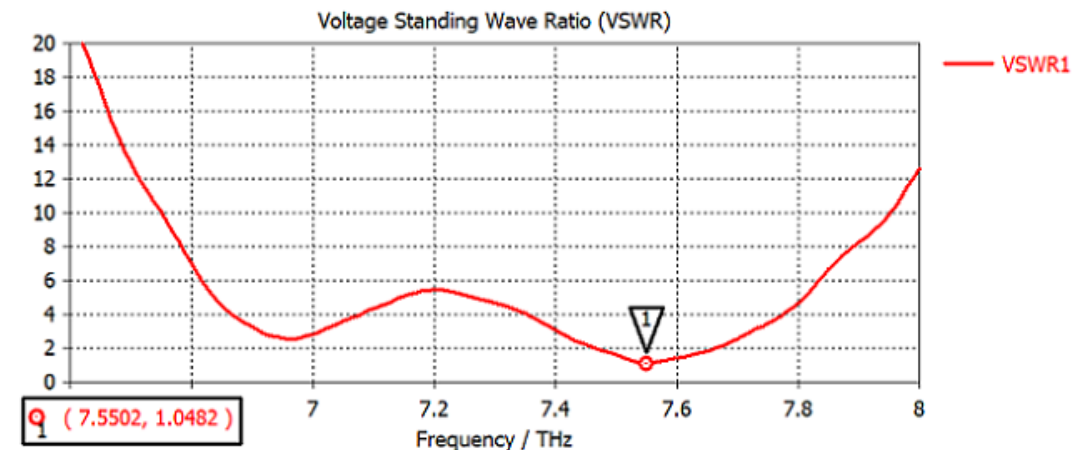
VSWR:

Figure 54: VSWR for single layer graphene rectangular patch antenna using Polyimide as Substrate

By using Polyimide as a substrate, we get a very good voltage standing wave ratio of around 1.044. The VSWR value is close to the optimum value of 1 which means the antenna is well matched with its feed line.

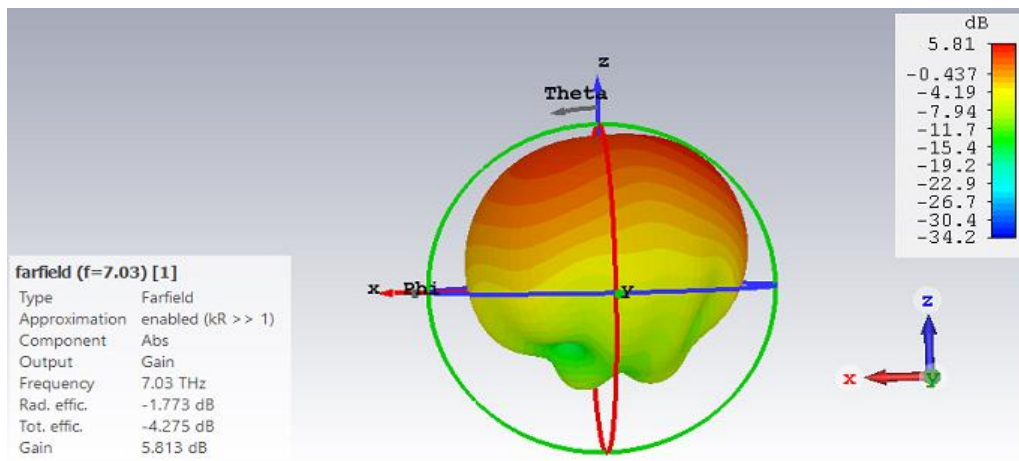
Radiation Pattern:

Figure 55: Radiation Pattern of single layer graphene rectangular patch antenna using Polyimide as Substrate

For Polyimide Substrate, we get a gain of 5.81 dB which is good compared to other antenna designs. The radiation efficiency of this design is -1.773 dB and the total efficiency is -4.275 dB.

Directivity:

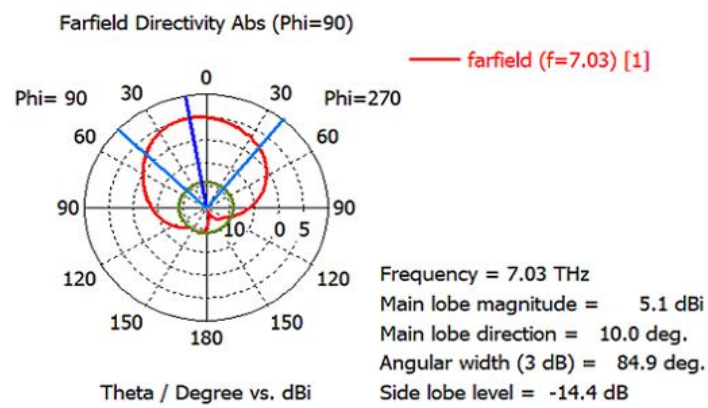


Figure 56: Polar Plot of Directivity of single layer graphene rectangular patch antenna using Polyimide as Substrate

Here, we have a directivity of 5.1 dBi which is decent compared to other antenna designs. There is a deviation main lobe direction by 10 degrees and has a smaller angular width of 84.9 degree. The side lobe level of this antenna is -14.4 dB.

6.1.3 Fr-4 As Dielectric Substrate

FR-4 is a dielectric material which is commonly used in microstrip patch antenna design in all over the world. The 'FR' in the FR-4 represents 'Flame Retardant'. It is a composite material reinforced by woven fiberglass with an epoxy resin. The incapability of absorption of water makes it a very good insulator. Moreover, this material possesses high electrical strength and flame resistance. The dielectric constant of FR-4 is 4.3. [94]

S-Parameter:

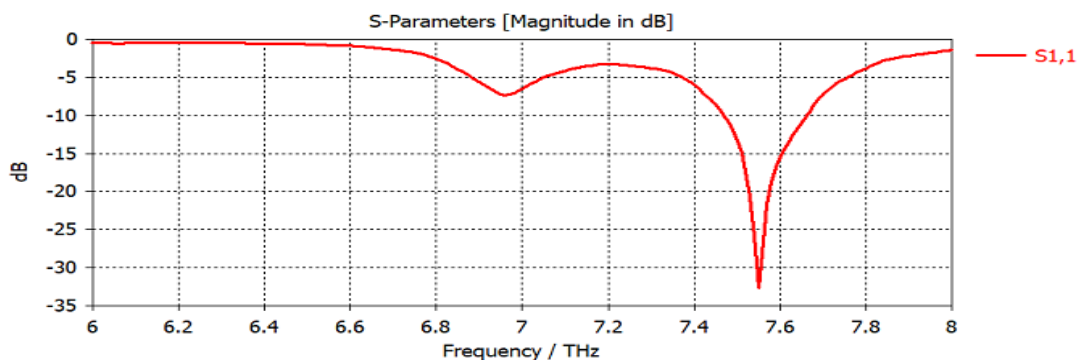


Figure 57: S Parameter for single layer graphene rectangular patch antenna using FR-4 as Substrate

From the simulation, we have a return loss of -32.71 dB at resonant frequency of 7.55 THz which is a very good value as it is in the ideal range of below -10 dB.

VSWR:

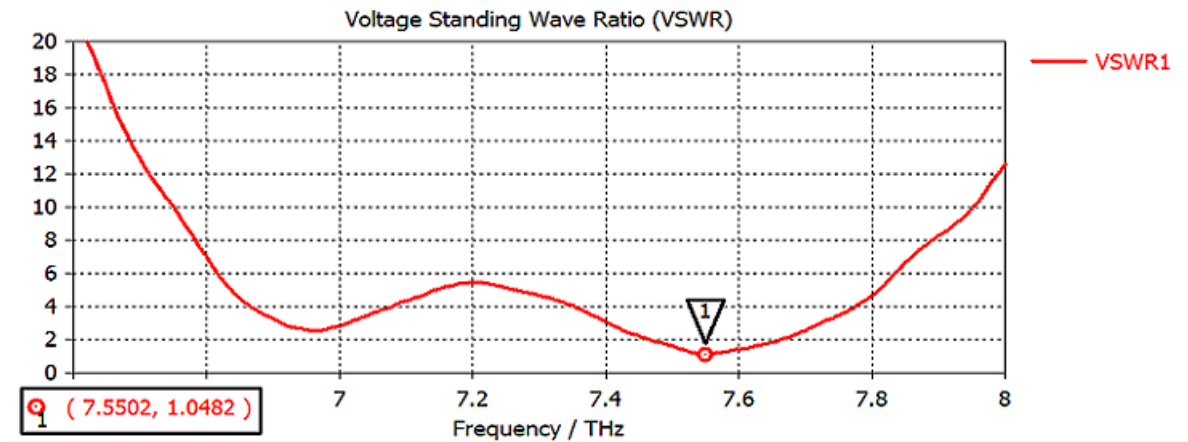


Figure 58: VSWR for single layer graphene rectangular patch antenna using FR-4 as Substrate

The Voltage Standing Wave Ratio of this design is 1.048 which is very good compared to other antenna designs as the value is closer to 1. The lower the VSWR value, the better the antenna is matched.

Radiation Pattern:

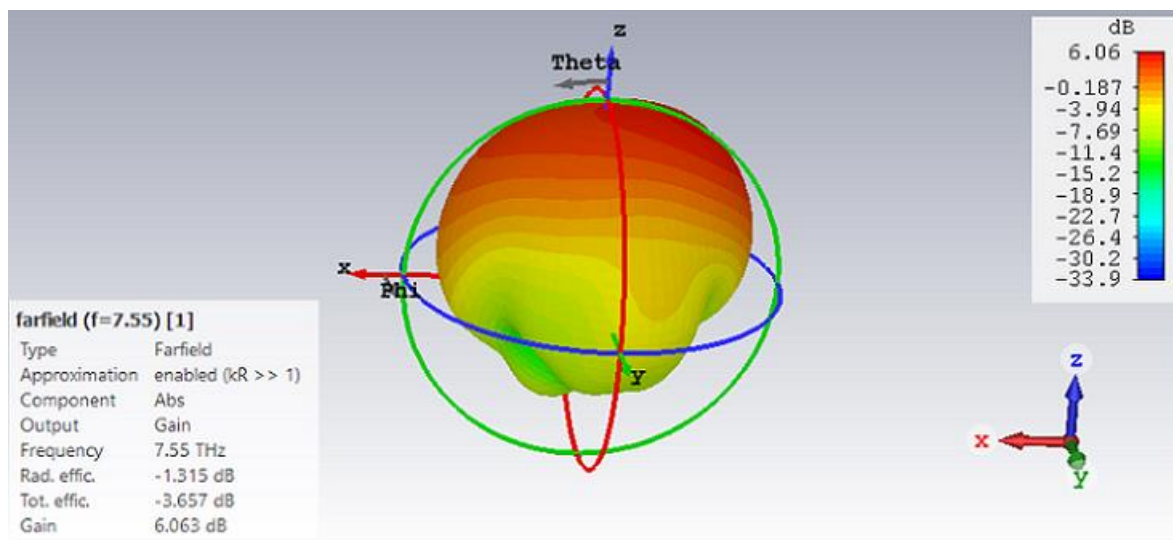


Figure 59: Radiation Pattern of single layer graphene rectangular patch antenna using FR-4 as Substrate

For FR-4 substrate, we get a gain of 6.06 dB which represents a good gain. The radiation efficiency of the antenna is -1.315 dB and the total efficiency is -3.657 dB.

Directivity:

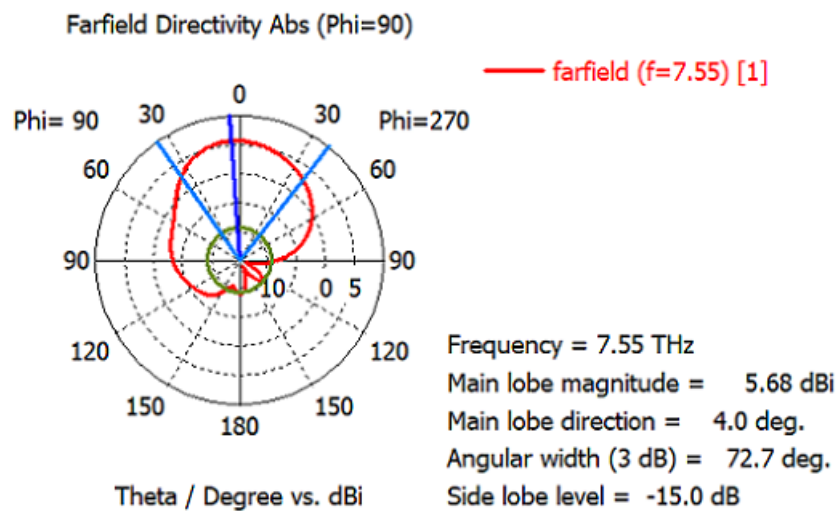


Figure 60: Polar Plot of Directivity of single layer graphene rectangular patch antenna using FR-4 as Substrate

This design provides a directivity of 5.68 dBi. The main lobe of the radiation pattern deviates by 4 degrees and has a smaller angular width of 72.7 degree. The side lobe level of the antenna is -15.0 dB.

6.1.4 Alumina (96%) as Dielectric Substrate

Alumina, commonly known as Aluminium Oxide is a progressive ceramic material which is drawing the attention of researchers all over the world for its novel characteristics such as high mechanical strength, thermal conductivity, enhance electrical insulation and exceptional corrosion resistance. These unique attributes make the material convenient to complement graphene as a material in several miniaturized wireless applications. The dielectric constant of Alumina is 9.4. [95]

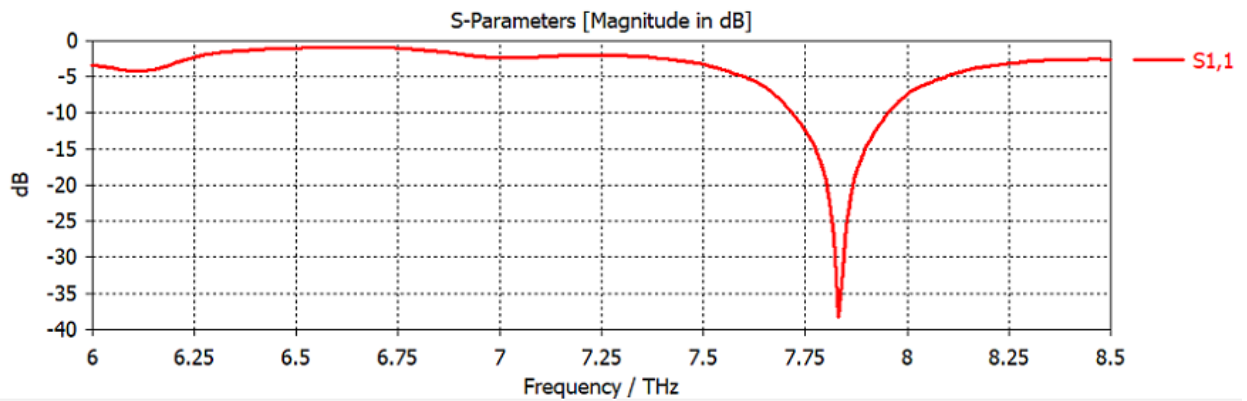
S-Parameter:

Figure 61: S Parameter for single layer graphene rectangular patch antenna using Alumina as Substrate

Using Alumina as substrate yields a return loss of -38.35 dB at 7.83 THz which is in the operating frequency range. As the s-parameter of this design is below -10 dB, the optimum result is achieved.

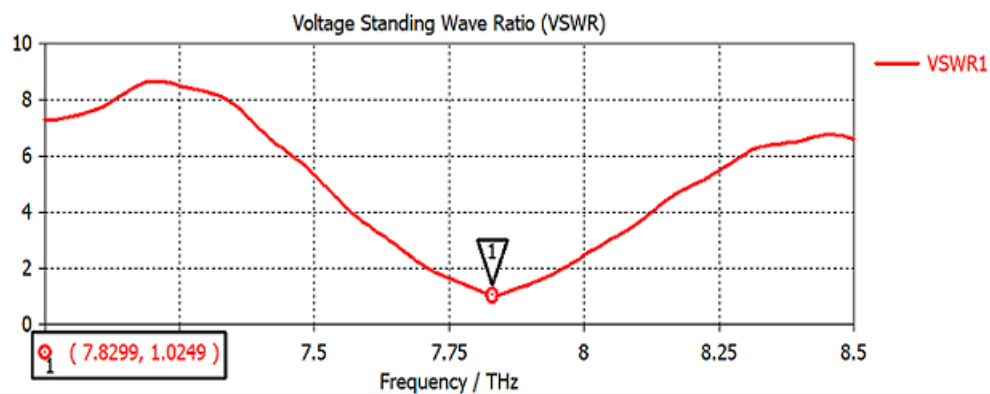
VSWR:

Figure 62: VSWR for single layer graphene rectangular patch antenna using Alumina as Substrate

From the simulation, we can see that the antenna is well matched with a voltage standing wave ratio of 1.025. VSWR of an antenna is considered to be optimum when its value is closer to 1.

Radiation Pattern:

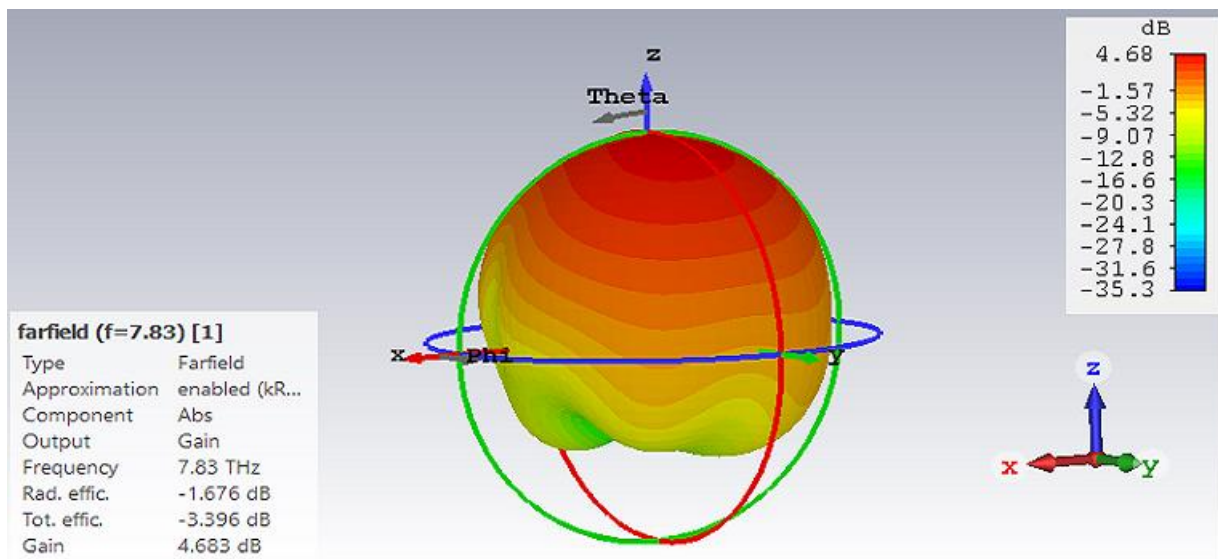


Figure 63: Radiation Pattern of single layer graphene rectangular patch antenna using Alumina as Substrate

This design provides a considerable gain of 4.68 dB. The radiation efficiency of the antenna is -1.676 dB and total efficiency is -3.396 dB.

Directivity:

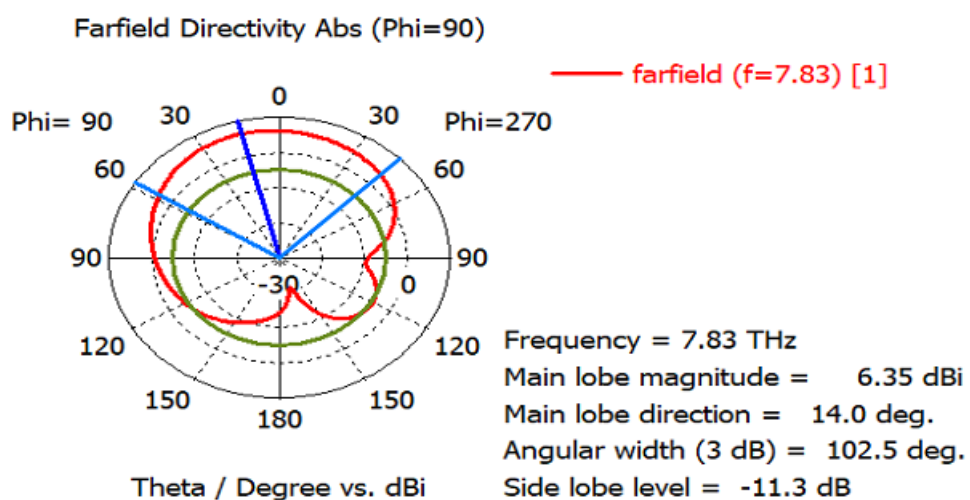


Figure 64: Polar Plot of Directivity of single layer graphene rectangular patch antenna using Alumina as Substrate

Here, the simulation shows that the antenna has a directivity of 6.35 dBi and the main lobe direction deviates by 14 degree. The angular width of the antenna is 102.5 degree and the side lobe level is -11.3 dB which is higher than the rest of the designs.

6.1.5 Comparison Among The Dielectric Substrates

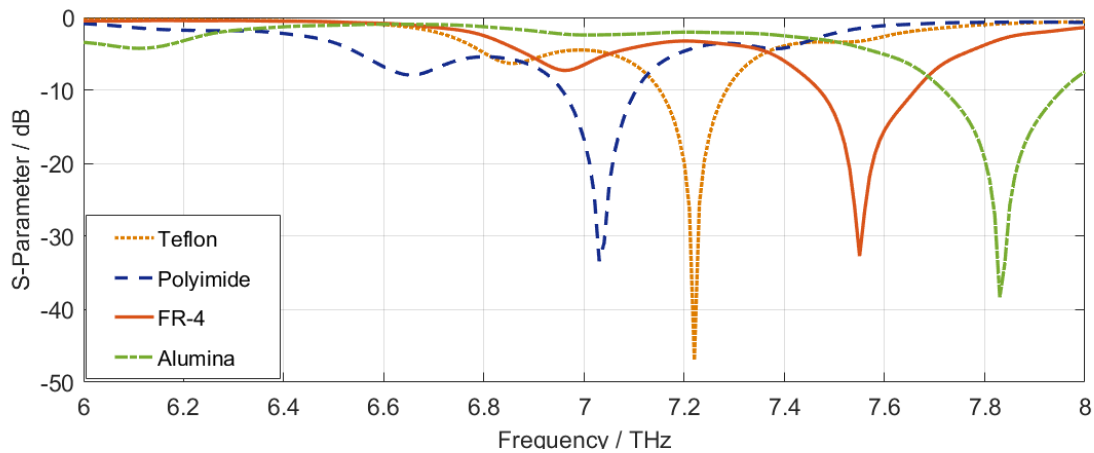


Figure 65: Comparison of s-parameter of rectangular patch antenna for different substrates

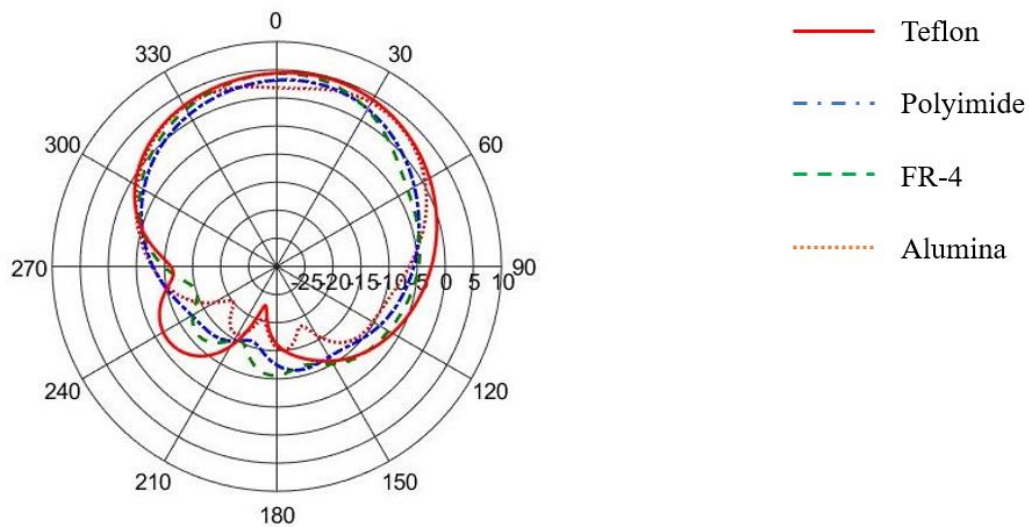


Figure 66: Polar plot of rectangular patch antenna for different substrates

Table 3: Comparison of rectangular patch antenna parameters for different substrates

Substrates	Resonant Frequency (THz)	S-Parameter(dB)	VSWR	Gain(dB)	Directivity (dBi)	Side Lobe Level(dB)
Teflon	7.22	-46.95	1.015	3.67	7.03	-18.7
Polyimide	7.03	-33.41	1.044	5.81	5.1	-14.4
FR-4	7.55	-32.71	1.048	6.06	5.68	-15
Alumina	7.83	-38.35	1.025	4.68	6.35	-11.3

The results obtained from the simulations are presented in the table above. All our designs show very good s parameter values in the desired frequency range with Teflon showing the best value of -46.95 dB. If we observe closely, we can see that as the dielectric constant of the substrate increases, the return loss increases except for the novel material alumina. A similar trend can be seen in terms of VSWR with Teflon showing the best match with a value of 1.015. Additionally, the side lobe level of the antenna increases along with the dielectric constant which is undesired as more power is drawn away from the main lobe. Moreover, the gain of the antenna increases with the dielectric constant of the substrate with alumina being the exception. In terms of gain, using FR-4 as a substrate yields the best result of 6.06 dB. Finally, we can see that all the designs provide good directivity values which is an important parameter in antenna design. From the analysis, we can notice that Teflon which has the lowest dielectric constant among all the substrates, shows the optimum antenna parameters and best performance with only gain being the exception but it can be compromised for a very low side lobe level.

6.2 Single Layer Graphene Circular Microstrip Antenna

The figure of single layer graphene circular microstrip antenna is given below:

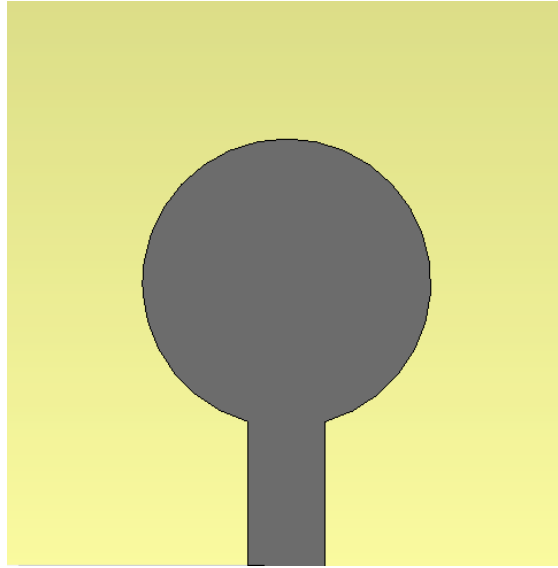


Figure 67: Single Layer Graphene Circular Patch Antenna

The parameters of single layer graphene circular microstrip antenna are given below:

Table 4: Parameters of Single Layer Graphene Circular Patch Antenna

Parameter	Values (in μm)
Substrate Length	35
Substrate Width	35
Substrate Height	1.5
Radius of the patch	8.9
Patch Thickness	0.000345
Feed Line Width	4.79

6.2.1 TEFLON AS DIELECTRIC SUBSTRATE

S-Parameter:

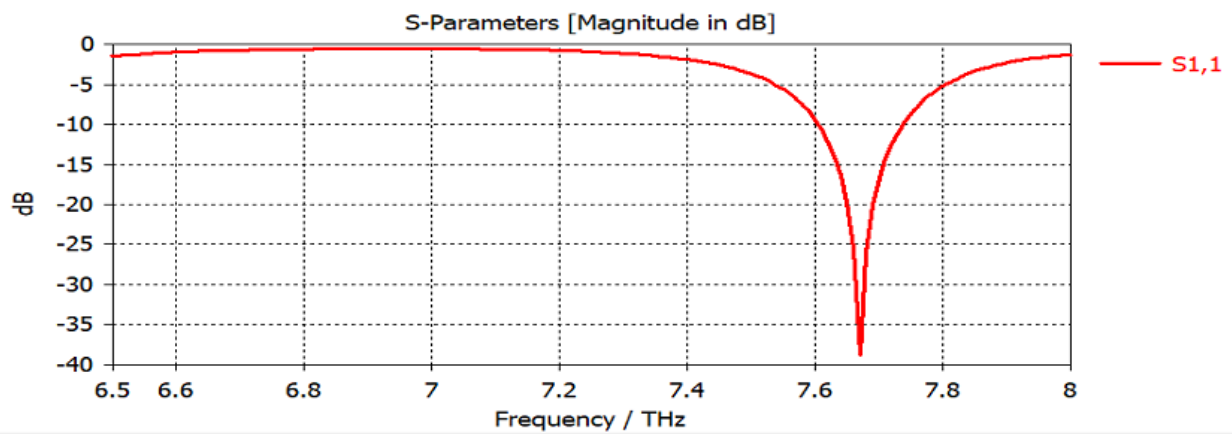


Figure 68: S Parameter for single layer graphene circular patch antenna using Teflon as Substrate

Here, the S-Parameter which represents the return loss of the antenna is -38.88 dB at 7.67 THz. It is a very good return loss as the value is below -10 dB.

VSWR:

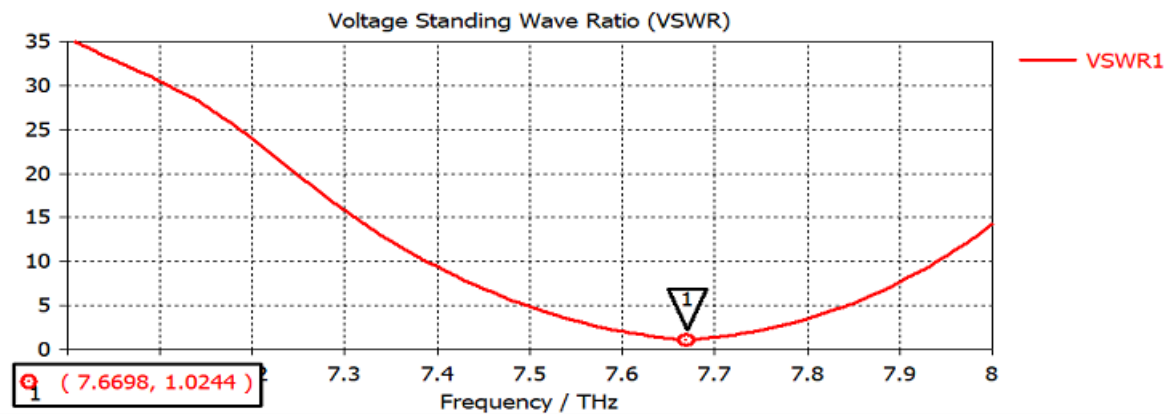


Figure 69: VSWR for single layer graphene circular patch antenna using Teflon as Substrate

The voltage standing wave ratio for this antenna is 1.024. We should always aim to make our VSWR as close to 1 as possible as it is the optimum result for VSWR.

Radiation Pattern:

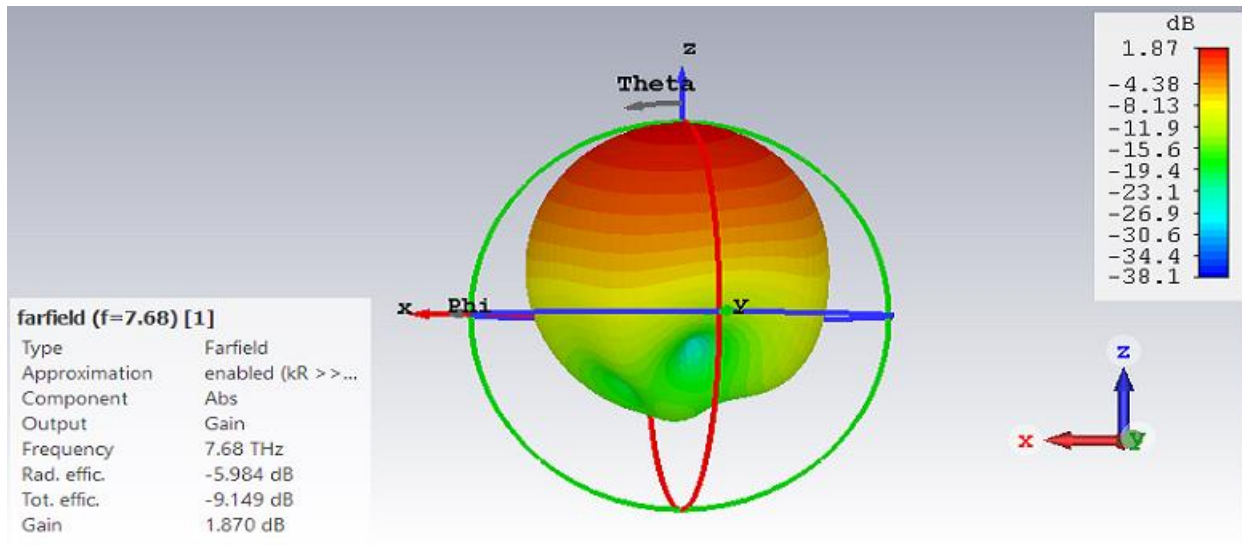


Figure 70: Radiation Pattern of single layer graphene circular patch antenna using Teflon as Substrate

From the simulation, we can see that the gain of the antenna is 1.87 dB. The radiation efficiency of the antenna is -5.984 dB and the total efficiency is -9.149 dB.

Directivity:

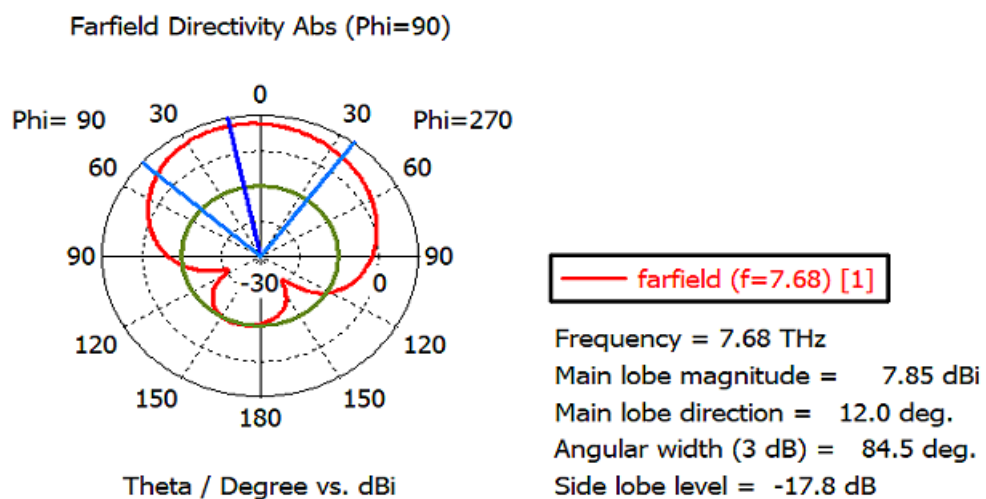


Figure 71: Polar Plot of Directivity of single layer graphene circular patch antenna using Teflon as Substrate

The antenna has a directivity of 7.85 dBi which signifies how much directive the antenna is. The main lobe deviates by 12.0 degree and the angular width of the lobe is 84.5 degree. The antenna has a good side lobe level of -17.8 dB.

6.2.2 Polyimide as Dielectric Substrate

S-Parameter:

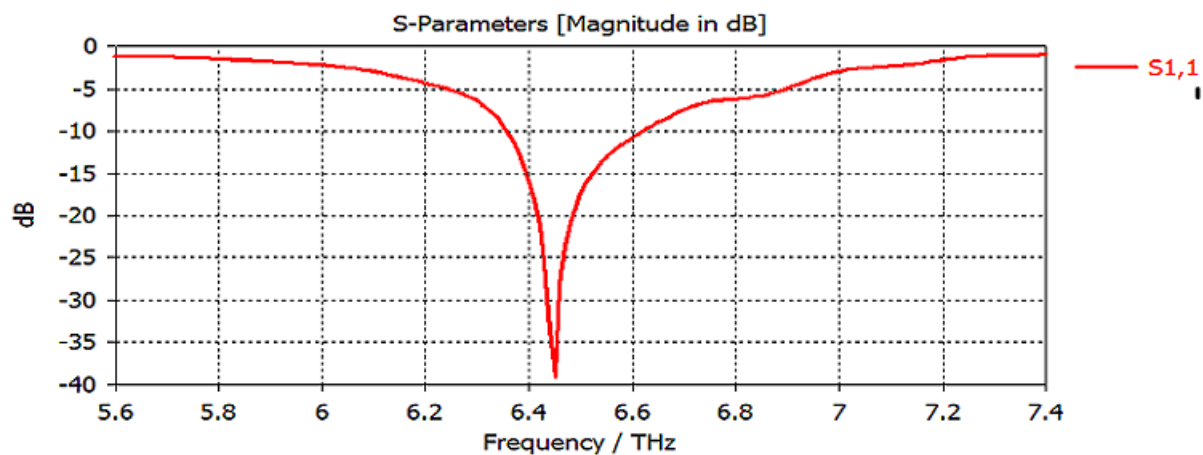


Figure 72: S Parameter for single layer graphene circular patch antenna using Polyimide as Substrate

The return loss of this antenna is -39.05 dB at the resonant frequency of 6.45 THz. Any s-parameter value less than -10 dB is considered to be a very good return loss for the antenna.

VSWR:

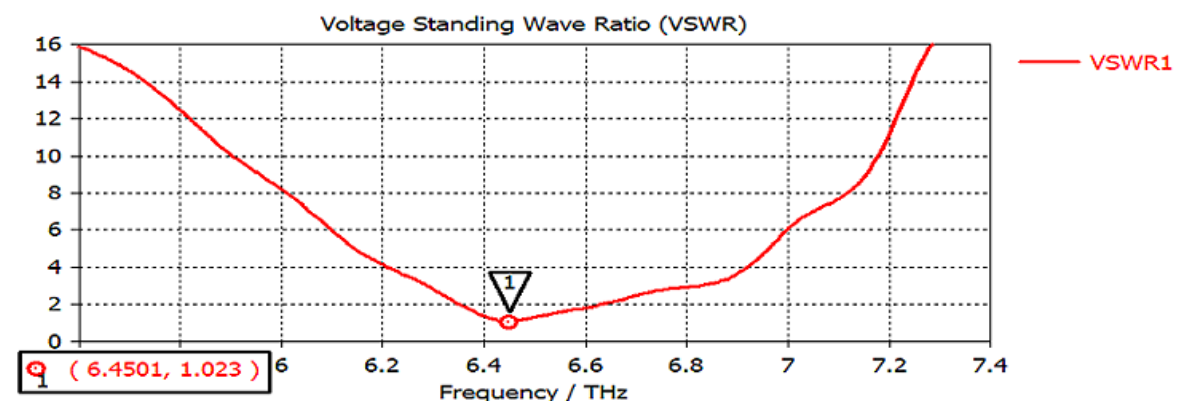


Figure 73: VSWR for single layer graphene circular patch antenna using Polyimide as Substrate

The voltage standing wave ratio for this antenna is 1.023. We should always aim to make our VSWR as close to 1 as possible as it is the optimum result for VSWR.

Radiation Pattern:

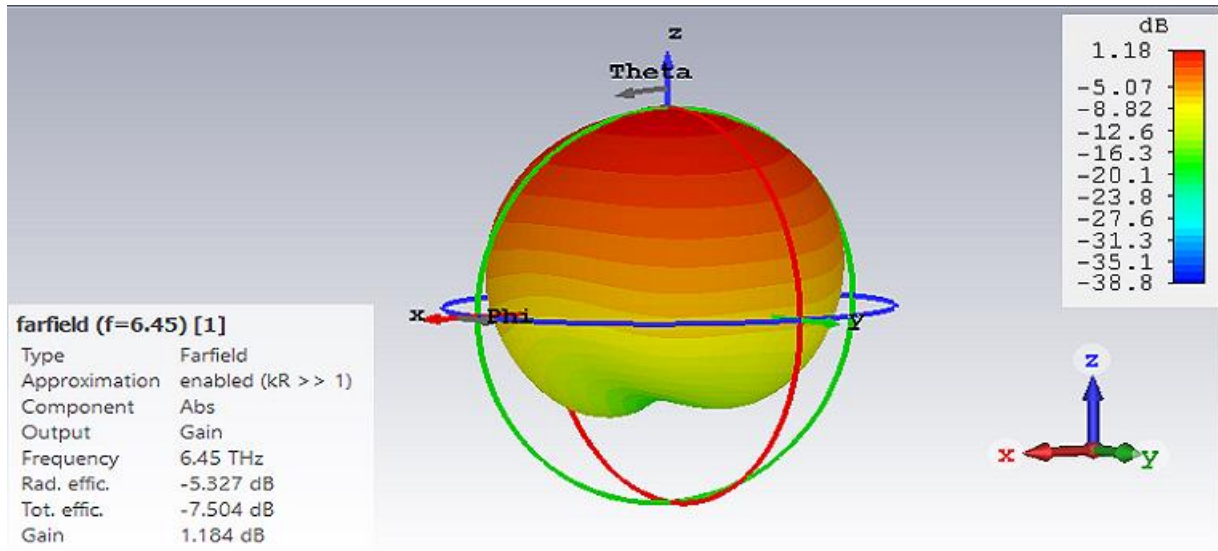


Figure 74: Radiation Pattern of single layer graphene circular patch antenna using Polyimide as Substrate

The gain of the antenna is 1.18 dB. The radiation efficiency of the antenna is -5.327 dB and the total efficiency is -7.504 dB.

Directivity:

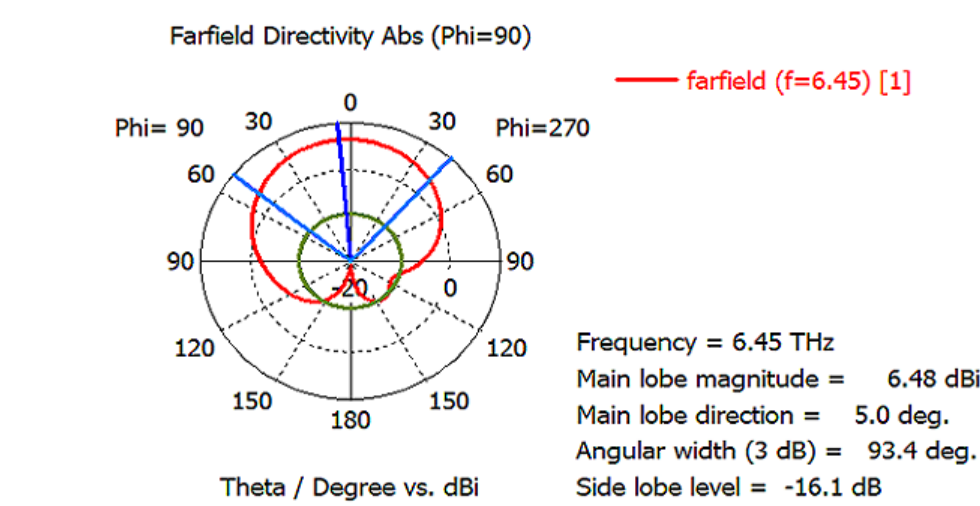


Figure 75: Polar Plot of Directivity of single layer graphene circular patch antenna using Polyimide as Substrate

This design has a directivity of 6.48 dBi which is good compared to other antenna designs. The angular width is 93.4 degree and the main lobe deviates by 5.0 degree. The antenna has a considerable side lobe level of -16.1 dB.

6.2.3 Fr-4 As Dielectric Substrate

S-Parameter:

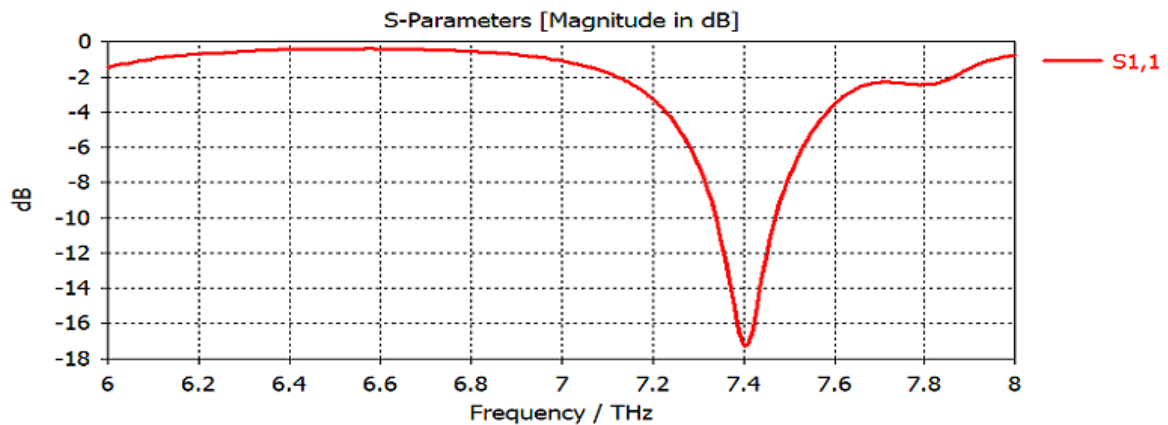


Figure 76: S Parameter for single layer graphene circular patch antenna using FR-4 as Substrate

For this design, we get a return loss value of -17.32 dB at resonant frequency of 7.4 THz. The s-parameter for FR-4 substrate is comparatively less than other designs though the value is well below the -10dB optimum range.

VSWR:

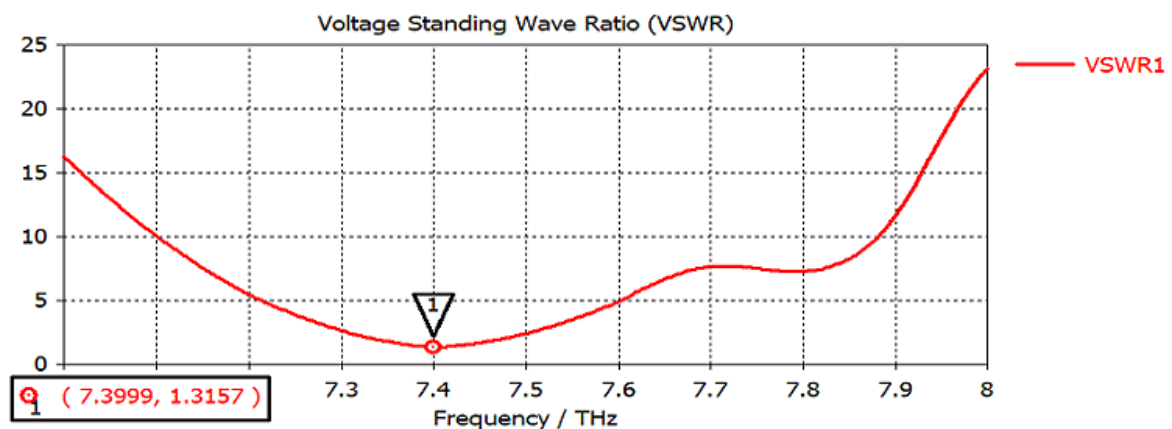


Figure 77: VSWR for single layer graphene circular patch antenna using FR-4 as Substrate

From the simulation, we can see that using FR-4 as substrate provides a standing wave ratio of 1.315 which is comparatively better than other antenna designs.

Radiation Pattern:

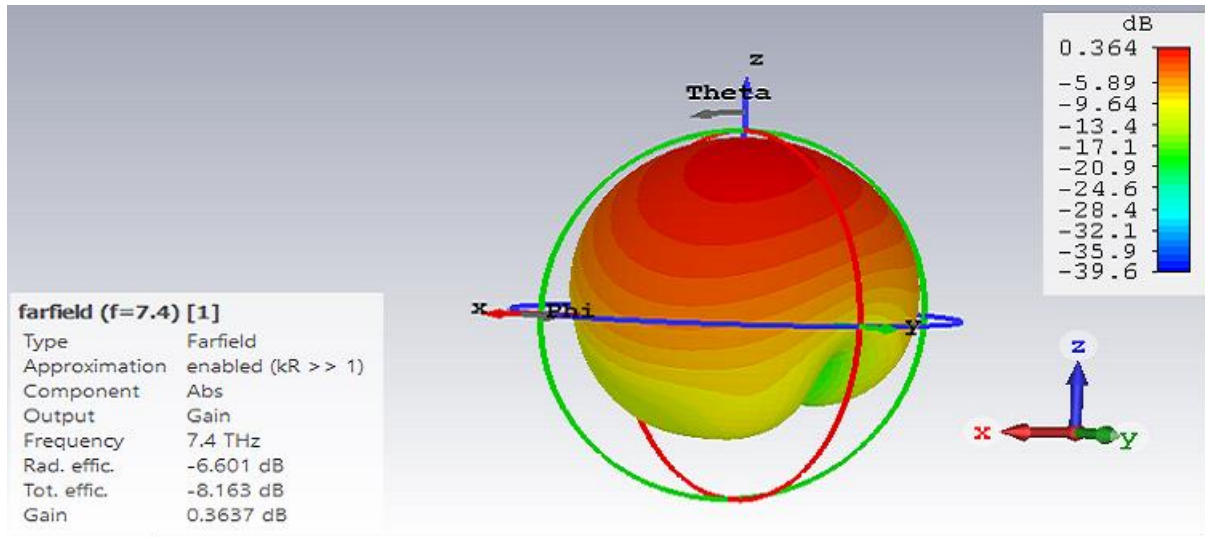


Figure 78: Radiation Pattern of single layer graphene circular patch antenna using FR-4 as Substrate

Here, we get a gain of 0.364 dB which is low compared to other antenna designs. For better antenna performance, the gain should be as high as possible. The radiation efficiency is -6.601 dB and total efficiency is -8.163 dB which are lower than other antenna designs.

Directivity:

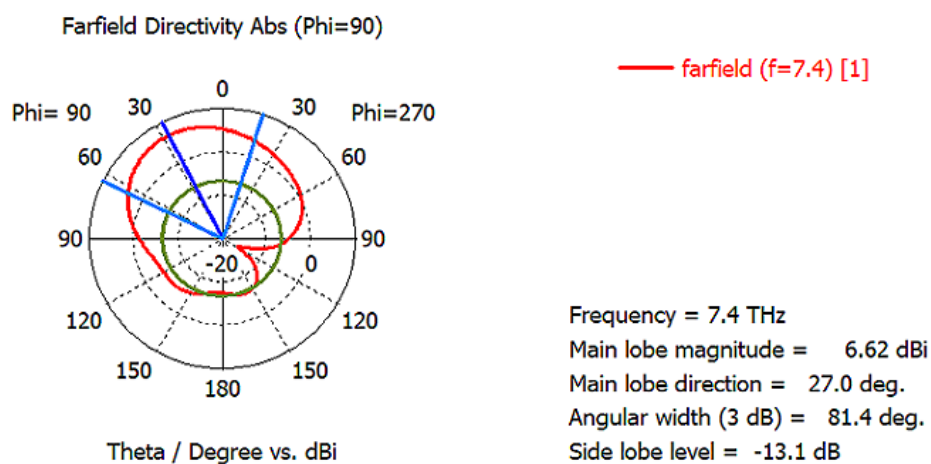


Figure 79: Polar Plot of Directivity of single layer graphene circular patch antenna using FR-4 as Substrate

From the simulation, we can see that the antenna has a directivity of 6.62 dBi with the deviation of main lobe direction by 27.0 degree. The angular width is 81.4 degree and the side lobe level is higher with the value of -13.1 dB.

6.2.4 Alumina (96%) As Dielectric Substrate

S-Parameter:

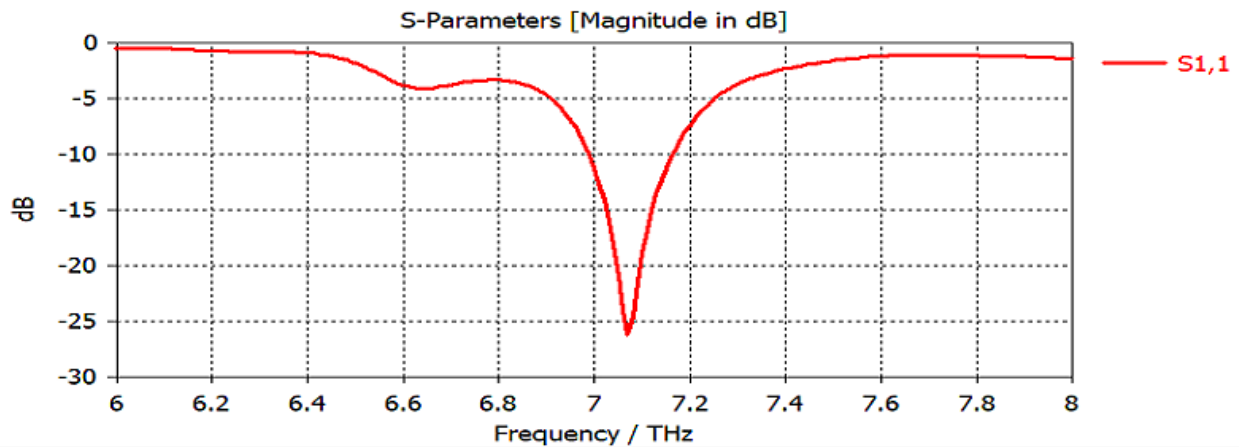


Figure 80: S Parameter for single layer graphene circular patch antenna using Alumina as Substrate

The return loss of the antenna is -26.2 dB at 7.07 THz. This design provides a good s-parameter value as it is below -10 dB.

VSWR:

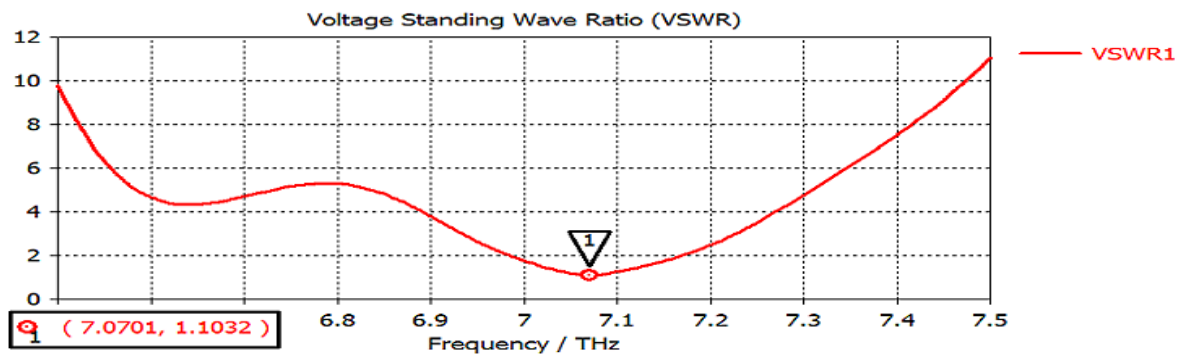


Figure 81: VSWR for single layer graphene circular patch antenna using Alumina as Substrate

From the simulation, we can see that using Alumina as substrate provides a standing wave ratio of 1.103 which is very good as the value is closer to the ideal value of 1.

Radiation Pattern:

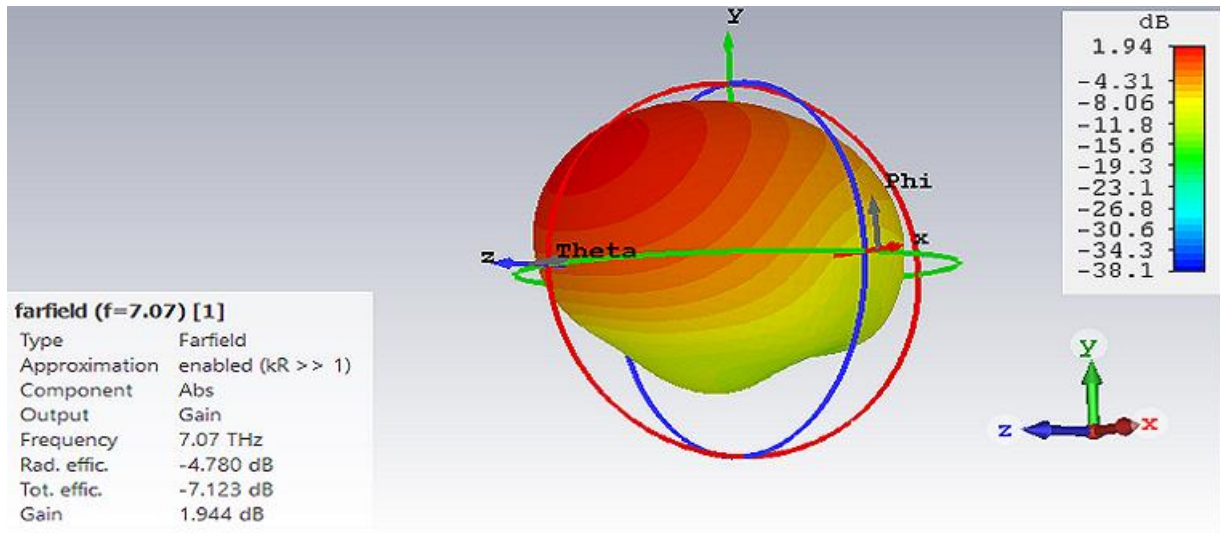


Figure 82: Radiation Pattern of single layer graphene circular patch antenna using Alumina as Substrate

This design provides a gain of 1.94 dB at 7.07 THz. The antenna has a radiation efficiency of -4.780 dB and a total efficiency of -7.123 dB.

Directivity:

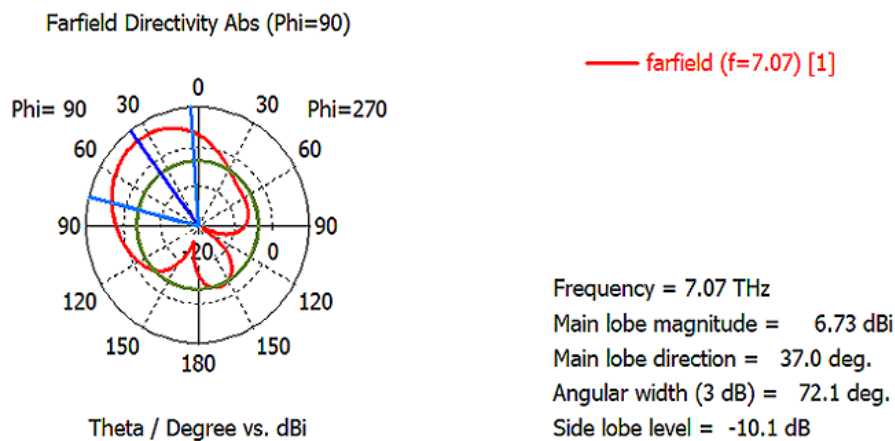


Figure 83: Polar Plot of Directivity of single layer graphene circular patch antenna using Alumina as Substrate

Here, the simulation shows that the antenna has a directivity of 6.73 dBi with the direction of the main lobe deviating by 37.0 degree. This design produces an angular width of 72.1 which ensures more directivity. Although, the antenna produces a higher side lobe level of -10.1 dB.

6.2.5 Comparison Among the Dielectric Substrates

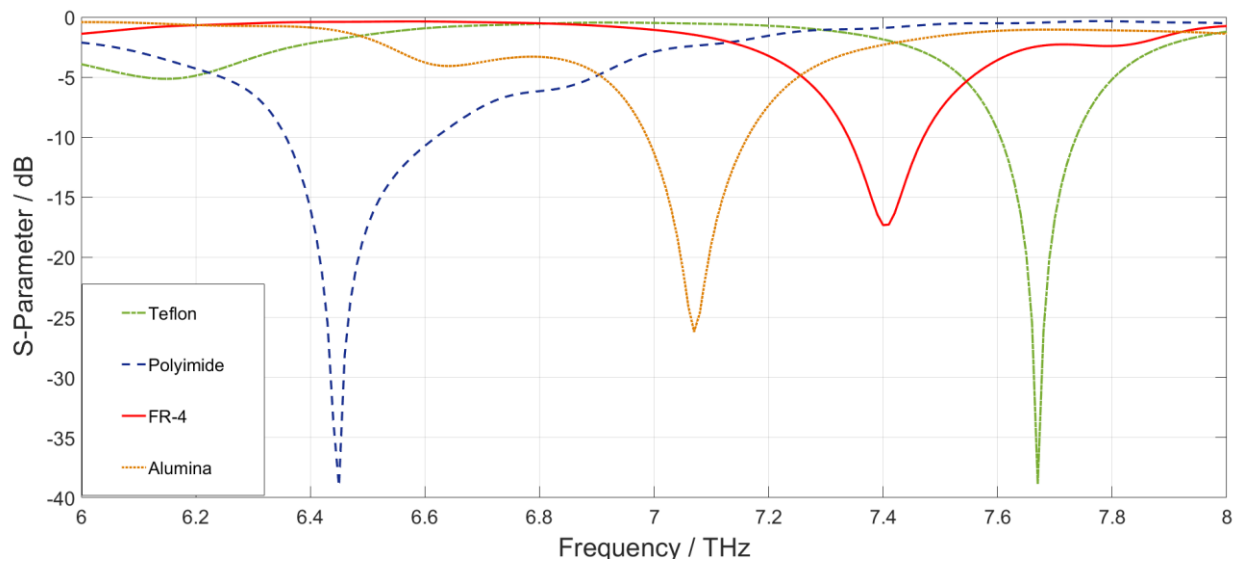


Figure 84: Comparison of s-parameter of circular patch antenna for different substrates

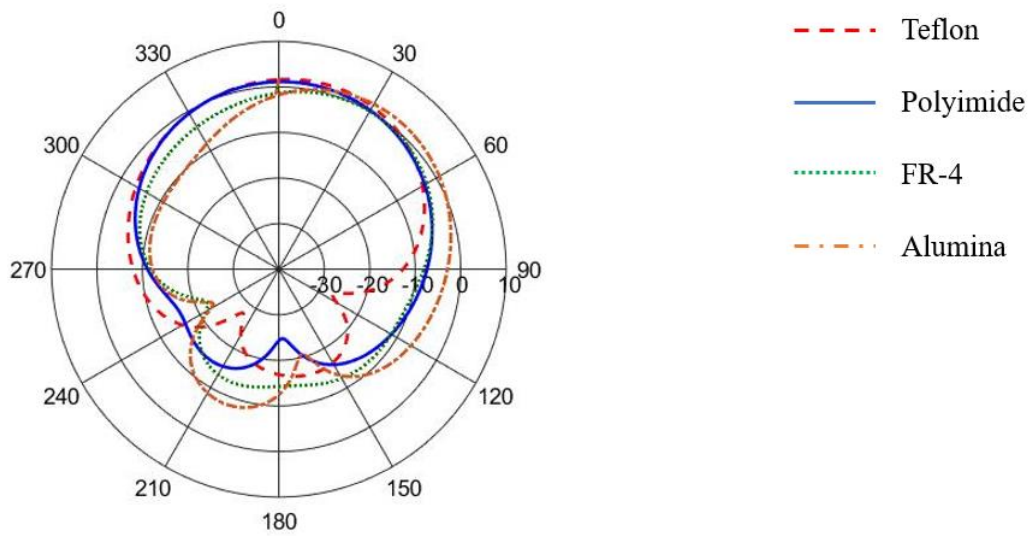


Figure 85: Polar plot of circular patch antenna for different substrates

Table 5: Comparison of circular patch antenna parameters for different substrates

Substrates	Resonant Frequency (THz)	S-Parameter(dB)	VSWR	Gain(dB)	Directivity (dBi)	Side Lobe Level(dB)
Teflon	7.67	-38.88	1.024	1.87	7.85	-17.8
Polyimide	6.45	-39.05	1.023	1.18	6.48	-16.1
FR-4	7.4	-17.32	1.315	0.364	6.62	-13.1
Alumina	7.07	-26.2	1.103	1.94	6.73	-10.1

The results obtained from all the simulated designs of circular patch antennas are provided in the table above. In terms of return loss, all the substrates yield good s parameter value with all the values being below -20 dB except FR-4 substrate whose return loss is a little bit higher than other antennas with a value of -17.32 dB. Voltage Standing Wave Ratio is an important parameter for antenna as it measures the amount of mismatch between the antenna and the feedline and all our designs provide ideal VSWR values of around 1. Moreover, the gain of the circular patch antennas is considerably low for all the dielectric materials with Alumina providing the highest gain of 1.94 dB. Directivity is another important parameter and all our designs show good directivity while using Teflon as a substrate produces the best directivity of 7.85 dBi. Lastly, the side lobe level increases with the increase of the dielectric constant of the substrate material. The antenna with Teflon as substrate produces the best side lobe level of -17.8 dB and alumina being the substrate material provides the highest side lobe level of -10.1 dB which is undesirable. Analysing all the antenna parameters for different substrate materials, it is safe to say that Teflon provides the best results among all the substrate materials for most of the antenna parameters.

6.3 Single Layer Graphene Triangular Microstrip Antenna

The figure of single layer graphene triangular microstrip antenna is given below:

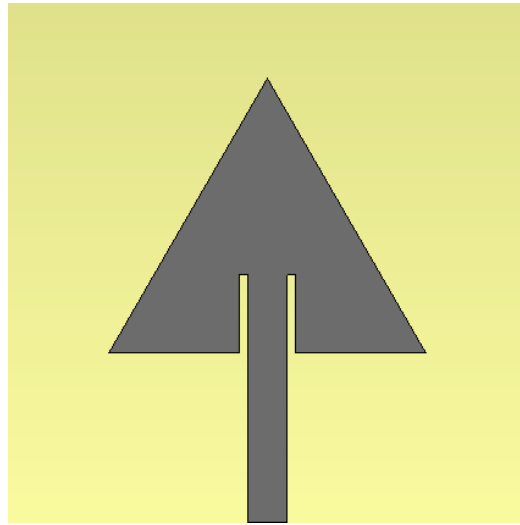


Figure 86: Single Layer Graphene Triangular Patch Antenna

The parameters of single layer graphene triangular microstrip antenna are given below:

Table 6: Parameters of Single Layer Graphene Triangular Patch Antenna

Parameter	Values (in μm)
Substrate Length	60
Substrate Width	60
Substrate Height	1.5
Side length of the patch	21.72
Patch Thickness	0.000345
Feed Line Width	4.79

6.3.1 Teflon As Dielectric Substrate

S-Parameter:

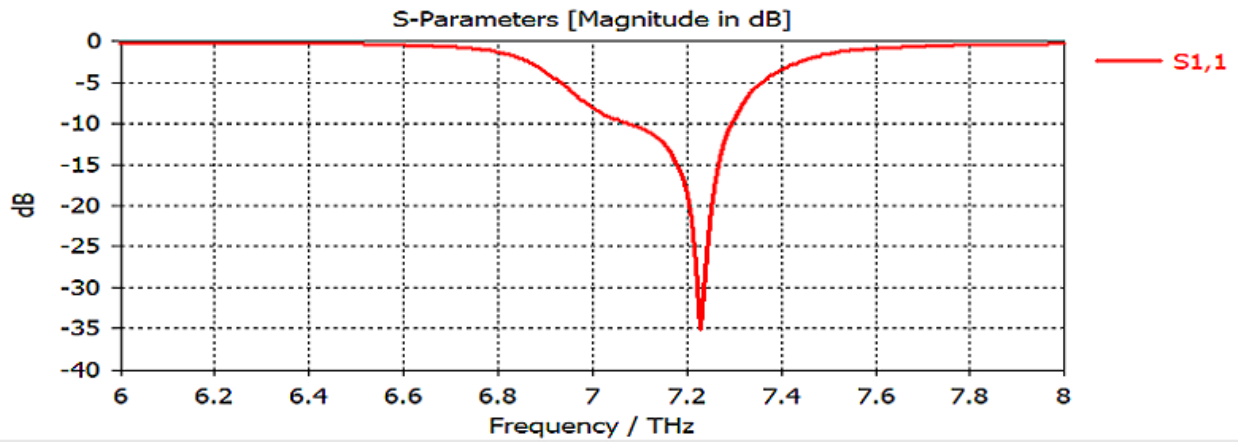


Figure 87: S Parameter for single layer graphene triangular patch antenna using Teflon as Substrate

For Teflon, we get a very good return loss of -35.04 dB at 7.23 THz which is in the operating frequency range. Return loss of an antenna is regarded as a good when the value of s parameter is lower than -10 dB.

VSWR:

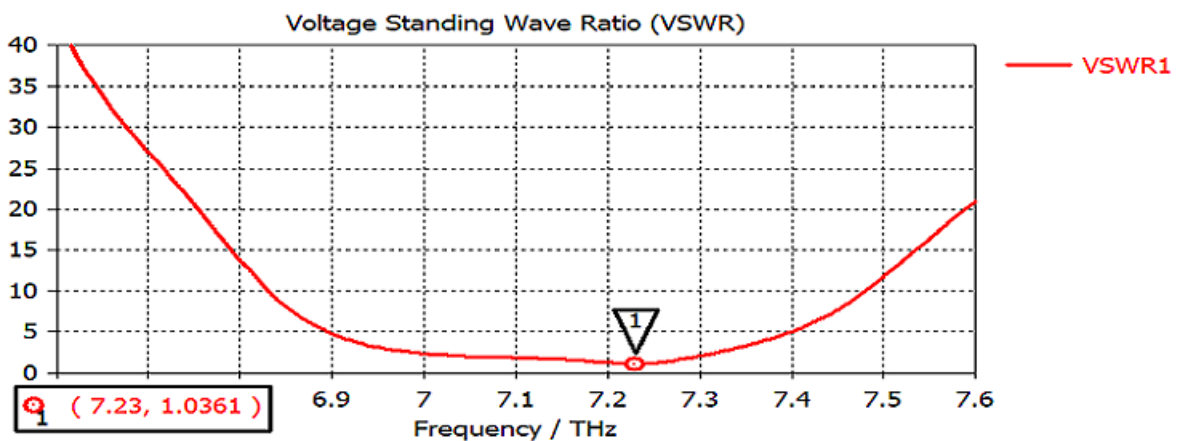


Figure 88: VSWR for single layer graphene triangular patch antenna using Teflon as Substrate

The Voltage Standing Wave Ratio of this design is 1.036, which is very good compared to other antenna designs as the value is closer to 1. The lower the value of VSWR, the better the antenna is matched.

Radiation Pattern:

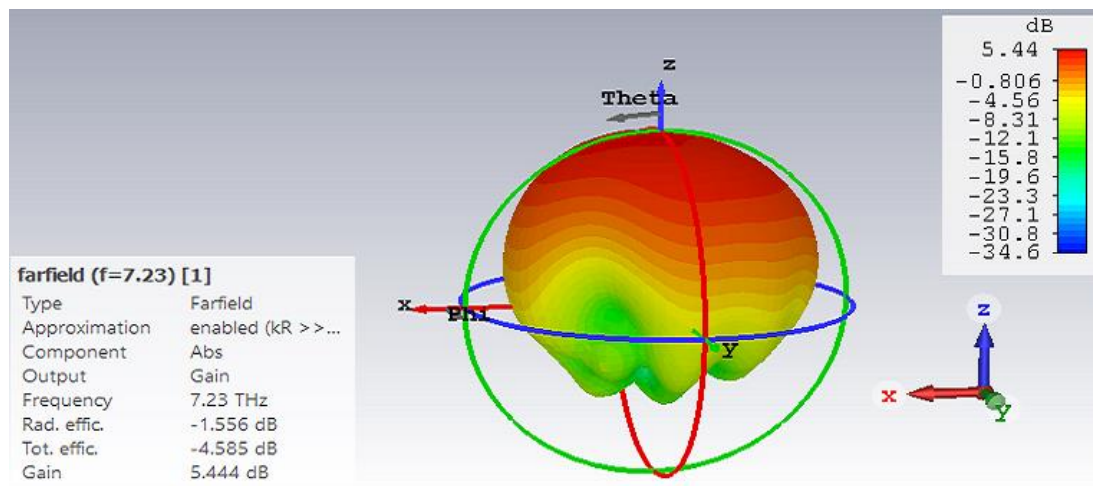


Figure 89: Radiation Pattern of single layer graphene triangular patch antenna using Teflon as Substrate

The designed antenna shows a very good gain of 5.44 dB at the desired frequency. Moreover, this design yields a very good radiation efficiency of -1.556 dB and total efficiency of -4.585 dB.

Directivity:

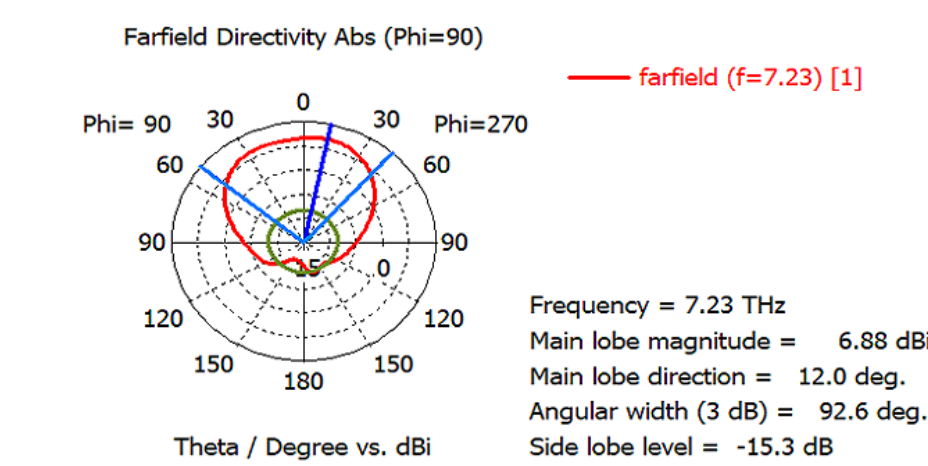


Figure 90: Polar Plot of Directivity of single layer graphene triangular patch antenna using Teflon as Substrate

From the simulation, we can see that the antenna has a directivity of 6.88 dBi with main lobe direction deviating by 12.0 degree and angular width of 92.6 degree. The side lobe level of this antenna is considerably good at -15.3 dB.

6.3.2 Polyimide as Dielectric Substrate

S-Parameter:

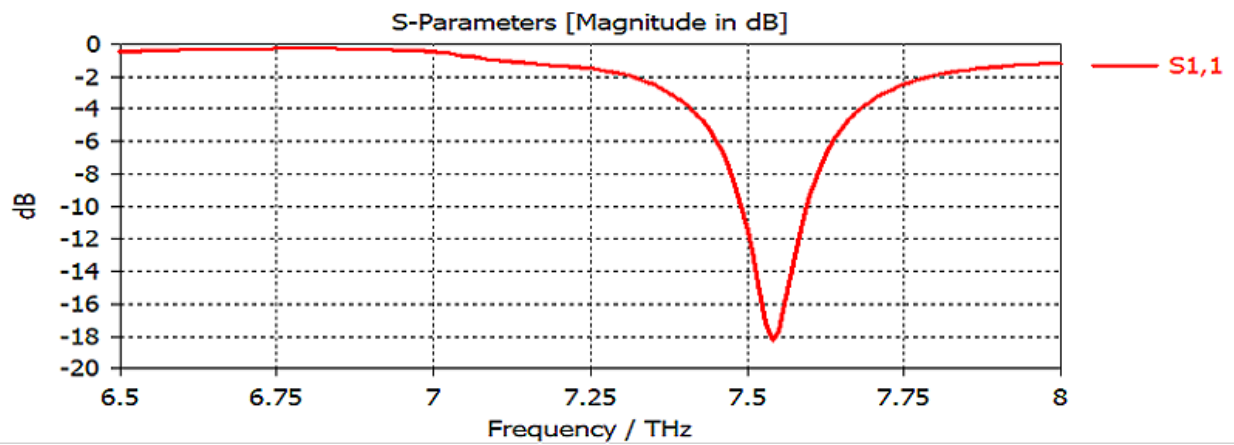


Figure 91: S Parameter for single layer graphene triangular patch antenna using Polyimide as Substrate

From the simulation, we have a return loss of -18.28 dB at resonant frequency of 7.54 THz which is an acceptable value as it is in the ideal range of below -10 dB.

VSWR:

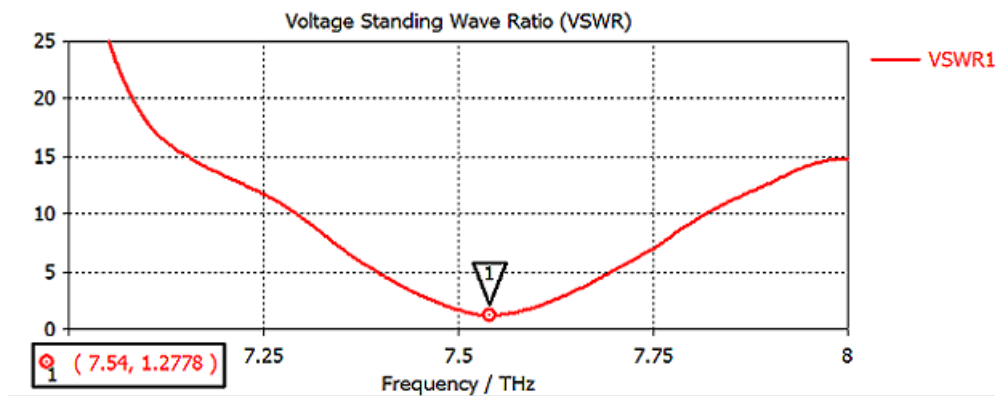


Figure 92: VSWR for single layer graphene triangular patch antenna using Polyimide as Substrate

The voltage standing wave ratio for this antenna is 1.277. We should always aim to make our VSWR as close to 1 as possible as it is the optimum result for VSWR.

Radiation Pattern:

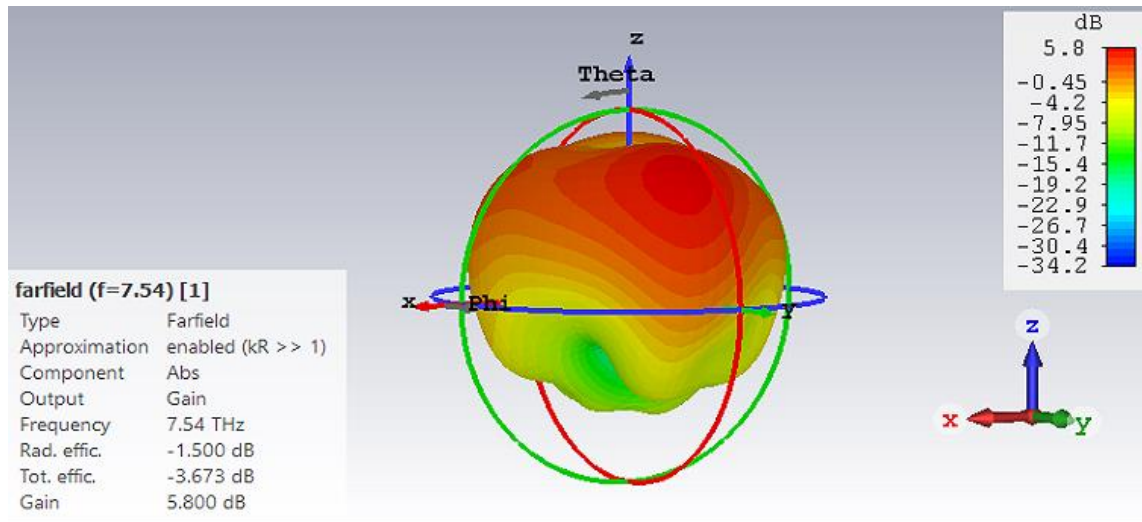


Fig 93: Radiation Pattern of single layer graphene triangular patch antenna using Polyimide as Substrate

The gain of the antenna is 5.8 dB. Moreover, the antenna provides a very good radiation efficiency of -1.5 dB dB and the total efficiency of -3.673 dB.

Directivity:

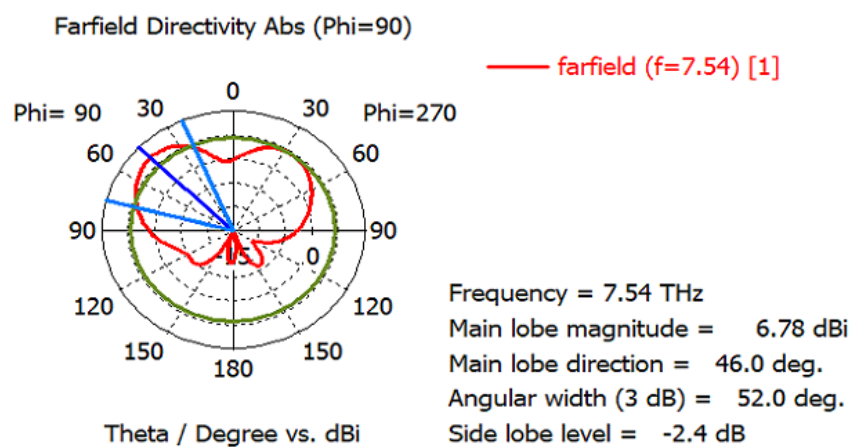


Figure 94: Polar Plot of Directivity of single layer graphene triangular patch antenna using Polyimide as Substrate

From the simulation, we can see that the antenna has a very good directivity of 6.78 dBi. The main lobe direction deviates by 52.0 degree. The angular is 52.0 degree which shows how directive the antenna is. However, the side lobe level for the antenna is -2.4 dB which is very high and unacceptable as more power is drawn away from the main lobe.

6.3.3 Fr-4 as Dielectric Substrate

S-Parameter:

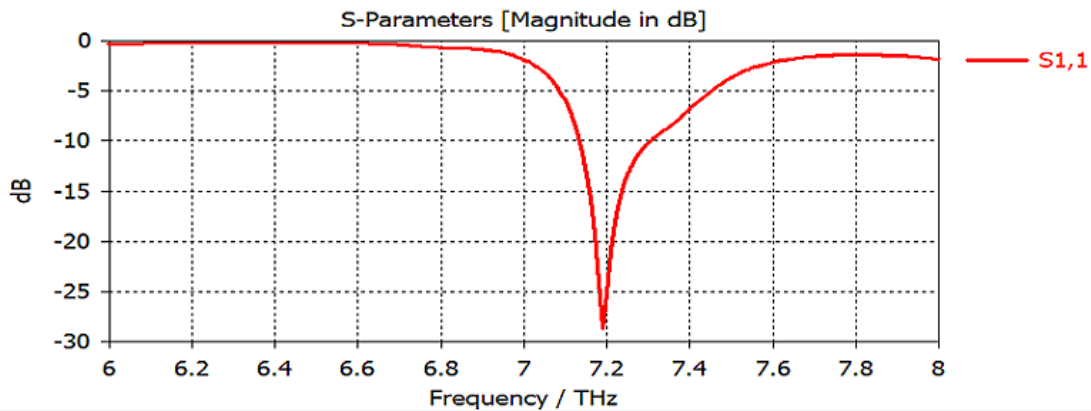


Figure 95: S Parameter for single layer graphene triangular patch antenna using FR-4 as Substrate

Here, the S-Parameter which represents the return loss of the antenna is -28.70dB at 7.19 THz. It is a very good return loss as the value is below -10 dB.

VSWR:

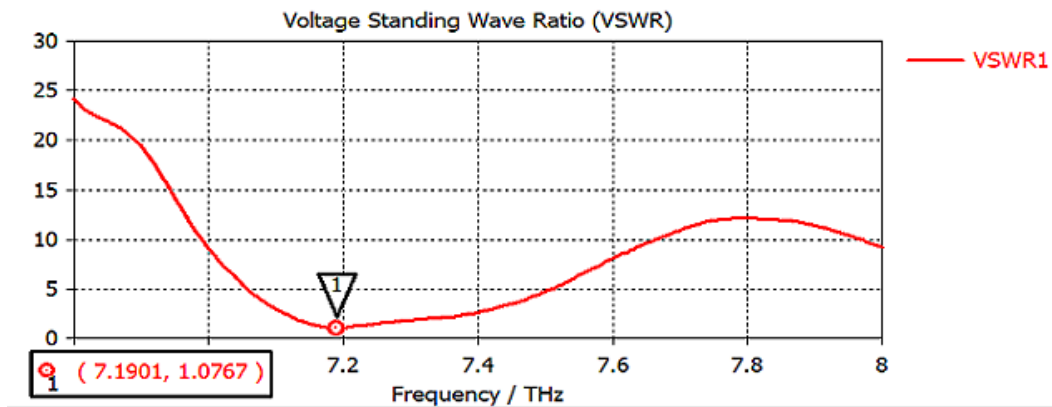


Figure 96: VSWR for single layer graphene triangular patch antenna using FR-4 as Substrate

The voltage standing wave ratio for this antenna is 1.076. We should always aim to make our VSWR as close to 1 as possible as it is the optimum result for VSWR.

Radiation Pattern:

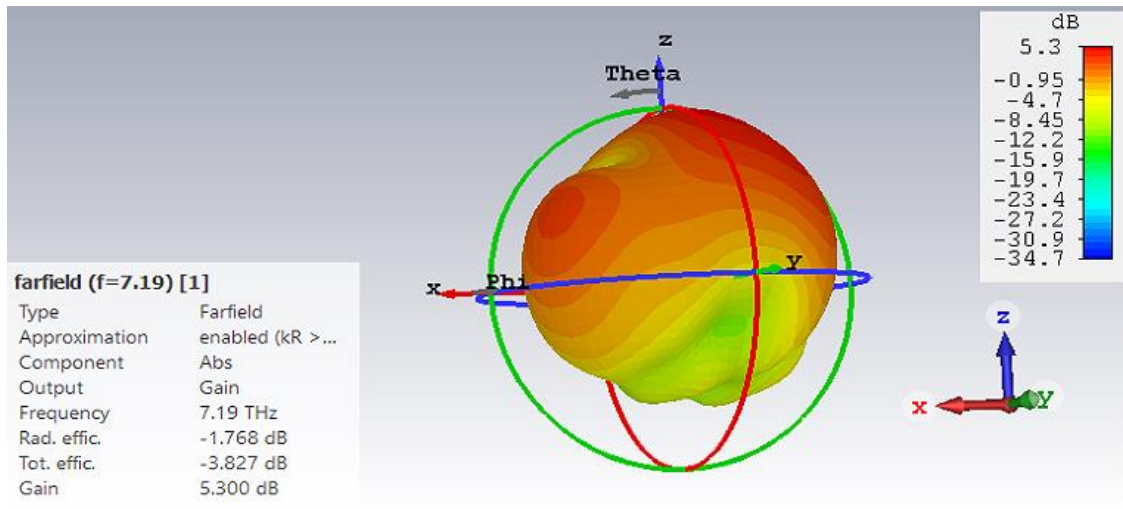


Figure 97: Radiation Pattern of single layer graphene triangular patch antenna using FR-4 as Substrate

From the simulation, we can see that the antenna provides a gain of 5.3 dB which is good compared to other designs. The antenna has a very good radiation efficiency of -1.768 dB and total efficiency of -3.827 dB.

Directivity:

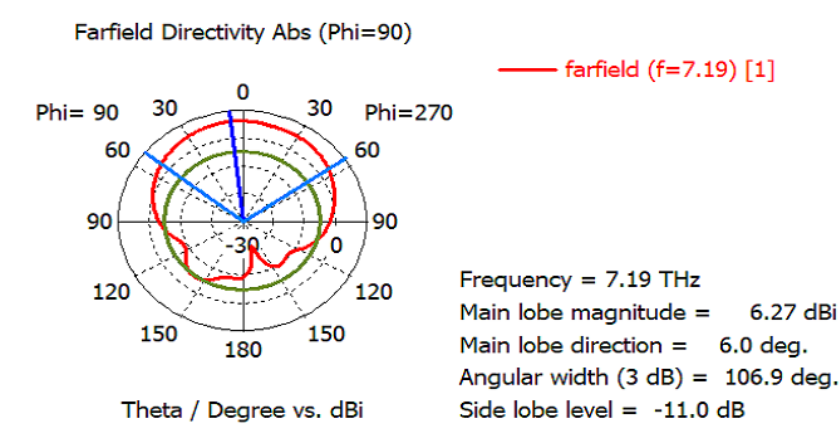


Figure 98: Polar Plot of Directivity of single layer graphene triangular patch antenna using FR-4 as Substrate

From the simulation, we can see that the antenna has a directivity of 6.27 dBi with the deviation of main lobe direction by 6.0 degree. The angular width is 106.9 degree and the side lobe level is higher with the value of -11.0 dB.

6.3.4 Alumina (96%) as Dielectric Substrate

S-Parameter:

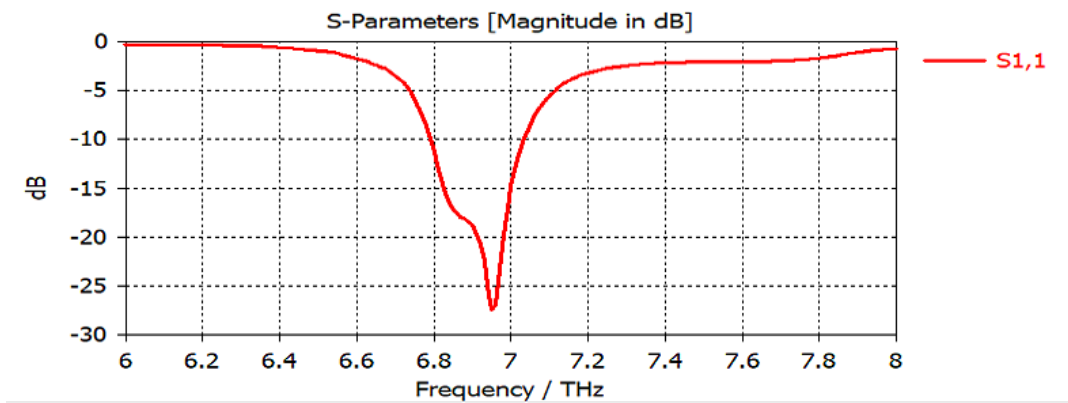


Figure 99: S Parameter for single layer graphene triangular patch antenna using Alumina as Substrate

Using Alumina as substrate yields a return loss of -27.5 dB at 6.95 THz which is in the operating frequency range. As the s-parameter of this design is below -10 dB, the optimum result is achieved.

VSWR:

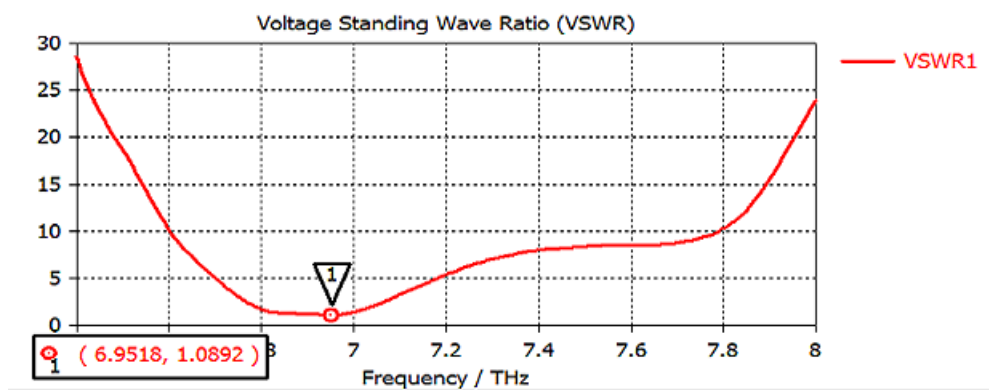


Figure 100: VSWR for single layer graphene triangular patch antenna using Alumina as Substrate

From the simulation, we can see that using Alumina as substrate provides a standing wave ratio of around 1.089 which is very good as the value is closer to the ideal value of 1.

Radiation Pattern:

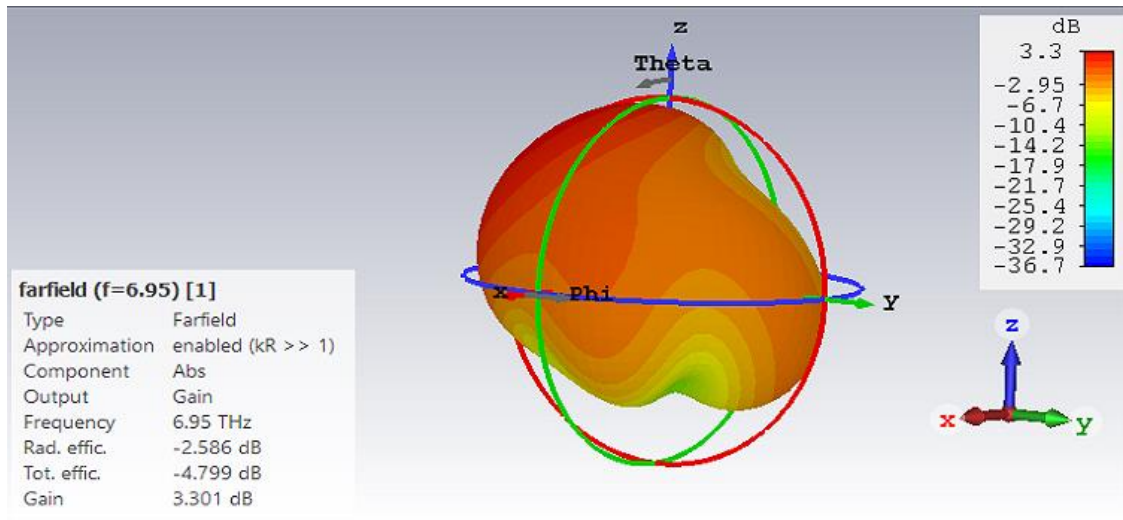


Figure 101: Radiation Pattern of single layer graphene triangular patch antenna using Alumina as Substrate

This design yields a gain of 3.3 dB which is decent. The antenna provides a good radiation efficiency of -2.586 dB and total efficiency of -4.799 dB.

Directivity:

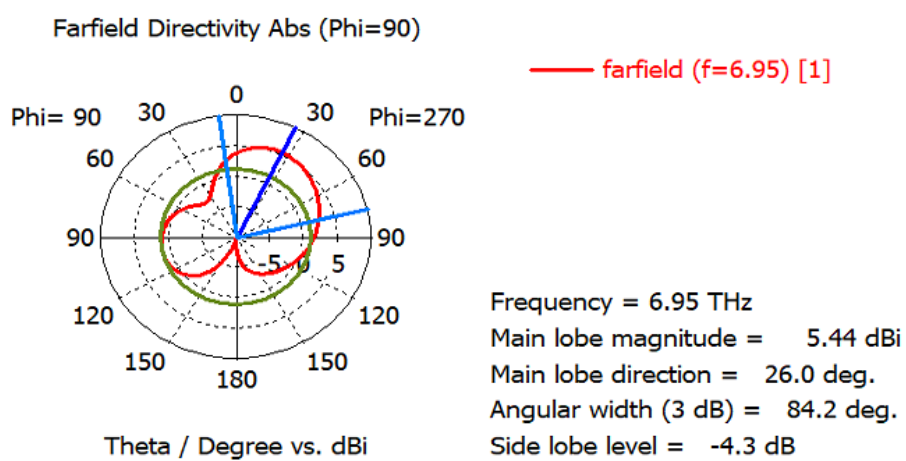


Figure 102: Polar Plot of Directivity of single layer graphene triangular patch antenna using Alumina as Substrate

From the simulation, we can see that the antenna has a directivity of 5.44 dBi with the deviation of main lobe direction by 26.0 degree. The angular width is 84.2 degree and the side lobe level is very high with the value of -4.3 dB.

6.3.5 Comparison Among the Dielectric Substrates

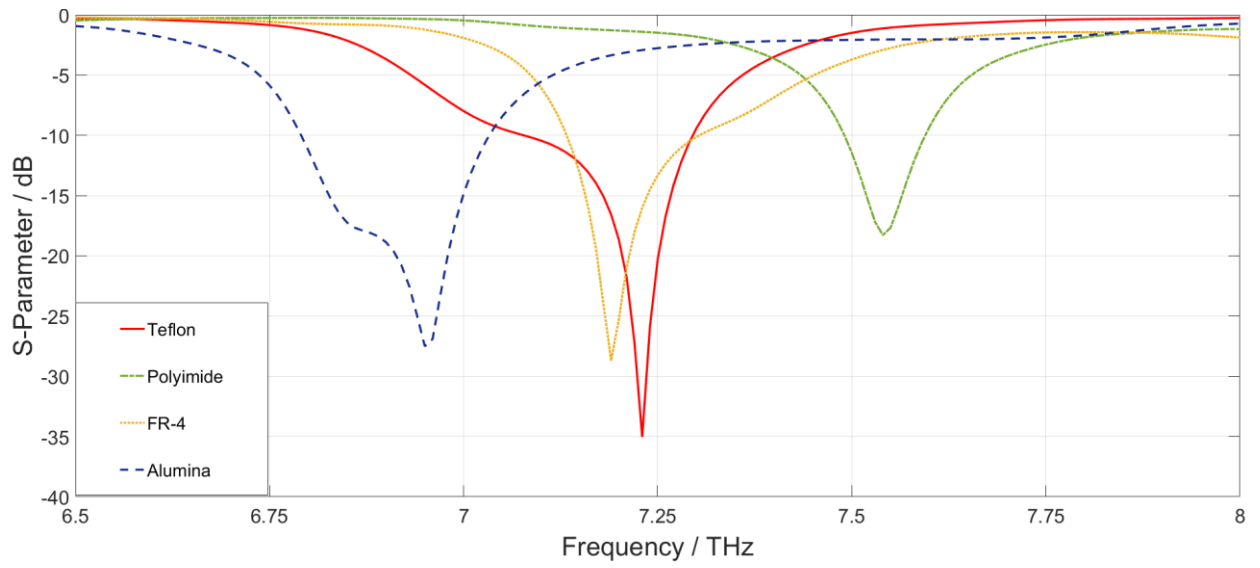


Figure 103: Comparison of s-parameter of triangular patch antenna for different substrates

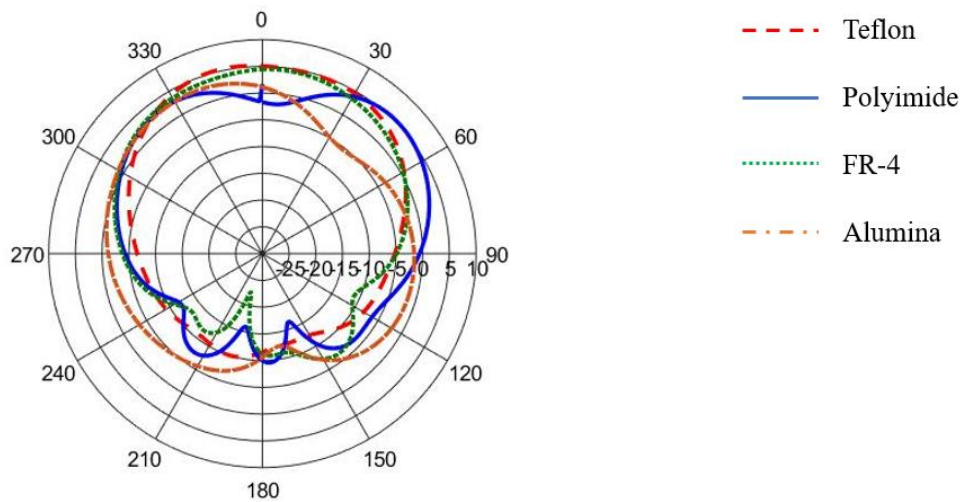


Figure 104: Polar plot of triangular patch antenna for different substrates

Table 7: Comparison of triangular patch antenna parameters for different substrates

Substrates	Resonant Frequency (THz)	S-Parameter(dB)	VSWR	Gain(dB)	Directivity (dBi)	Side Lobe Level(dB)
Teflon	7.23	-35.04	1.036	5.44	6.88	-15.3
Polyimide	7.54	-18.28	1.277	5.8	6.78	-2.4
FR-4	7.19	-28.70	1.076	5.3	6.27	-11.0
Alumina	6.95	-27.5	1.089	3.3	5.44	-4.3

The table above comprises all the experimental results and data obtained from the simulations. The s-parameter of an antenna evaluates how much power is reflected by the antenna. From the table, we can see that all the antenna designs show a good s parameter value with Teflon providing the best value of -35.04 dB. In terms of VSWR, the antenna provides a very good value for all the dielectric materials while using Teflon as a substrate yields the best performance. However, the designed antennas show identical gain values for Teflon, Polyimide and FR-4 dielectric materials whereas Alumina substrate shows relatively lower gain of 3.3 dB. Moreover, directivity is an important parameter and all our designs show good directivity values with Teflon providing the best performance with 6.88dBi. If we observe closely, we can see that directivity decreases with the increase of dielectric constant of the substrate materials. Among all the designs, Teflon as substrate provide the lowest side lobe level of -15.3 dB. On the other hand, Polyimide and Alumina produce very high side lobe levels of -2.4 dB and -4.3 dB respectively which is undesired as more power is drawn away from the main lobe. Comparing all the results for different substrate materials, it can be concluded that Teflon provides the best results among all the substrate materials for triangular patch antenna.

6.4 Comparison Among Antenna Shapes For Different Dielectric Materials

At this point, it is also essential to study and analyse the differences among parameters such as gain, directivity, return loss and Voltage Standing Wave Ratio with respect to specific dielectric substrate by changing the design of the patch.

6.4.1 For Teflon Substrate

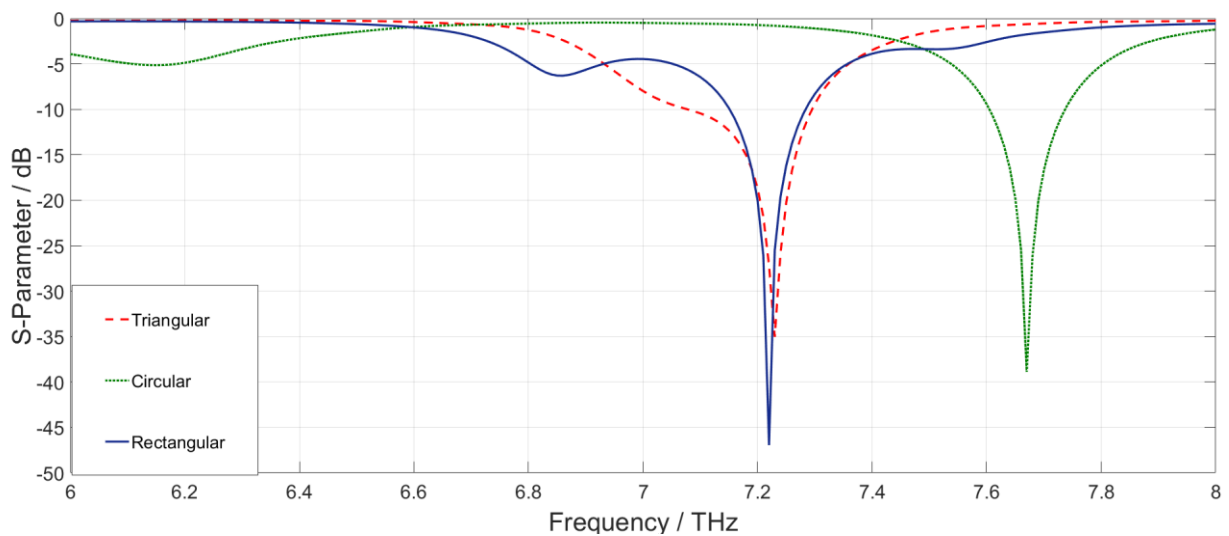


Figure 105: S-Parameters of different patch antennas for Dielectric Substrate Teflon

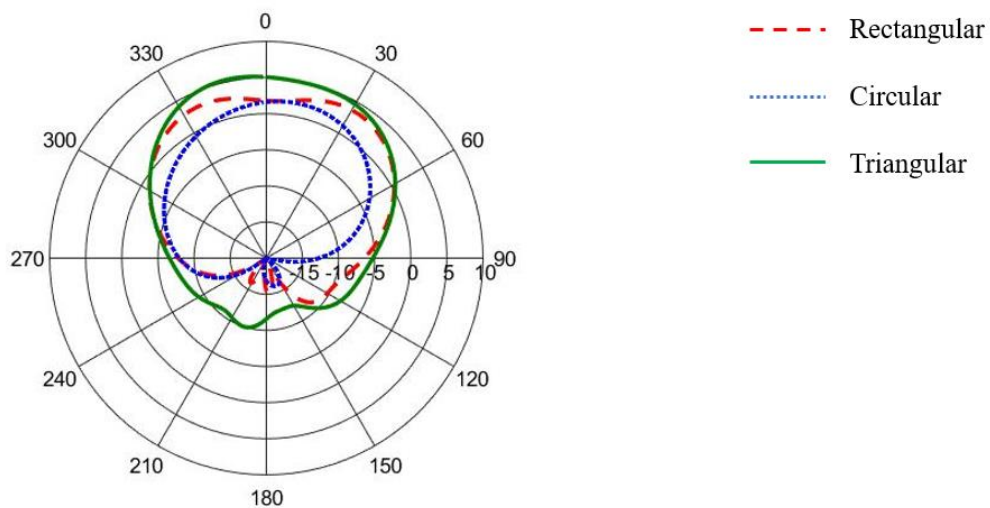


Figure 106: Polar plot of different patch antenna for Dielectric Substrate Teflon

Table 8: Comparison among the different patch antenna for Dielectric Substrate Teflon

Shape of patch	Resonant Frequency (THz)	S-Parameter(dB)	VSWR	Gain(dB)	Directivity (dBi)	Side Lobe Level(dB)
Rectangular	7.22	-46.95	1.015	3.67	7.03	-18.7
Circular	7.67	-38.88	1.024	1.87	7.85	-17.8
Triangular	7.23	-35.04	1.036	5.44	6.88	-15.3

From the above table we can draw several conclusions in terms of S-parameters, VSWR, gain, directivity and side lobe level. We have tried to compare different patches designs using a specific dielectric substrate in this case Teflon. At first it is observed that the resonant frequency for both rectangular and triangular patch is around 7.22 THz. However, the resonant frequency for circular patch is found at 7.67 THz. The best return loss is obtained at -46.95 dB for rectangular patch design. It is mandatory to keep the S-Parameter below -10dB so that 90% power can be reflected. Similarly, rectangular graphene patch shows the best value for VSWR which is 1.015. In terms of gain the highest value is obtained for triangular graphene which is 5.44 dB. Though rectangular graphene shows gain of 3.67 dB which is laudable but in case of circular patch it is very minimal showing about 1.87 dB. On the other hand, maximum directivity is shown by circular patch graphene which is 7.85 dBi. Finally, in terms of dB the side lobe level of rectangular antenna is lowest at -18.7 dB than circular and triangular patches. It is to be understood that the more the side lobe level more power is drawn away from the main lobe.

6.4.2 For Polyimide Substrate

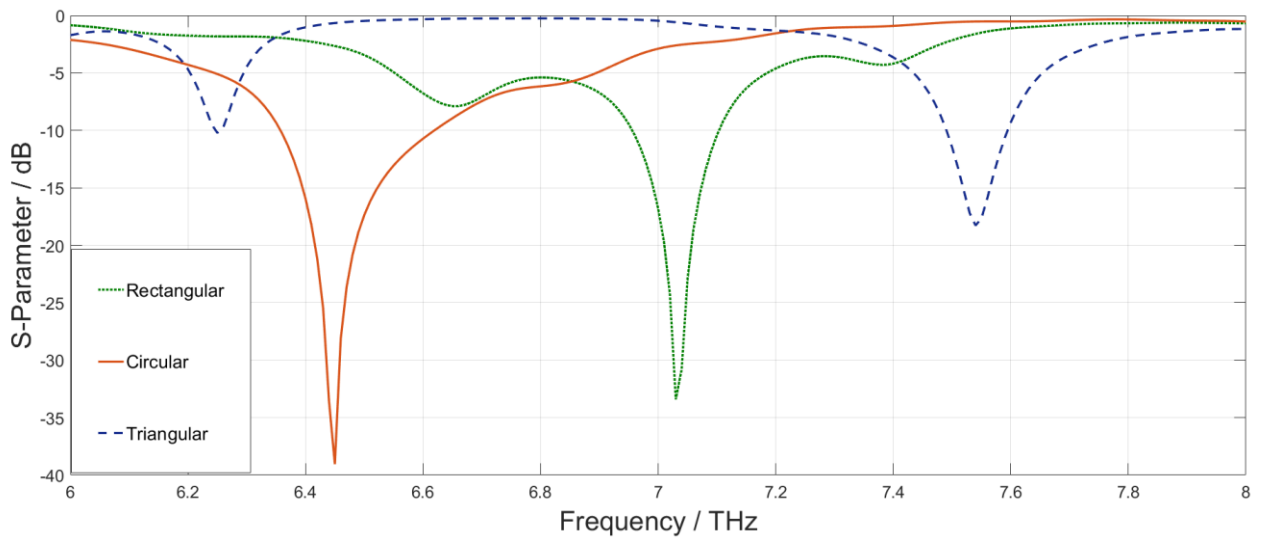


Figure 107: S-Parameters of different patch antenna for Dielectric Substrate Polyimide

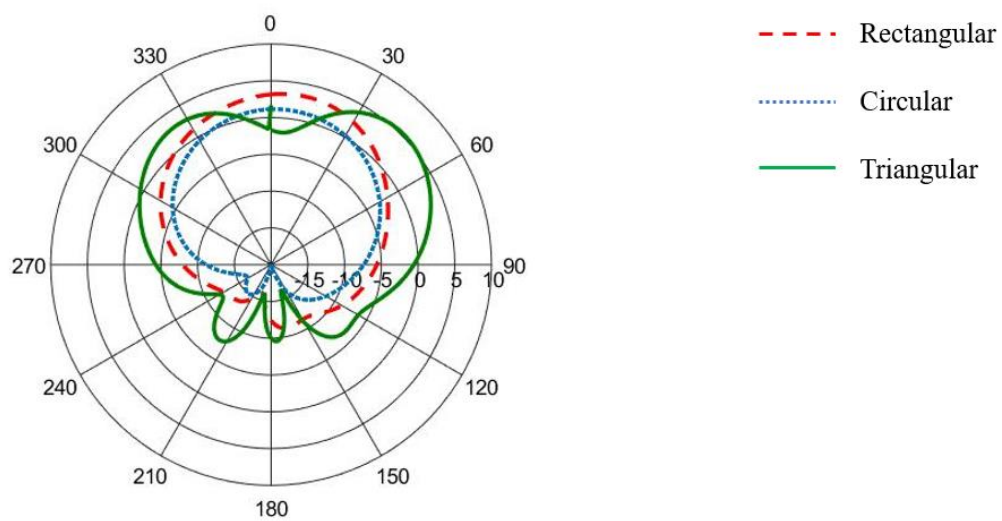


Figure 108: Polar plot of different patch antenna for Dielectric Substrate Polyimide

Table 9: Comparison among the different patch antenna for Dielectric Substrate Polyimide

Shape of patch	Resonant Frequency (THz)	S-Parameter(dB)	VSWR	Gain(dB)	Directivity (dBi)	Side Lobe Level(dB)
Rectangular	7.03	-33.41	1.044	5.81	5.1	-14.4
Circular	6.45	-39.05	1.023	1.18	6.48	-16.1
Triangular	7.54	-18.28	1.277	5.8	6.78	-2.4

The above table shows comparison for different patch designs using a specific dielectric substrate in this case Polyimide. At first it is observed that the resonant frequency is irregular for different kinds of patches. The resonant frequency for circular patch is found at 6.45 THz whereas rectangular and triangular patch resonates around 7.03 THz and 7.54 THz respectively. The best return loss is obtained at -39.05 dB for circular patch. It is mandatory to keep the S-Parameter below -10dB so that 90% power can be reflected. Similarly, circular graphene patch shows the best value for VSWR which is 1.023. In terms of gain both triangular and rectangular graphene shows the highest value which is 5.8 dB. However, gain of circular patch is very minimal showing about 1.18 dB. Furthermore, the maximum directivity is shown by triangular patch graphene which is 6.78 dBi. Finally, in terms of dB the side lobe level both rectangular and circular graphene antenna shows values lower than at -14.4 dB. It is to be understood that the more the side lobe level more power is drawn away from the main lobe. In case of triangular patch, the side lobe level is more i.e. -2.4 dB. Hence the side lobe of triangular graphene draws more power than circular and rectangular.

6.4.3 For Fr-4 Substrate

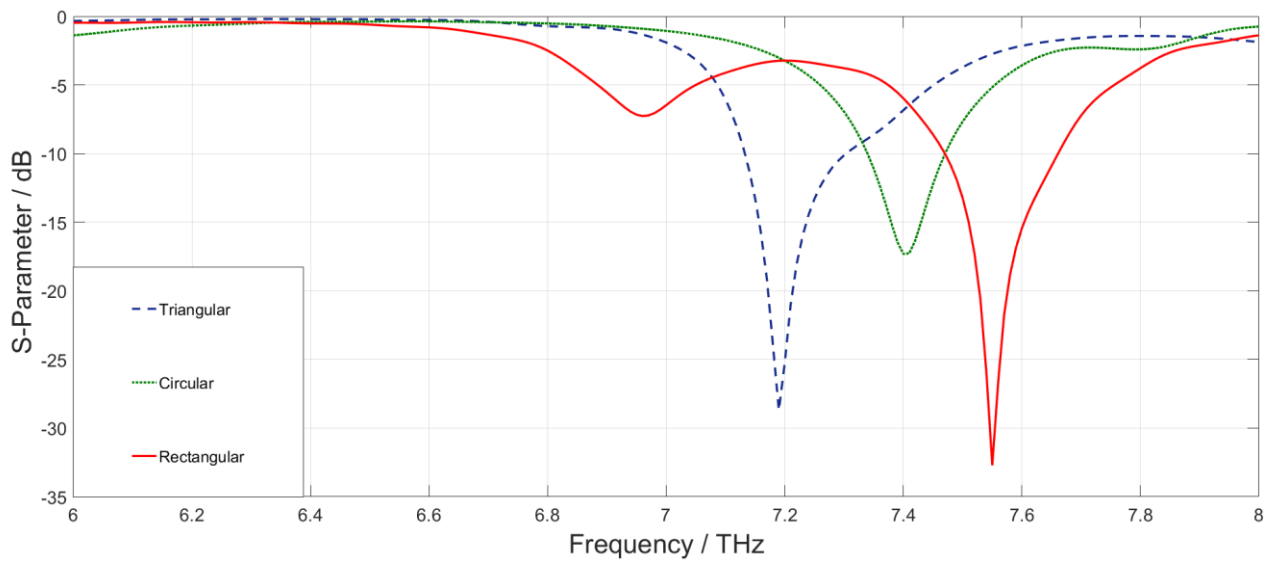


Figure 109: S-Parameters of different patch antenna for Dielectric Substrate FR-4

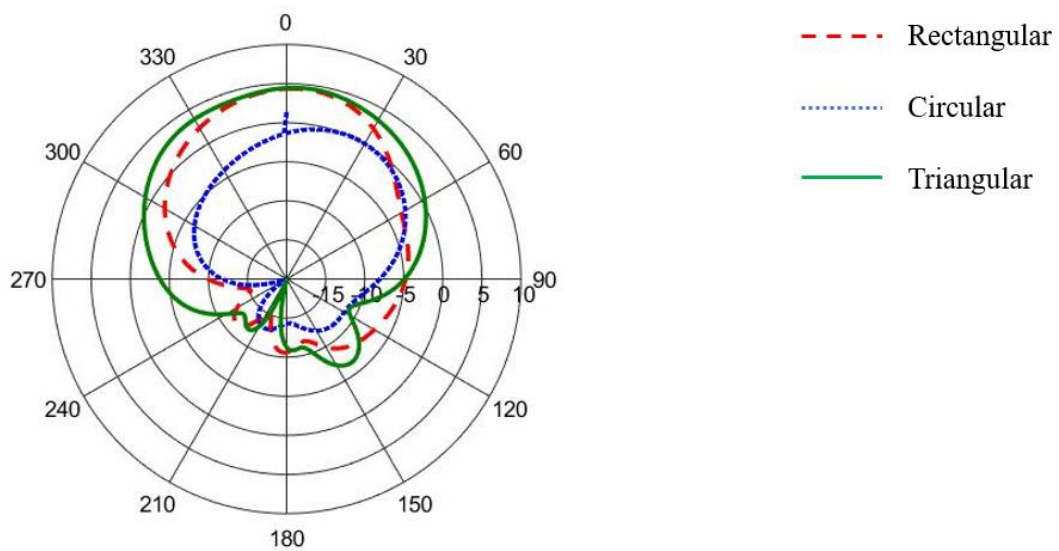


Figure 110: Polar plot of different patch antenna for Dielectric Substrate FR-4

Table 10: Comparison among the different patch antenna for Dielectric Substrate FR-4

Shape of patch	Resonant Frequency (THz)	S-Parameter(dB)	VSWR	Gain(dB)	Directivity (dBi)	Side Lobe Level(dB)
Rectangular	7.55	-32.71	1.048	6.06	5.68	-15
Circular	7.4	-17.32	1.315	0.364	6.62	-13.1
Triangular	7.19	-28.70	1.076	5.3	6.27	-11.0

The above table discusses comparison for different patch designs using a specific dielectric substrate in this case FR-4. At first it is observed that the resonant frequency for both rectangular and circular patch is close around 7.5 THz. However, the resonant frequency for triangular patch is found at 7.19 THz. The best return loss is obtained at -32.71 dB for rectangular patch. It is mandatory to keep the S-Parameter below -10dB so that 90% power can be reflected. Similarly, rectangular graphene patch shows the best value for VSWR which is 1.048. In terms of gain the highest value is found for rectangular graphene which is 6.06 dB. Though triangular graphene shows gain of 5.3 dB which is laudable but in case of circular patch it is very minimal showing about 0.364 dB. On the other hand, maximum directivity is shown by circular patch graphene which is 6.62 dBi. Finally, in terms of dB the side lobe level of rectangular antenna is lowest at -15 dB than circular and triangular patches. It is to be understood that the more the side lobe level more power is drawn away from the main lobe.

6.4.4 For Alumina (96%) Substrate

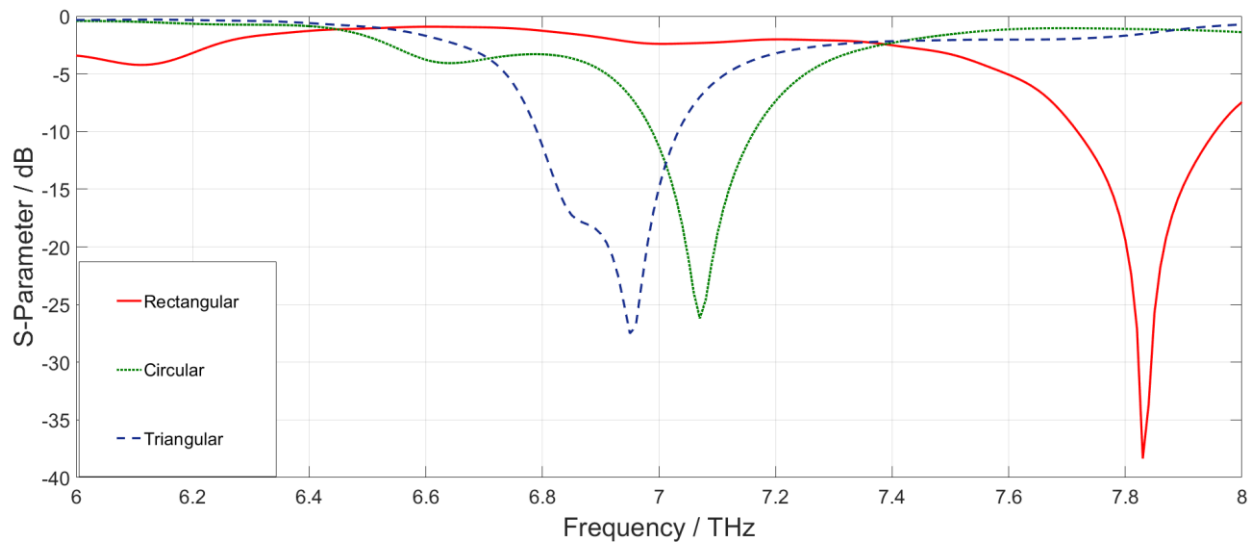


Figure 111: S-Parameters of different patch antenna for Dielectric Substrate Alumina (96%)

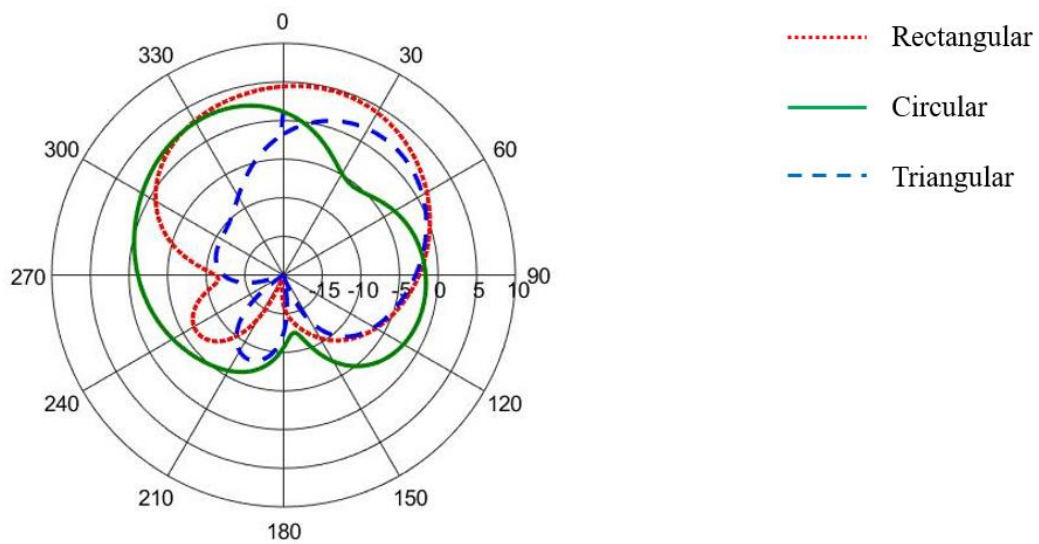


Figure 112: Polar plot of different patch antenna for Dielectric Substrate Alumina (96%)

Table 11: Comparison among the different patch antenna for Dielectric Substrate Alumina (96%)

Shape of patch	Resonant Frequency (THz)	S-Parameter(dB)	VSWR	Gain(dB)	Directivity (dBi)	Side Lobe Level(dB)
Rectangular	7.83	-38.35	1.025	4.68	6.35	-11.3
Circular	7.07	-26.2	1.103	1.94	6.73	-10.1
Triangular	6.95	-27.5	1.089	3.3	5.44	-4.3

From the above table comparison for different patch designs using a specific dielectric substrate in this case Alumina (96%) is shown. At first it is observed that the resonant frequency for both circular and triangular patch is around 7 THz. However, the resonant frequency for rectangular patch is found at 7.83 THz. The best return loss is obtained at -38.35 dB for rectangular patch. It is mandatory to keep the S-Parameter below -10dB so that 90% power can be reflected. Similarly, rectangular graphene patch shows the best value for VSWR which is 1.025. In terms of gain the highest value is obtained for rectangular graphene which is 4.68 dB. Though triangular graphene shows gain of 3.3 dB which is laudable but in case of circular patch it is very minimal showing about 1.94 dB. On the other hand, maximum directivity is shown by circular patch graphene which is 6.73 dBi. Finally, in terms of dB the side lobe level of both rectangular and circular graphene antenna is lower than -10.1 dB. It is to be understood that the more the side lobe level more power is drawn away from the main lobe. In case of triangular patch, the side lobe level is more i.e. -4.3 dB. Hence the side lobe of triangular graphene draws more power than circular and rectangular.

Chapter 7

Conclusion and Future Scopes

7.1 Conclusion

In recent times, the demand for higher speed wireless communication with larger bandwidth is becoming inevitable as the amount of data an average person transfers or uses is increasing vastly. The frequencies in the terahertz band has shorter wavelengths than microwave radiation, and therefore has a higher bandwidth capacity for larger data transmissions. Along with that, terahertz radiation is more concentrated and focused, and thus provides improved communication efficiency and less power consumption. It will provide several attractive properties like terabit-per-second communication links, miniature transceivers, zero latency, and potentially, high energy efficiency. Existing materials that are being used for conventional antennas such as copper, aluminium, brass etc. does not have the high electron mobility that is needed to produce terahertz radiation. Graphene, an allotrope of carbon with high electron mobility, has the capabilities to function properly in producing and operating in terahertz radiations. Our approach was to create an antenna made of graphene that will exhibit excellent performances at high frequencies. Our choice of antenna was the microstrip patch antenna, because it can be easily modified and fabricated, and has a wide range of applications. We hoped that our results will pave a path and ease the difficulties faced in making higher speed wireless communication systems a reality.

In our research, we opted to design microstrip patch antenna for three shapes: rectangular, circular and triangular and analyse the antenna performance based on different substrate materials as the properties of the materials such as dielectric constant, loss tangent and surface wave excitation are crucial for antenna performance. The substrate materials used in our thesis are Teflon, Polyimide, FR-4 and Alumina (96%). At first, we designed rectangular microstrip patch antennas for four different substrate materials. From the results, it can be concluded that Teflon provides the optimum results for rectangular shape with return loss of -46.95 dB, VSWR of 1.015 and a high directivity of 7.03 dBi. The only parameter where Teflon falls behind other materials is gain with a value of 3.67 dB, but it can be compromised as Teflon provides a lower side lobe level of -18.7 dB than other dielectric materials. Similarly, circular shaped graphene patch antennas for different substrates have been designed. It can be concluded that circular shaped patch antenna shows poor gain for all the dielectric materials. Among the four dielectric

materials for circular patch, Teflon stands out showing excellent return loss of -38.88 dB and directivity of 7.85 dB along with the fact that it shows lower side lobe level of -17.8 dB. Finally, we designed triangular patch antennas with the four substrates and found optimum antenna performance for Teflon. Comparing the three patch shapes, Teflon has shown outstanding antenna performance as a substrate. Analysing all our designs, it can be deduced that the combination of a rectangular single-layer graphene patch with Teflon as the dielectric substrate will give the best antenna performance.

Overall, our analysed designs have helped us to find out a better combination of patch shape and substrate material that will exhibit excellent antenna performances at terahertz frequencies. However, there are opportunities to make further modifications and improvements to provide superior results. Hopefully, we will be able to make upgrades to our work and contribute to a better wireless communication system.

7.2 Future Scopes

Graphene possesses such magnificent and prolific attributes which can easily bring the world of wireless communication to a new horizon. Our aim was to design a simple versatile microstrip antenna primarily made of pure single layer graphene so that it can operate in higher order terahertz regime since classical antenna cannot be shrunk into few micro meters. But this is not the end. Graphene's far reaching capabilities have opened the door to immense possibilities. Future scope of this research is to make a comparative study and analyse the characteristics and radiation properties of graphenna having multiple layers. In addition to it, we can also add impurities such as MoS₂ and analyse its effects on antenna parameters such as efficiency, gain, return loss, radiation pattern etc. Moreover, we will try to implement on other types of antenna such as arrays, Yagi-Uda and so on. Furthermore, study can also be done by changing feeding tetchiness and using shorting pins. We also hope to integrate such miniature size antennas in IoNT devices. As a result, very high data communication can be established.

References

- [1] Bevelacqua, P. (n.d.). Welcome to Antenna-Theory.com! Retrieved July 15, 2017, from <http://www.antenna-theory.com/>
- [2] Notes, e. Yagi Antenna | Yagi-Uda Aerial | Electronics Notes. Retrieved from <https://www.electronics-notes.com/articles/antennas-propagation/yagi-uda-antenna-aerial/basics-overview.php>
- [3] Microstrip Patch Antennas. Retrieved from http://emlab.utep.edu/ee4382_AntennaEngineering/Topic%205%20--%20Microstrip%20Patch%20Antenna.pdf
- [4] Log-periodic antenna. Retrieved from https://en.wikipedia.org/wiki/Log-periodic_antenna
- [5] Design and Simulation of Dual Band Planar Inverted F Antenna (PIFA) For Mobile Handset Applications. (2015). *International Journal of Antennas (JANT)*, 1(1). Retrieved from https://www.academia.edu/34722020/Design_and_Simulation_of_Dual_Band_Planar_Inverted_F_Antenna_PIFA_For_Mobile_Handset_Applications
- [6] Puri, S., Kaur, K., & Kumar, N. (2014). A Review of Antennas for Wireless Communication Devices. *International Journal of Electronics and Electrical Engineering*, 199-201. doi: 10.12720/ijeee.2.3.199-201
- [7] Radiation Pattern of Antenna. Retrieved from http://www.idc-online.com/technical_references/pdfs/electronic_engineering/Radiation_Pattern_of_Antenna.pdf
- [8] Pozar, David M. (2012). *Microwave engineering*. Hoboken, NJ: Wiley,
- [9] Reflector Antennas. Retrieved from <https://www.cv.nrao.edu/course/ast534/ReflectorAntennas.html>
- [10] Reflector (antenna). Retrieved from [https://en.wikipedia.org/wiki/Reflector_\(antenna\)](https://en.wikipedia.org/wiki/Reflector_(antenna))
- [11] Antenna Theory Log-periodic Antenna. Retrieved from https://www.tutorialspoint.com/antenna_theory/log_periodic_antenna_theory.htm
- [12] Notes, E. Log Periodic Antenna | LPDA Aerial Array | Electronics Notes. Retrieved from <https://www.electronics-notes.com/articles/antennas-propagation/log-periodic-lpda-antenna/log-periodic-basics.php>
- [13] Antenna types. Retrieved from https://en.wikipedia.org/wiki/Antenna_types
- [14] Antenna Theory - Aperture. Retrieved from https://www.tutorialspoint.com/antenna_theory/antenna_theory_aperture.htm

- [15] Antenna Theory - Horn. Retrieved from
https://www.tutorialspoint.com/antenna_theory/antenna_theory_horn.htm
- [16] Antenna Theory - Slot. Retrieved from
https://www.tutorialspoint.com/antenna_theory/antenna_theory_slot.htm
- [17] C. A. Balanis, "Antenna theory: analysis and design. Hoboken", NJ: Wiley Interscience, 2005.
- [18] UHA 9125 D, half-wave dipole antenna, 1.0 - 4 GHz , digital image, Wikipedia, accessed 21 April, 2019,
https://en.wikipedia.org/wiki/Dipole_antenna#/media/File:Half_%E2%80%93_Wave_Dipole.jpg
- [19] ANT50D - Folded Dipole Antenna, 45 - 54 MHz, digital image, Telewave, Inc. , accessed 21 April 2019, <https://www.telewave.com/product/ant50d-folded-dipole-antenna-45-54-mhz/>
- [20] Aomway High Gain 5.8G 11dbi Helical Antenna Internal Thread Needle, FPV Model, digital image, accessed 21 April 2019, https://www.fpvmodel.com/aomway-high-gain-5-8g-11dbi-helical-antenna-internal-thread-needle_g504.html
- [21] Yagi-Uda Antenna (Yagi-Uda the III (close-up), digital image, SOTA outings by KØMOS and contributors, accessed 21 April 2019,
<http://www.schnizer.com/SOTAblog/equipment/yagiuda-iii/>
- [22] Rectangular Microstrip Patch Antenna (Shafiei, M. M., Moghavvemi, M., Mahadi, W. N. L., 2015) (Shafiei, M. M., Moghavvemi, M., Mahadi, W. N. L. (2015), experimental antenna, "Antenna tackles Wi-Fi and WiMAX," *Microwaves & RF*, January 16, 2015
- [23] Planar Inverted-F Antenna (from H. Chattha, Y. Huang, M. Ishfaq and S. Boyes, 2012) (H. Chattha, Y. Huang, M. Ishfaq and S. Boyes.(2012), PIFA used for experiment, "A Comprehensive Parametric Study of Planar Inverted-F Antenna," *Wireless Engineering and Technology*, Vol. 3 No. 1, 2012, pp. 1-11. doi: 10.4236/wet.2012.31001
- [24] _Paraboloid Reflector with Cassegrain Feed, digital image, Antenna Theory, Tutorialspoint, accessed 21 April 2019,
https://www.tutorialspoint.com/antenna_theory/antenna_theory_parabolic_reflector.html
- [25] A VSAT (Very Small Aperture Terminal) antenna used for home or business satellite communications. (Very Small Aperture Antenna, digital image, iDirect Satellite Equipment, GROUNDCONTROL Global Satellite Communications, accessed 21 April 2019, http://www.groundcontrol.com/Satellite_Dish_Equipment.htm

- [26] The Log Periodic Dipole Antenna LPDA 400-4000 MHz, digital image, EMC Antenna, BAZ special antennas - Germany, accessed 21 April 2019, <http://www.amateur-radio-antenna.com/images/lpda4004000mhz.jpg>
- [27] Waveguide Antenna (Open-Ended Waveguide Antenna, digital image, accessed 21 April 2019, https://www.labvolt.com/solutions/9_telecommunications/60-9555-00_open_ended_waveguide_antenna
- [28] Horn Antenna (Double ridged broadband horn antenna BBHA 9120 B, digital image, Schwarzbeck Dual Polarized Broadband Horn Antenna, accessed 21 April 2019, http://www.ramayes.com/Snap_Mount_Antennas.htm
- [29] Slot Antenna (UHF RFID Slot Antenna H86-AS-SMA, digital image, HL, accessed April 2019, <http://www.hl-rfidtag.com/product/uhf-rfid-slot-antenna-h86-as-sma/>
- [30] Radiation pattern in 2D (Radiation pattern in 2D, digital image, Antenna Theory, Tutorialspoint, accessed 21 April 2019, https://www.tutorialspoint.com/antenna_theory/antenna_theory_radiation_pattern.htm
- [31] Omnidirectional Antenna Radiation Pattern (Omnidirectional dipole antenna radiation pattern, digital image, Omnidirectional Antenna Radiation Pattern, MP Antenna, accessed 21 April 2019, <https://www.mpantenna.com/omnidirectional-antenna-radiation-patterns/>
- [32] Isotropic Antenna Radiation Pattern (Antenna Pattern of an Isotropic Antenna in the vertical and horizontal plane, digital image, Everything RF, accessed 21 April 2019, <https://www.everythingrf.com/community/what-is-an-isotropic-antenna>
- [33] 3D radiation pattern of an isotropic antenna (3-D Antenna Pattern of an Isotropic Antenna, digital image, Everything RF, accessed 21 April 2019, <https://www.everythingrf.com/community/what-is-an-isotropic-antenna>
- [34] Yagi antenna directional radiation pattern, Yagi antenna RF pattern, digital image, EVDO Tips and Tweaks, accessed April 2019, <http://evdotips.blogspot.com/2008/02/directional-antennas.html>
- [35] 3D representation of the antenna pattern of a Yagi antenna, digital image, Principal of Operation, Yagi Antenna, radartutorial.eu, accessed 23 April 2019, <http://www.radartutorial.eu/06.antennas/Yagi%20Antenna.en.html>
- [36] Directivity- Antenna, retrieved from: <http://www.antenna-theory.com/basics/directivity.php>
- [37] Garg, R., Bhartia, P., Bahl, I. and Ittipiboon, A. (2001) Microstrip Antenna Design Handbook. 1st Edition, Artech House, Norwood.

- [38] Novoselov, K. S., Geim, A. K., Morozov, S. V., Jiang, D., Zhang, Y., Dubonos, S. V., Grigorieva, I. V., and Firsov, A. A. 2004. Electric field effect in atomically thin carbon films. *Science* 306 (5696): 666–669.
- [39] Bolotin, K. I., Sikes, K. J., Jiang, Z., Klima, M., Fudenberg, G., Hone, J., Kim, P., and Stormer, H. L. 2008. Ultrahigh electron mobility in suspended graphene. *Solid State Communications* 146 (9–10): 351–355.
- [40] Bunch, J. S., van derZande, A. M., Verbridge, S. S., Frank, I. W., Tanenbaum, D. M., Parpia, J. M., Craighead, H. G., and McEuen, P. L. 2007. Electromechanical resonators from graphene sheets. *Science* 315 (5811): 490–493.
- [41] Lee, C., Wei, X., Kysar, J. W., and Hone, J. 2008. Measurement of the elastic properties and intrinsic strength of monolayer graphene. *Science* 321 (5887): 385–388.
- [42] Bae, S., Kim, H., Lee, Y., Xu, X., Park, J.-S., Zheng, Y., Balakrishnan, J., Lei, T., Ri Kim, H., Song, Y. I., Kim, Y.-J., Kim, K. S., Ozyilmaz, B., Ahn, J.-H., Hong, B. H., and Iijima, S. 2010. Roll-to-roll production of 30-inch graphene films for transparent electrodes. *Nature Nanotechnology* 5 (8): 574–578.
- [43] Kim, K. S., Zhao, Y., Jang, H., Lee, S. Y., Kim, J. M., Kim, K. S., Ahn, J.-H., Kim, P., Choi, J.-Y., and Hong, B. H. 2009. Large-scale pattern growth of graphene films for stretchable transparent electrodes. *Nature* 457 (7230): 706–710.
- [44] Balandin, A. A., Ghosh, S., Bao, W., Calizo, I., Teweldebrhan, D., Miao, F., and Lau, C. N. 2008. Superior thermal conductivity of single-layer graphene. *Nano Letters* 8 (3): 902–907.
- [45] GEIM, A. and NOVOSELOV, K. (2007). *The rise of graphene*. [online] Nature Publishing Group. Available at: <http://www.nature.com/naturematerials> [Accessed 18 Sep. 2018].
- [46] H. Philip Wong and D. Akinwande, *Carbon nanotube and graphene device physics*. Cambridge University Press 2011, p. pages 49.
- [47] Geim and K. Novoselov, "The Rise of Graphene", *Arxiv.org*, 2019. [Online]. Available: <https://arxiv.org/pdf/cond-mat/0702595>. [Accessed: 17- Apr- 2019]
- [48] "The history of graphene | Graphene Flagship", *Graphene-flagship.eu*, 2019. [Online]. Available: <https://graphene-flagship.eu/material/Pages/The-history-of-graphene.aspx>. [Accessed: 17- Apr- 2019].

- [49] B. Helbig, "1. Propagation of Electromagnetic Waves in Graphene Waveguides", Physik.uni-augsburg.de, 2019. [Online]. Available: <https://www.physik.uni-augsburg.de/lehrstuehle/theo2/downloads/helbig.pdf>. [Accessed: 13- Apr- 2019].
- [50] Wallace, P. R. The band theory of graphite. Phys. Rev. 71, 622{634 (1947).URL <http://link.aps.org/doi/10.1103/PhysRev.71.622>.
- [51] Slonczewski, J. C. & Weiss, P. R. Band structure of graphite. Phys. Rev. 109, 292{297 (1958).
- [52] S. A. Mikhailov. Frequency Mixing Effects in Graphene, in: Physics and Applications of Graphene {Theory, ISBN: 978-953-307-152-7, edited by Sergey Mikhailov (InTech, Rijeka, Croatia, 2011); chapter 25, pp. 519{534.
- [53] Tudorovskiy, T. &Mikhailov, S. A. Intervalley plasmons in graphene. Phys. Rev. B 82, 073411 (2010).URL <http://link.aps.org/doi/10.1103/PhysRevB.82.073411>.
- [54] Hausler, W. Lecture 'quasi-relativistic electrons in graphene' (2011).
- [55] Castro Neto, A. H., Guinea, F., Peres, N. M. R., Novoselov, K. S. &Geim, A. K. The electronic properties of graphene. Rev. Mod. Phys. 81, 109{162 (2009).URL <http://link.aps.org/doi/10.1103/RevModPhys.81.109>.
- [56] Geim, A. K. &Novoselov, K. S. The rise of graphene. Nature Materials 6, 183{191 (2007).
- [57] Llatser, I.; Kremers, C.; Cabellos-Aparicio, A.; Jornet, J.M.; Alarcon E.; and Chigrin D.N. (2012). Graphene - based nano-patch antenna for terahertz radiation. Photonics and Nanostructures-Fundamentals and Applications, 10(4), 353-358.
- [58] L. Falkovsky, S. Pershoguba, Optical far-infrared properties of a graphene monolayer and multilayer, Physical Review B 76 (2007) 1–4.
- [59] G.W. Hanson, Dyadic Green's functions for an anisotropic, nonlocal model of biased graphene, IEEE Transactions on Antennas Propagation 56 (2008) 747–757.
- [60] Bechtel, H.A.; Chen, C.; Crommie, M.F.; Geng, B.; Girit, C.; Horng, J.; Hao, Z.; Martin, M.; Shen, Y.R.; Wang, F.; Zhang, Y.; and Zettl, A. (2011). Intraband optical transitions in graphene. CLEO: 2011 - Laser Science to Photonic Applications, 1-2.

- [61] Kashuba, A.B. (2008). Conductivity of defect less graphene. *Physical Review B* 78 (085415).
- [62] Razavizadeh M. S, "2017 Simulation of Graphene in CST Microwave v2015 and COMSOL Multiphysics5.2a2017[Online]Available: https://www.researchgate.net/publication/312146956_Simulation_of_Graphene_in_CST_Microwave_v2015_and_COMSOL_Multiphysics_52a. [Accessed: 11- Apr- 2019].
- [63] I. LLATSER et al., "Radiation Characteristics of Tunable Graphennas in the Terahertz Band."
- [64] GEORGE, P. A., STRAIT, J., DAWLATY, J., and others, Ultrafast Optical-Pump Terahertz-Probe Spectroscopy of the Carrier Relaxation and Recombination Dynamics in Epitaxial Graphene. *Nano Letters*, 2008, vol. 8, no. 12, p. 4248 - 4251.
- [65] TRUSHIN, M., SCHLIEMANN, J. Anisotropic photoconductivity in graphene. *EPL*, 2011, vol. 96, 37006.
- [66] HU, J., RUAN, X., CHEN, Y. P. Thermal Conductivity and Thermal Rectification in Graphene Nanoribbons: A Molecular Dynamics Study. *Nano Letters*, 2009, vol. 9, no. 7, p. 2730 - 2735.
- [67] RYZHII, V., RYZHII, M., OTSUJI, T. Negative dynamic conductivity of graphene with optical pumping. *Journal of Applied Physics*, 2007, vol. 101, 083114.
- [68] B. R., M. A. and M. S., "MATHEMATICAL FORMULATION OF SURFACE CONDUCTIVITY FOR GRAPHENE MATERIAL", *Core.ac.uk*, 2019. [Online]. Available: <https://core.ac.uk/display/88830145>. [Accessed: 23- Apr- 2019].
- [69] "Significance of Antenna in Communication System - Article | ATG", *Atg.world*, 2018. [Online]. Available: <https://www.atg.world/viewarticle/Significance%20Of%20Antenna%20In%20Communication%20System-1878>.
- [70] S. Adnan and M. Goni, "Graphene Nanoribbon based Antenna for Terahertz Band Communication", in *Proceedings of International Conference on Electrical Information and Communication Technology (EICT 2015)*, 2015.

- [71] Y. Dong, P. Liu, D. Yu, G. Li and F. Tao, "Dual-Band Reconfigurable Terahertz Patch Antenna with Graphene-Stack-Based Backing Cavity", *IEEE Antennas and Wireless Propagation Letters*, vol. 15, pp. 1541-1544, 2016.
- [72] J. Jornet and I. Akyildiz, "Graphene-Based Nano-Antennas for Electromagnetic Nano communications in the Terahertz Band."
- [73] E. Carrasco, "Reflect array Antenna at Terahertz Using Graphene", in *IEEE ANTENNAS AND WIRELESS PROPAGATION LETTERS, VOL. 12, 2013 253*, 2013.
- [74] I. Llatser, C. Kremers, A. Cabellos-Aparicio, J. Jornet, E. Alarcón and D. Chigrin, "Graphene-based nano-patch antenna for terahertz radiation", *Photonics and Nanostructures - Fundamentals and Applications*, vol. 10, no. 4, pp. 353-358, 2012.
- [75] T. Zhou, Z. Cheng, H. Zhang, M. Le Berre, L. Militaru and F. Calmon, "Miniaturized tunable terahertz antenna based on graphene", *Microwave and Optical Technology Letters*, vol. 56, no. 8, pp. 1792-1794, 2014.
- [76] W. Fuscaldo, P. Burghignoli, P. Baccarelli and A. Galli, "A Reconfigurable Substrate–Superstrate Graphene-Based Leaky-Wave THz Antenna", *IEEE Antennas and Wireless Propagation Letters*, vol. 15, pp. 1545-1548, 2016.
- [77] Tamagnone, M., Gómez-Díaz, J. S., Mosig, J. R., & Perruisseau-Carrier, J. (2012). Analysis and design of terahertz antennas based on plasmonic resonant graphene sheets. *Journal of Applied Physics*, 112(11), 114915. doi:10.1063/1.4768840
- [78] Wang, X.-C., Zhao, W.-S., Hu, J., & Yin, W.-Y. (2015). Reconfigurable Terahertz Leaky-Wave Antenna Using Graphene-Based High-Impedance Surface. *IEEE Transactions on Nanotechnology*, 14(1), 62–69. doi:10.1109/tnano.2014.2365205,
- [79] Li, J., He, M., Wu, C., & Zhang, C. (2017). Radiation-pattern-reconfigurable graphene leaky-wave antenna at terahertz band based on dielectric grating structure. *IEEE Antennas and Wireless Propagation Letters*, 16, 1771-1775.
- [80] Dragoman, M., Muller, A. A., Dragoman, D., Coccetti, F., & Plana, A. R. (2010). Terahertz antenna based on graphene. *Journal of Applied Physics*, 107(10), 104313.

- [81] Tamagnone, M., Diaz, J. S. G., Mosig, J., & Perruisseau-Carrier, J. (2013, June). Hybrid graphene-metal reconfigurable terahertz antenna. In *Microwave Symposium Digest (IMS), 2013 IEEE MTT-S International* (pp. 1-3). IEEE.
- [82] Huang, Y., Wu, L. S., Tang, M., & Mao, J. (2012). Design of a beam reconfigurable THz antenna with graphene-based switchable high-impedance surface. *IEEE Transactions on Nanotechnology*, 11(4), 836.
- [83] Esquiús-Morote, M., Gómez-Dí, J. S., & Perruisseau-Carrier, J. (2014). Sinusoidally modulated graphene leaky-wave antenna for electronic beam scanning at THz. *IEEE Transactions on Terahertz Science and Technology*, 4(1), 116-122.
- [84] Cheng, Y., Wu, L. S., Tang, M., Zhang, Y. P., & Mao, J. F. (2017). A Sinusoidally-Modulated Leaky-Wave Antenna with Gapped Graphene Ribbons. *IEEE Antennas and Wireless Propagation Letters*, 16, 3000-3004.
- [85] Tamagnone, M., Gomez-Diaz, J. S., Mosig, J. R., & Perruisseau-Carrier, J. (2012). Reconfigurable terahertz plasmonic antenna concept using a graphene stack. *Applied Physics Letters*, 101(21), 214102.
- [86] Rodrigues, N. R., de Oliveira, R. M., & Dmitriev, V. (2017, August). A terahertz graphene antenna with dynamical control of its radiation pattern. In *Microwave and Optoelectronics Conference (IMOC), 2017 SBMO/IEEE MTT-S International* (pp. 1-4). IEEE.
- [87] Zhang, H., Jiang, Y., Wang, J., Cao, W., Gao, X., Yu, X., & Wang, L. (2016, October). A broadband terahertz antenna using graphene. In *Antennas, Propagation and EM Theory (ISAPE), 2016 11th International Symposium on* (pp. 149-152). IEEE.
- [88] Ultra-Wide Band Antenna: M. H. Sagor, Q. H. Abbasi, A. Alomainy and Y. Hao, "Compact and conformal ultra-wideband antenna for wearable applications," Proceedings of the 5th European Conference on Antennas and Propagation (EUCAP), Rome, 2011, pp. 2095-2098.
- [89] Transparent and flexible antenna for 5G /mm Wave applications: S. Rahman, S. Alam, M. Haque, N. S. Siddique and M. H. Sagor, "Transparent and flexible Y-shaped antenna for 5G wireless applications," 12th European Conference on Antennas and Propagation, London, 2018, pp. 1-3.

- [90] Metamaterial Based Antenna: S. Al Nahiyah, A. R. Salehin, M. R. C. Mahdy and M. H. Sagor, "Modification of higher order natural mode in metamaterial loaded patch antenna," in *IET Microwaves, Antennas & Propagation*, vol. 13, no. 4, pp. 442-447, 27 3 2019.
- [91] Callaghan, P., Huelin, R., & Sagor, M. H. (2016). Investigation into use of double-layer grid structures as frequency selective surfaces for buildings. *IET Microwaves, Antennas & Propagation*, 10(13), 1372–1377. doi:10.1049/iet-map.2016.0065
- [92] Azizi, M.K., Ksiksi, M.A., Ajlani, H., Gharsallah, A., "Terahertz Graphene-Based Reconfigurable Patch Antenna," *Progress in Electromagnetics Research Letters*, 71, 69–76 (2017)
- [93] Mahamine, S. D., Parabat, R.S., Bodake, S. H., & Aher, M.P., "Effects of Different Substrates on Rectangular Microstrip Patch Antenna for S-band," 2016 International Conference on Automatic Control and Dynamic Optimization Techniques (ICACDOT).
- [94] "Printed Circuit Board (PCB) FR-4 - Sunstone Circuits", *Sunstone.com*, 2019. [Online]. Available: <https://www.sunstone.com/pcb-manufacturing-capabilities/detailed-capabilities/pcb-materials/fr-4-material>. [Accessed: 23- Apr- 2019].
- [95] "Alumina Ceramic | 96% Alumina Al₂O₃ | Elan Technology", *Elan Technology*, 2019. [Online]. Available: <https://www.elantechnology.com/ceramics/ceramic-materials/alumina-ceramics/96-alumina/>. [Accessed: 23- Apr- 2019].
- [96] side view, sp² hybridization, digital image, Organic Chemistry, Socratic, accessed on 23 April 2019, <https://socratic.org/questions/how-does-sp2-hybridized-carbon-differ-from-sp3>